Organization and functional effects of perisomatic inhibition on principal cell activity in the basolateral amygdala

Ph.D. thesis

Judit Veres

Semmelweis University

János Szentágothai Doctoral School of Neurosciences

Supervisor: Norbert Hájos, PhD, DSc

Official Reviewers of the Ph.D. Dissertation: Zita Puskár, PhD

Zoltán Kisvárday, PhD, DSc

Members of the Final Examination Board: Anita Kamondi, PhD, DSc

Lucia Wittner, PhD

Tibor Zelles, PhD

Budapest

2016

Table of Contents

List of Abbreviations

5-HT	5-hydroxytryptamine
AAC	Axo-axonic cell
ACSF	Artificial cerebrospinal fluid
AIS	Axon initial segment
BAC	Bacterial artificial chromosome
BC	Basket cell
BDA	Biotinylated dextran amine
BLA	Basolateral amygdala
BMA	Basomedial amygdala
Calb	Calbindin
CB_1	Type 1 cannabionoid receptor
CCK	Cholecystokinin
CeA	Central amygdala
CeL	Centrolateral amygdala
CeM	Centromedial amygdala
CR	Calretinin
CS	Conditioning stimulus
Ctx	Cortex
DAB	Diaminobenzidine
DSI	Depolarization-induced suppression of inhibition
GABA	Gamma-amino butyric acid
GAD	Glutamic acid decarboxylase
GFP	Green fluorescent protein
HC	Hippocampus
IC	Current clamp
IN	Interneuron
IPSC	Inhibitory postsynaptic current
IPSP	Inhibitory postsynaptic potential
ISI	Interneuron-selective interneuron
ITC	Intercalated cell

LA	Lateral amygdala
NGFC	Neurogliaform cell
NMDA	N-methyl-D-aspartate
NPY	Neuropeptide Y
PB	Phosphate buffer
PC	Principal cell
PFA	Paraformaldehyde
PP	Perforated patch
PTI	Perisomatic region-targeting interneuron
PV	Parvalbumin
SOM	Somatostatin
Str	Striatum
TBS	Tris buffered saline
Thal	Thalamus
US	Unconditioned stimulus
VC	Voltage clamp
VGAT	Vesicular GABA transporter
VGLUT1	Type 1 vesicular glutamate transporter
VGLUT2	Type 2 vesicular glutamate transporter
VGLUT3	Type 3 vesicular glutamate transporter
VIP	Vasoactive intestinal polypeptide
WCR	Whole cell recording

1. Introduction

Information processing in cortical networks relies on the precise, spatiotemporally coordinated interaction of billions of neurons. The accurate activity of the ensemble is ensured and controlled by various mechanisms at subcellular, cellular, synaptic and network levels. At network levels, the intricate wiring and precisely orchestrated excitatory and inhibitory interactions between the components are crucial for proper cortical functions, and even seemingly slight changes in the connections can lead to severe pathological states like epileptic seizures or schizophrenic symptoms (Gonzalez-Burgos et al., 2010). Unraveling the basic principles of connectivity patterns and the effects of different connections on the activity of the network components is indispensable for understanding cortical information processing.

Cortical ensembles consist of two main neuronal cell types: 80-90% of the neurons are excitatory principal cells (PCs) and 10-20% are inhibitory interneurons (INs). Cells belonging to the two main categories are thought to play different roles in cortical functions: PCs are proposed to be responsible for information processing, storage and recall, whereas INs control and tune the electrical activity of PCs at both subcellular and cellular levels as well as synchronize their rhythmic firing (Buzsaki and Chrobak, 1995, Paulsen and Moser, 1998, Engel et al., 2001). PCs use glutamate as neurotransmitter and give rise to both local collaterals and projecting axons out of the local circuit to form the main output of the given cortical area. PCs have either spherical or pyramidal-like somata from which 3-7 spiny dendrites can emerge , while their axon can emanate from the soma or the proximal dendrites (Faber et al., 2001, Thome et al., 2014). These distinct compartments have different basic functions: the dendrites receive the majority of the incoming inputs, and can locally integrate and propagate the signals towards the soma, where the inputs arriving from various dendritic branches are integrated. The proximal part of the axon, called the axon initial segment (AIS) has the lowest threshold for action potential generation, therefore here the inputs of the cell are translated into all-or-none output signals. In cortical networks, the distinct membrane domains of PCs are controlled by a massive inhibitory input originated from heterogeneous local interneuronal populations. In general, although there are some exceptions, interneurons have aspiny dendrites, use ɣ-amino butiryc acid (GABA) as

main neurotransmitter, and their axon collaterals are restricted to the local circuits. The remarkable heterogeneity of cortical interneurons observed in their morphology, electrophysiological properties, postsynaptic target distribution and cell type-specific expression of calcium binding proteins or neuropeptides may all serve to fulfil their different functions in cortical processing.

The majority of our knowledge on cortical networks comes from the investigation of the hippocampus and several neocortical areas like the somatosensory or visual cortices. Based on comparative studies we know that the main features of cortical wiring principles are similar across various cortical areas, often referring to this notion as canonical microcircuits (Douglas and Martin, 1991). Therefore, the characteristics of these well-described wiring structures- taking into account the possibility of some regional differences- can be regarded as common properties of cortical networks. The basolateral amygdala (BLA), which is in the focus of this study, belongs structurally and developmentally to cortical areas and this region is known to play a critical role in fear and extinction memory formation (Aggleton, 1993, Sah et al., 2003). Examination of the building blocks of the networks and the interactions among the elements in this region therefore can contribute to understanding of information processing and learning mechanisms in cortical areas. In the next section I will summarize our recent knowledge on the different cortical interneuronal types in general, then I will describe and compare the properties of the network in the basolateral amygdala.

1.1. Interneuron diversity in cortical networks

As mentioned above, the different subcellular compartments of PCs serve for different physiological roles, which may imply that the inhibitory inputs arriving to the distinct compartments should have different regulatory effects on PC function (Cobb et al., 1995, Miles et al., 1996). Therefore, a functional approach to IN classification can be based on the specificity in the innervation of separate subcellular domains of PCs. Accordingly, the majority of the INs in distinct cortical regions can be divided into three groups (Freund and Buzsáki, 1996): (I) perisomatic region-targeting interneurons, which form synapses on the soma, proximal dendrites and axon initial segment of PCs,

(II) dendrite-targeting interneurons, which preferentially target PC dendrites and (III) interneuron-selective interneurons, which selectively innervate other GABAergic cells. To provide a complete view of cortical interneurons, I will present the different interneuron types with a special emphasis on perisomatic region-targeting interneurons, which are in the focus of the experimental work of this thesis.

1.1.1. Perisomatic region-targeting interneurons

Perisomatic region-targeting interneurons (PTIs) predominantly innervate the cell body, proximal dendrites and axon initial segment of excitatory neurons, membrane domains of PCs where the inputs are finally integrated and the action potentials are generated. Thus, these interneurons are in the critical position to powerfully regulate the output of individual PCs as well as to synchronize the spiking activity of large neural ensembles (Buhl et al., 1994b, Miles et al., 1996). PTIs can be further subdivided into axo-axonic cells and at least two types of basket cells.

The proximal part of the axon, the axon initial segment (AIS) plays a crucial role in the generation of action potentials, therefore any input, which targets this region is thought to have a profound influence on the firing of the cells. In cortical regions a type of interneuron is specialized to innervate the AIS of PCs, the so-called chandelier or axo-axonic cell (AAC) (Somogyi, 1977). Specific innervation of the AIS in various cortical regions by AACs is a general phenomenon, since these interneurons have been identified in paleo-, archi- and neocortical areas (Inda et al., 2009). In the cortical regions investigated so far, it has been found that AACs show the highest target specificity: they form 2-30 synapses almost exclusively on AISs of PCs and avoid other cellular compartments as well as other cell types (Somogyi, 1977, Soriano et al., 1990, Han et al., 1993). AACs show typical fast spiking characteristics: they fire action potentials at high rates and there is only a moderate accommodation in their firing pattern evoked by a depolarizing current step pulse. In may cortical regions, AACs express the calcium binding protein parvalbumin (PV), a potent calcium buffer, which can also facilitates the temporally precise, fast release of neurotransmitters from their axon terminals (Eggermann and Jonas, 2012). AACs influence their postsynaptic partners via A-type GABA receptors. The intracellular chloride concentration, which

primarily sets the reversal potential for GABAergic responses, varies in distinct developmental (Ben-Ari, 2002) and pathological states (Cohen et al., 2002), and it can be controlled locally in different subcellular compartments (Szabadics et al., 2006, Foldy et al., 2010). Previous results show that the effects of AACs on their postsynaptic partners are also variable and can either inhibit or promote firing in PCs depending on several factors, including the membrane potential of the postsynaptic cell and the Cl^- reversal potential in the AIS (Buhl et al., 1994b, Szabadics et al., 2006, Glickfeld et al., 2009, Woodruff et al., 2011). Thus, to understand the role of AACs in different network states, it is indispensable to have information both on their firing activity as well as their instantaneous effect on their postsynaptic partners.

The other types of PTIs are basket cells. This cell type targets predominantly the soma and proximal dendrites of PCs, and occasionally also forms few synapses on axon initial segments (Somogyi et al., 1983a, Halasy et al., 1996). Their name refers to the characteristic, basket like axon terminal plexus around PC cell bodies formed by the convergent terminals of this cell type. An individual basket cell forms on average 1-10 boutons on the perisomatic region of single PCs (Gulyás et al., 1993, Miles et al., 1996, Kubota et al., 2015), however they also innervate more distal dendritic segments in varying proportions. In the neocortex, 25-30% of the basket cell terminals contact the perisomatic region, whereas in the hippocampus this number can reach up to 80%, indicating higher target specificity in this archicortical area. In contrast to AACs, basket cells also innervate other interneurons, mainly other basket cells (Galarreta and Hestrin, 2002, Pfeffer et al., 2013). The two main type of basket cells, PV-immunopositive, fast spiking basket cells (PVBCs) and cholecystokinin (CCK) and type 1 cannabinoid receptor (CB_1)-expressing, regular spiking basket cells (CCK/CB_1BCs) differ in various morphological and electrophysiological properties as well as in protein expression patterns. PVBCs have low input resistance and short membrane time constant, which enables them to respond fast to incoming inputs and faithfully monitor the neural activity in excitatory networks (Galarreta and Hestrin, 2001, Papp et al., 2013). Similarly to AACs, PVBCs generate narrow action potentials at high rates, show moderate- or non-accommodating firing (Papp et al., 2013, Povysheva et al., 2013). In their presynaptic terminals, the calcium influx upon spike invasion is mediated by P/Q type (Cav2.1) channels. These voltage gated Ca^{2+} channels and Ca^{2+} sensors at their

synapses are tightly coupled, forming nanodomain release machinery, which facilitates the fast, temporally precise and reliable GABA release from their axon varicosities (Poncer et al., 1997, Bucurenciu et al., 2008). CCK/CB_1BCs on the other hand have different intrinsic membrane properties: they show higher input resistance and longer membrane time constant than PVBCs enabling them to integrate incoming multiple inputs more efficiently (Glickfeld and Scanziani, 2006). Their peak firing rate is lower than those of PVBCs, and show marked accommodation in their firing (Szabó et al., 2010). As shown in the hippocampus, various subtypes of these cells can be formed based on the expression of the type 3 vesicular glutamate transporter (VGLUT3) and the vasoactive intestinal polypeptide (VIP), but the presence and functional significance of these subtypes in other cortical regions has not been clarified yet (Freund and Buzsáki, 1996). In contrast to PVBCs, the calcium influx into the presynaptic terminals of CCK/CB_1BCs is mediated by N-type calcium channels ($Ca_v2.2$), and the calcium sensors are loosely coupled to these voltage gated Ca^{2+} channels, which provides a less precise timing in transmitter release, but may enable presynaptic forms of synaptic plasticity (Hefft and Jonas, 2005, Ahmed and Siegelbaum, 2009, Lenkey et al., 2015).

There is growing evidence supporting the concept that the two types of basket cells have distinct inhibitory roles during network activities (Freund and Katona, 2007). Most of this knowledge comes from results obtained in the hippocampus, a brain region, in which the network activities and the underlying synaptic mechanisms are the most investigated among cortical areas. This is due to the fact that its circuit is relatively simple and thoroughly described, the characteristic network activities can be induced in *in vitro* preparations, and it is accessible for *in vivo* recordings. It has been shown in the hippocampus that PVBCs can effectively inhibit the firing of their postsynaptic partners and precisely regulate the function of large populations of PCs; i.e. they are well suited to operate as high-precision clockworks during network oscillations. In contrast, due to the different input integration and release properties, CCK/CB_1BCs provide a less precise synaptic inhibition (Freund and Katona, 2007). Remarkably, by expressing specific receptors, the activity of this latter cell type can be influenced by the ascending subcortical pathways, like serotoninergic (via 5-HT_3 receptors) and cholinergic ($\alpha7$ nicotinic receptors) afferents, therefore it is proposed to be involved in fine-tuning of local network activities. Thus, PVBCs can effectively synchronize PC activity

generating rhythmic patterns, while CCK/CB_1BCs appear to be able to modulate network dynamics conveying information from subcortical areas about emotional, motivational and general physiological states. In line with this concept, distinct PTI types may contribute distinctly to different pathological conditions: PVBCs are implicated in epilepsy; an abnormal rhythmic synchrony in cortical networks, whereas CCK/CB_1BCs may be rather involved in mood disorders like excessive anxiety (Freund, 2003, Cossart et al., 2005).

1.1.2. Dendrite-targeting interneurons

Dendrites of PCs in the cortex are complex structures specialized to receive the vast majority of inputs arriving to the cell. There is emerging evidence showing that PC dendrites have not a mere passive role as input receivers, but in various brain regions they can non-linearly integrate the incoming inputs by active local electrogenesis. This capacity is due to the expression of voltage-gated channels present in specific dendritic regions, which profoundly influence their integration properties. The all-or-none activation of voltage-gated Ca^{2+} and Na^{+} channels, as well as NMDA type of glutamate receptors can evoke local dendritic spikes in excitable segments called "hotspots", which propagate, sometimes in a regenerative manner, along the dendritic tree. This enables specific dendritic branches to summate excitatory inputs supralinearly, e.g. the synchronous activation of neighbouring inputs can evoke higher voltage responses than the mathematical sum of their individual responses, thereby performing space and time specific input integration (Magee, 2000, Magee and Cook, 2000). The supralinear integration of inputs has deep influence on the activity of the cell: dendritic spikes can trigger action potentials and facilitate burst firing at the soma (Golding and Spruston, 1998, Larkum et al., 1999, Ariav et al., 2003, Losonczy and Magee, 2006), and the local dendritic depolarization and Ca^{2+} influx can be sufficient to induce synaptic plasticity (Golding et al., 2002, Remy and Spruston, 2007). Therefore, any inhibitory input targeting these specific dendritic domains - besides shunting the excitatory inputs - is in a strategic position to control dendritic integration linearity by changing the gain and offset of the input-output function (Mitchell and Silver, 2003, Isaacson and Scanziani, 2011, Mullner et al., 2015). Thereby, dendrite-targeting interneurons may even be able

to control the action potential output in an all-or-none manner (Buzsaki et al., 1996, Takahashi and Magee, 2009, Lovett-Barron et al., 2012, Muller et al., 2012). The expression pattern of the voltage gated ion channels along the PC dendritic tree and therefore the signal integration mode of dendrites show high degree of cell type specificity and even single cell types can switch between integration modes according to specific inputs (Lavzin et al., 2012, Jia et al., 2014).

In cortical structures most of the incoming inputs arriving from other cortical or subcortical regions is arranged in a layer-specific manner, therefore dendritic branches present in different layers can receive source specific input(s). Dendrite-targeting inhibitory cells, which arborize in specific layers are in the position to control the input and integration mode of PCs in an input source-selective manner. In the neocortex and hippocampus, a large variety of dendrite-targeting inhibitory cells is present to inhibit the distinct dendritic segments of PCs (Somogyi and Klausberger, 2005). Some of the interneurons have axonal arborization restricted to well-defined layers, which receive a specific input. For example, in the hippocampus, oriens-lacunosum moleculare cells restrict their innervation to the layer where the entorhinal and thalamic inputs contact the apical tuft of PCs (Gulyás et al., 1993, McBain et al., 1994). On the other hand, there are dendrite-targeting interneurons, which are less specific for dendritic subregions, like Martinotti cells in the neocortex, which innervate both the apical trunk, oblique dendrites and apical tuft of PCs (Wang et al., 2004). Overall, dendrite-targeting interneurons in the neocortex and hippocampus show a large heterogeneity across cortical regions regarding their layer (and target) specificity and neurochemical marker expression.

However, it should be noted that a recent theoretical study, which investigated the impact of inhibition on local excitatory inputs proposed a concept that the maximal effect of inhibition can be far from the actual site of the synapses (Gidon and Segev, 2012). Based on experimental data these computational modelling studies showed that due to the passive cable properties of dendrites, the centripetal (from distal to proximal) spread of the shunting impact of inhibition is more effective than the centrifugal (from proximal to distal). This implies that distal inhibitory conductances can more effectively dampen excitatory inputs on proximal dendritic regions than locally at their contact sites. Interestingly, they also proposed that this condition holds only if the inhibition

consists of at least three synchronously activated synapses. Importantly, it was also shown, that the distal "off-path" inhibition could inhibit the spread of dendritic calcium spikes from the hotspot to the soma more effectively than the proximal, "on-path" inhibition. I think this modelling data has an extreme importance, if it turns out to be true in real neurons, because it shows that if an IN type targets a PC dendrite region, which receives a specific excitatory input, this does not necessarily imply that the given IN type is the best suited to control that particular input. Therefore, to elucidate the effect of distinct IN populations on PC input processing we need an integrated view, which takes into account the exact inhibitory contact pattern (e.g. the number and location of synapses), the release properties of those synapses, as well as the firing activity and synchronization level of that particular IN population in line with the network activity and the incoming inputs.

1.1.3. Interneuron-selective interneurons

The main target of the majority of local GABAergic interneurons are PCs, although many INs innervate other INs at about the frequency of their occurrence (Gulyás et al., 1993). However, it was described first in the hippocampus and later in many other cortical circuits that there are GABAergic cell types, which preferentially, if not selectively innervate other INs in the local circuits (Acsády et al., 1996, Gulyas et al., 1996, David et al., 2007). Most of the described interneuron-selective interneurons (ISI) in the cortex express the calcium binding protein calretinin and/or the neuropeptide VIP, which can be therefore used as a potential marker for these neurons (although VIP expression is not restricted to this IN group, some other GABAergic cells, e.g. a subpopulation of CCK/CB_1BCs also expresses this protein). ISIs possess rarely branching local axonal tree with irregular bouton distribution. A group of ISIs besides innervating local interneurons, can give rise to long-range projections targeting other cortical or sucbortical areas (Gulyas et al., 2003) (but see (Jinno et al., 2007) for *in vivo* filled cells). Locally, ISIs tend to target predominantly somatostatin or calbindin immunopositive dendrite-targeting interneurons both in the hippocampus and the cortex (Acsády et al., 1996, Pi et al., 2013). By innervating local interneurons, the effect of ISIs on PCs is disinhibitory: it has been shown *in vivo* that upon their activation, local

INs are inhibited, and the activity of PCs is elevated due to the release of their inhibitory input (Pi et al., 2013). Despite their relatively low occurrence their impact on the local networks has been shown to be impressive: although they represent only 1-2% of the local cells, their simultaneous activity can alter the firing of 20% of the cells in a given microcircuit (Pi et al., 2013). The dendrites of these cells are often restricted to specific layers, which receive source specific excitatory inputs (Freund and Buzsáki, 1996). Therefore, by the specific innervation of local interneurons, these cells are in the position to ensure the input specific dendritic disinhibiton of large PC populations.

1.2. Neuronal circuits of the rodent basolateral amygdala involved in fear memory formation

1.2.1. Basic structure of the amygdala and its role in fear memory learning

An approach to understand the cellular mechanisms of cortical learning processes is to investigate model networks, which have well-defined roles in specific learning tasks. One of the most investigated learning paradigm is the classical Pavlovian conditioned fear learning, where the subject learns to associate a neutral stimulus (conditioned stimulus-CS) with a noxious stimulus (unconditioned stimulus, US). Fear conditioning is a relatively easily inducible, reliable memory test, which makes it an excellent model for studying the cellular mechanisms of memory formation. The amygdaloid complex is a medial temporal lobe structure, which has a central role in emotional processing (Aggleton, 1993, Scott et al., 1997). This brain region has been proved to be essential for learning the emotional significance of a stimulus in the environment, recognizing emotions on faces, especially fear and anger, and has a dynamic role in interpreting the emotions during social interactions (Phelps and LeDoux, 2005, Adolphs, 2010). Abnormal development and activity of the amygdala is associated with various mental disorders e.g. autism, Williams syndrome, social phobia and epilepsy (Schumann et al., 2011). In general, in these disorders the hyperactivity of the amygdala leads to increased anxiety states and impairment of social interactions (Schumann et al., 2011). It has been proved that this region is indispensable for

learning, storage and retrieval of conditioned fear and extinction memories (Armony et al., 1995, Herry et al., 2008, Pape and Pare, 2010). To understand the cellular mechanisms of emotional information processing in this region in health and disease, it is necessary to uncover the organization of the local connectivity and the features of synaptic communication between the neural elements.

The amygdaloid complex comprises different nuclei, which can be divided into three main groups based on their structure, main input sources and developmental origin (Sah et al., 2003) (Fig. 1A). (I) The basolateral amygdala complex (or deep cortical nuclei) has a cortex-like network structure, shares its developmental origin with cortical structures and it is composed of several nuclei: the lateral (LA), basal(BA)(or also called basolateral; BLA) and the accessory basal amygdala nucleus (AB)(or basomedial amygdala (BMA). The LA is traditionally considered as the input site of the amygdala receiving various specific and polymodal sensory inputs from the cortex and thalamus.

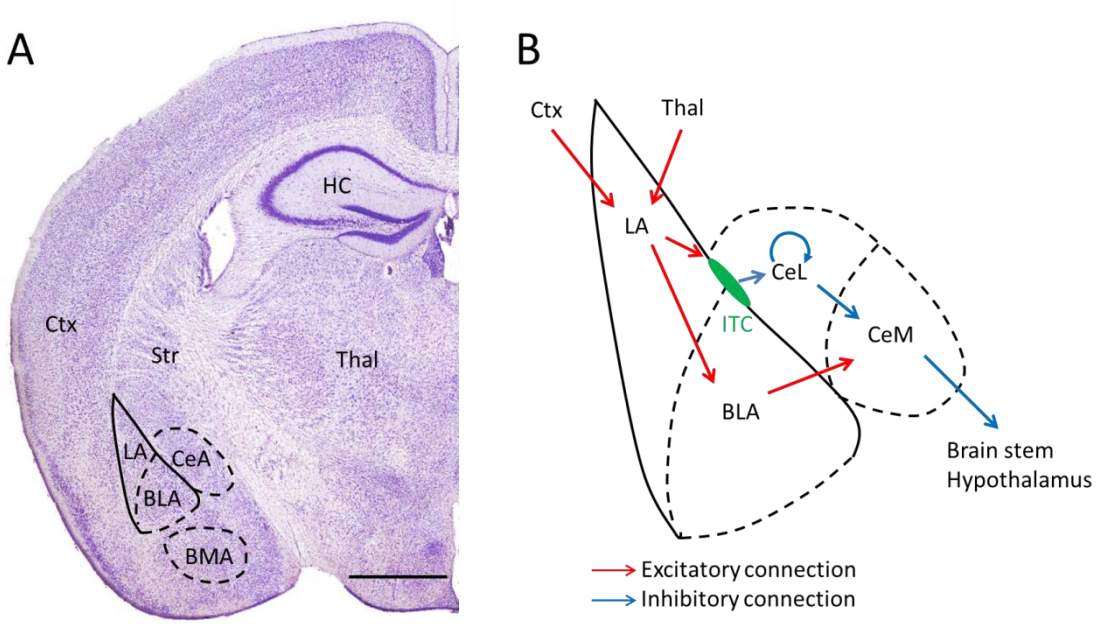

Figure 1. *Location of the amygdala and the main routes of information flow*

A, Location of the main amygdala nuclei in coronal mouse brain section (Bregma -1.94 mm). Adopted from (Paxinos G, 2001). B, The main information flow routes involved in fear memory learning in a schematic amygdala. Predominantly excitatory connections shown in red, inhibitory connections in blue. BLA: basolateral amygdala, BMA: basomedial amygdala, CeA: central amygdala, Ctx: cortex, HC: hippocampus, ITC: intercalated cell mass, LA: lateral amygdala, Str: striatum, Thal: thalamus. Scale bar: 1 mm

(II) The superficial cortical like nuclei, as the name suggests, also have cortical structure and origin, and comprise the nucleus of the lateral olfactory tract, the bed nucleus of the accessory olfactory tract, the anterior and posterior cortical nucleus and the periamygdaloid cortex. The main input of this complex arrives from the olfactory system and other amygdalar nuclei. (III) The central amygdala has a striatum-like network structure, derives from striatal progenitors, and includes the centrolateral (CeL), centromedial (CeM) nuclei, the medial nucleus and the amygdaloid part of the bed nucleus of stria terminalis. The CeM is considered as the main output region of the amygdala by innervating various regions responsible for autonomic responses in the hypothalamus, brain stem, and by modulating the ascending monoaminergic and cholinergic systems. In addition to these three main groups of nuclei, there are separate sets of nuclei that don't belong to any of these three groups: the intercalated cell masses (ITCs), which are small groups of GABAergic cells with striatal origin, located in the capsules surrounding the basolateral nuclei; the anterior amygdala area and the amygdalohippocampal area. Besides the classically described main inputs and outputs, almost all amygdala nuclei receive other cortical and subcortical inputs and give rise to efferent projections to various brain regions, which might further enable the amygdala to integrate, associate and process a large variety of information during emotional memory formation.

The basolateral amygdala complex is proposed to play a crucial role in the fear conditioning learning paradigm. The neutral CS and noxious US are associated in the LA via the integration of the converging multisensory and higher order cortical inputs, and fear learning induces the potentiation of these excitatory synapses (Rogan et al., 1997). Thalamic inputs are proposed to deliver rapid, unprocessed multisensory information to the LA, whereas processed information arrives from visual, auditory or somatosensory cortices (Li et al., 1996, LeDoux, 2000, Szinyei et al., 2000). The integrated information from the LA reaches the effector area of the amygdala, the CeM indirectly, through several routes (Fig. 1B). Projection cells of the LA excite PCs in the BLA, which in turn excite CeM cells. Within the BLA the information is further processed by the interaction of the local interneurons and PCs: local INs can provide feedforward inhibition due to their excitation by LA neurons, or they can be recruited by the activity of BLA PCs thereby forming a feedback inhibitory loop. The second

route of information flow from the LA to the CeM is through the ITC cells, which also produce disinhibition of CeM projection neurons. Numerous studies confirmed that information processing in these parallel routes is involved in fear memory processes (Anglada-Figueroa and Quirk, 2005, Herry et al., 2008, Likhtik et al., 2008, Haubensak et al., 2010, Busti et al., 2011). In the last two decades, information processing in the BLA has received special attention. Much evidence shows that the sophisticated network structures and the plastic changes in the inhibition within the BLA can control fear learning. Local inhibitory circuits in the amygdala have been shown to play major roles in controlling the acquisition, expression and extinction of fear memories (Herry et al., 2010, Tye et al., 2011, Wolff et al., 2014). Similar to other cortical regions, local interneurons of the BLA show large diversity regarding their electrophysiological properties and postsynaptic target distribution, which might endow them with specific role during information processing. Recent advancements in recording techniques enabled the targeted investigation of different IN populations, which significantly facilitates the exploration of the function of diverse INs in fear memory processes. In the next section, I will summarize our recent knowledge on the physiological and anatomical properties of BLA PCs and INs and their proposed role during network activities.

1.2.2. Principal cells of the BLA

As in other cortical networks, PCs in the BLA form about 80% of the neuronal population. Morphologically, they have either triangular pyramidal-like or rounded somata with 15-20 μm diameter and 3-7 rapidly tapering spiny dendrites (McDonald, 1992, Washburn and Moises, 1992). As the amygdala is not a layered structure, the dendrites are not arranged and oriented strictly in one plane, but emerge from the soma at random directions (Faber et al., 2001). However, some PCs have one or two thicker, apical-like dendrites, but the difference in their inputs or electrophysiological properties compared to other dendrites has not been showed yet. According to the presence or absence of an apical-like dendrite, PCs can have pyramidal-cell like or stellate cell-like appearance. However, it is difficult to group the cells into these two types, since they rather form a morphological continuum. As in other cortical structures (Megias et al.,

2001), the glutamatergic synaptic inputs arrive predominantly on their spines or thin dendritic shafts, whereas GABAergic synapses are formed mainly on their somata, AIS and dendritic shafts and spine necks (Carlsen, 1988, McDonald et al., 2002). Their axon emerges from the soma or from a proximal dendrite, and forms local collaterals before leaving the BLA to innervate e.g. the CeA, hippocampus, prefrontal cortex, nucleus accumbens and thalamus. They use glutamate as neurotransmitter and express the type 1 vesicular glutamic acid transporter (VGLUT1), as other cortical projecting cells. These neurons produce broad action potentials, relatively low spontaneous firing rate (0.1-0.3 Hz) and often fire spike bursts (Gaudreau and Pare, 1996, Bienvenu et al., 2012). It has been shown in cats that the membrane potential of PCs intrinsically oscillates at theta frequency *in vivo*, which shapes the cell's firing probability (Lang and Pare, 1997, Pape and Driesang, 1998). Moreover, as shown in rats *in vitro*, large periodic IPSPs arrive onto PCs inhibit and/or synchronize their firing. Interestingly, these periodic IPSPs might be induced by the activity of a small subset of local PCs which excite local INs, suggesting that there might be a subpopulation of PCs, which orchestrates the synchronous activity in local inhibitory networks (Popescu and Pare, 2011). This implies the inhomogeneity in amygdalar PC populations, however, clear morphological or electrophysiological differences between the subgroups in this study could not be shown. Another source of inhomogeneity in BLA PCs is the difference in the input and projection of individual cells. It has been shown that there are at least two different PC populations, which might have different roles in amygdala functions: one group, receiving information from the hippocampus is involved in fear memory formation, whereas another, receiving input and projecting to the medial prefrontal cortex is implicated in fear extinction. In summary, although PCs are usually considered as a homogenous cell population, there is emerging evidence that separate sub-networks can be present, which may have different functions in amygdala processes.

1.2.3. Interneurons of the BLA: types, firing during network activity and role in network function

GABAergic interneurons form about 20% of the BLA cell population (McDonald, 1985, McDonald and Augustine, 1993, Sah et al., 2003). The first

approaches to classify BLA INs were based on the expression of calcium binding proteins or neuropeptides. Early studies described two main non-overlapping groups: 50% of the INs expresses calbindin (Calb) and ~20% calretinin (CR) (Kemppainen and Pitkanen, 2000, McDonald and Mascagni, 2001). These groups can be further divided by the expression of PV, VIP, CCK and somatostatin (SOM). Immunocytochemical analysis using electron microscopy showed that axon terminals containing different markers contact specific compartments of BLA PCs: e.g. PV+ terminals often form synapses with PC somata, large caliber dendrites and axon initial segments, CCK+ terminals contact soma and large caliber dendrites, whereas SOM+ terminals often synapse on small caliber dendrites (Katona et al., 2001, McDonald and Betette, 2001, Muller et al., 2006, 2007a). These data imply that INs expressing a specific combination of markers might restrict their input to specific compartments on the PCs. As mentioned in the previous sections, INs targeting distinct subcellular compartments of PCs may have different effects on their activity, therefore a functional approach to classify INs can be based on their postsynaptic target distribution.

However, to precisely define the target distribution of different IN groups, it is necessary to label individual INs from each group and analyse their targets, preferably at the electron microscopic level. This can be achieved by various methods. Golgi staining can label the dendritic and axonal processes of few random cells in the preparation, which can be analyzed at the light and electron microscopic levels. This technique, however, doesn't allow targeted labeling of specific cell types. In addition, cells can be labeled after single cell *in vivo* recordings, which enables the investigation of multiple features of the recorded neuron: basic electrophysiological properties, which can be informative about the type of the cell (e.g., shape of the action potential, resting membrane potential, passive and active membrane properties), it's firing pattern upon stimulation and during induced or spontaneous network activity. Importantly, the labeled cells can be processed for various anatomical investigations: multiple immunolabeling with fluorescent microscopy, reconstruction of the cell's morphology and analysis of its targets at the electron microscopical level. This method, therefore, is perfectly suited to collect information for the classification of interneurons, however, it has several drawbacks. First, these experiments are very time consuming, and in an ideal case, only one cell is labeled in every animal, therefore the data productivity of

this method is very slow, and collecting statistically sufficient data to characterize cell groups can take years. Second, the targeted recordings from specific cell groups is still difficult, although there are several methods to identify cells *in vivo* based on the shape of the action potentials or with optogenetic tagging of specific interneuron types. These disadvantages can be overcome by labeling single cells in *in vitro* slice preparations. Various transgenic animal strains exist, in which different IN types are labeled with fluorescent proteins due to their controlled expression by cell type specific protein promoters. By using an *in vitro* recording setup equipped with a fluorescent microscope, the different IN types can be targeted very specifically and effectively. The labeled cells then can be processed for the same anatomical investigations as the *in vivo* filled cells. Naturally, while using this technique, one always has to keep in mind that due to the slicing procedure and the artificial environment, the electrophysiological and anatomical properties of the cells can change, therefore the interpretation of the results should be done with caution and their *in vivo* confirmation is desired. Based on the data obtained with these methods in the last two decades, local interneurons in the BLA can be functionally categorized into (at least) seven groups.

Axo-axonic cells (AACs)

The first study, which suggested the existence of AACs in the BLA described Golgi stained spine-free neurons forming characteristic cartridges presumably surrounding axon initial segments (McDonald, 1982). Later, electron microscopic studies revealed that axon terminals immunostained for the calcium binding protein PV formed symmetrical synapses on the AIS of PCs in the BLA (Muller et al., 2006), suggesting the presence of AACs in this cortical region. A recent *in vivo* study obtained in the rat (Bienvenu et al., 2012) finally undoubtedly proved that there is a GABAergic interneuron type in the BLA specialized to target exclusively AISs. In this study they showed that AACs are PV+ and Calb-, and can fire action potentials with narrow half width at high frequencies. Despite the recognition of AACs in the BLA, it is still uncertain how effective the regulation of PC firing by single AACs is, and how many presynaptic AACs have to discharge synchronously to veto PC action potential generation. In addition, it is also unknown that how the distribution of AAC output synapses along the AIS relates to the action potential generation site. These basic

questions are unanswered not only in the BLA but in other cortical regions as well. The above mentioned *in vivo* study also demonstrated that AACs in the BLA can be effectively activated by noxious stimulation, which suggests their role in regulating PC spiking during fear-memory related information processing. Therefore, the investigation of how this cell type is embedded in the local networks and its effect on the output of the BLA can help us to understand the mechanisms of fear memory processes in health and disease.

Parvalbumin-positive basket cells (PVBCs)

PV+ terminals in the BLA were described to surround PC somata forming characteristic, basket like structures, which indicated the presence of basket cells in the BLA (McDonald and Betette, 2001). Numerous studies investigated the electrophysiological properties of PV+ cells in the BLA. These studies showed that PV+ cells can generate action potentials with narrow width at high frequencies with little or no accommodation, and can be clustered into groups based on their firing patterns (Rainnie et al., 2006, Woodruff and Sah, 2007b). An *in vitro* study showed that a population of PV+ cells in the BLA is capable to inhibit PC spiking, and synchronize the firing of their postsynaptic partners (Woodruff and Sah, 2007a). Moreover, a recent study has proved that optogenetic manipulation of PV+ cells can effectively modulate the acquisition of fear memories in an auditory fear learning task (Wolff et al., 2014). Unfortunately, in these studies the various PV+ IN types (e.g. AACs, BCs and other PV+ GABAergic cells) were not identified anatomically, thus the correlation between the electrophysiological parameters characterizing a subgroup and cell type specificity is not clarified yet. Recently, it has been shown that the firing of anatomically identified PVBCs *in vivo* were found to be weakly coupled to theta oscillation recorded in dorsal CA1 or some of these cells' firing was not even coupled to this hippocampal rhythm. Interestingly, this cell type displayed heterogeneous and generally moderate responses to noxious stimuli (Bienvenu et al., 2012). Thus, their role -instead of pacing theta rhythm in the BLA as speculated previously (Ehrlich et al., 2009)- might be the tonic inhibition of PCs and setting their baseline activity level, i.e. the gain control. The synaptic output of PVBCs might contribute to the source of large amplitude IPSPs recorded in PCs during both spontaneous and evoked synaptic activity, which inhibitory

input can set the characteristic low firing rate of PCs in the BLA (Lang and Pare, 1997). Similarly to AACs, there are many questions still unanswered about the effectiveness of the inhibition provided by individual PVBCs, and that how individual cells can influence the timing of PC firing. Moreover, the basic anatomical features of individual PVBC-PC connections are also unknown.

Cholecystokinin and type 1 cannabinoid receptor-positive basket cells (CCK/CB_1BCs)

Early studies described that CCK-positive GABAergic neurons in the BLA can be divided into two groups according to the size of the cell body (McDonald and Pearson, 1989). Those cells, which have small soma size, lack the CB_1 receptor immunolabeling from their cell body and are proposed to innervate distal dendrites of PCs, whereas cells with large soma express CB_1 receptor in their terminals and often form basket-like multiple contacts around PC somata (Katona et al., 2001, Mascagni and McDonald, 2003), therefore called CCK/CB_1 basket cells. CCK+ cells in the rat colocalize with Calb, but not with VIP and calretinin (Mascagni and McDonald, 2003). *In vitro* this cell type discharges relatively broad action potentials, can have marked AHP and regular spiking or adapting firing pattern. A recent study showed that in rats large CCK cells can be further divided into two subgroups based on their electrophysiological properties, although the functional difference between these groups has not been shown (Jasnow et al., 2009). Unfortunately, there is no *in vivo* data about the firing activities of amygdalar CCK/CB_1BCs during hippocampal theta oscillation or noxious stimuli, probably because the shape of their action potential is similar to PCs, thus they usually are not separated from PCs during *in vivo* recordings. However, the role of CCK/CB_1BCs in the normal function of the amygdala in fear memory processes can be crucial, as their synapses can undergo CB_1 receptor dependent depolarization-induced suppression of inhibition (DSI) (Zhu and Lovinger, 2005) and endocannabinoid-mediated long-term depression (Marsicano et al., 2002), which has been shown to be necessary for the extinction of fear memories (Chhatwal et al., 2009). In addition, a population of CCK/CB_1BCs expresses 5HT-3 type serotonin receptor (Muller et al., 2007b) suggesting that 5-HT may exert its anxiolytic effects by modulation of the transmitter release from this cell type. To assess their role in the

amygdalar network functions, it is necessary to unravel the basic properties of their synapses, their ability to control local principal cells and the underlying anatomical structures of their connections.

Dendrite-targeting INs

Previous studies described that SOM-positive terminals often form symmetrical synapses on thin caliber dendrites and spines. Besides these compartments, terminals containing SOM also target perikarya and large caliber dendrites, but in a much less extent (37% on thin dendrites, 51% on spines, 4% on perikarya and 6% on thick dendrites) (Muller et al., 2007a). Therefore, SOM+ cells, which represent 11-18% of the GABAergic neurons of the BLA, are proposed to be dendrite-targeting interneurons (McDonald and Mascagni, 2002). The majority (90%) of SOM+ cells are Calb-positive, but does not express PV or calretinin. A recent publication using optogenetic manipulation showed a crucial role of SOM+ dendrite targeting interneurons in fear learning (Wolff et al., 2014).

A detailed study using electron microscopy on the inhibitory input of BLA PCs showed that about half of the symmetrical synapses arriving onto the dendritic shafts, and occasionally onto spines is PV-immunopositive (Muller et al., 2006), which suggested the presence of another, PV+ dendrite-targeting IN type in the BLA. There has been only 3 cells described in the literature, labelled *in vivo*, which has proved to be selectively targeting dendrites (Bienvenu et al., 2012). Like PVBCs, these cells were Calb+, however their behavior was remarkably different from the perisomatic region-targeting interneurons: their firing was deeply modulated by hippocampal theta oscillations, which might enable this cell type to modulate the integration of incoming dendritic inputs and synaptic plasticity processes in accordance with the ongoing oscillation. These cells, however, did not contain SOM, which clearly separates them from the above mentioned dendrite-targeting cell group.

Unfortunately there is no data yet about the role of Calb+ dendrite-targeting cells in fear learning, therefore there is no information whether the two major dendrite-targeting cells play different, maybe complementary role in BLA network activities.

AStria cells

A special PV+ cell type was recently described in the BLA (Bienvenu et al., 2012), which -besides targeting the soma and dendrites of local PCs- project out from the BLA to the amygdalostriatal transition area, where they innervate the soma and dendrites of medium spiny neurons. These cells have dense axonal arbor and profoundly branching, very tortuous dendrites. Interestingly, and in contrast to other BLA INs, these cells are robustly inhibited by noxious stimuli. These properties clearly separate them from other PV+INs, but their role in BLA network function is presently unknown.

Neurogliaform cells

Most of the INs mentioned so far are known to provide fast, phasic GABAergic inputs, however, there is a special interneuron type, called the neurogliaform cell (NGFC), which provides 5-10 times slower inhibition on the PCs than the above mentioned INs (Manko et al., 2012). NGFCs in the BLA are neuropeptide Y (NPY) and SOM positive, and likely express nitric oxide synthase (McDonald et al., 1993). NGFCs target somata and dendrites mainly with non-synaptic juntions (77%), and only the minority of their terminals form synapses (23%) (Manko et al., 2012). Like PV- and Calb-positive dendrite-targeting INs, the firing of NGFCs is strongly coupled to the hippocampal theta oscillation. This two cell types together can provide a rhythmic inhibition on the dendrites with complementary temporal profiles, which might be necessary for the coordination of hippocampal-amygdala theta oscillations emerging during fear memory retrieval (Seidenbecher et al., 2003).

Interneuron selective interneurons

As already mentioned, VIP expressing interneurons in the hippocampus or in the neocortex selectively inhibit other IN types, thereby providing a disinhibitory effect on local PCs. The presence of VIP+ cells which target local INs has been described in the BLA circuits, however, their interneuron target selectivity has not been proven yet (Muller et al., 2003). However, there is evidence showing that a strong interneuron specific inhibitory source exists in the BLA, which provide phasic inhibition on local PV+ and SOM+ cells during auditory fear conditioning. The suppression of interneuron firing leads to a phasic disinhibition of the entire somatodendritic domain of PCs in the

BLA (Wolff et al., 2014). Possible candidates for this disinhibitory source are local VIP cells, in analogy to the auditory cortex (Pi et al., 2013) however this theory in the BLA is not proven yet.

1.2.4. Wiring properties of the neural networks in the BLA, emerging questions

To understand the mechanisms of different network activities in health and disease, a basic step is to describe the elements of the neural ensembles, the logic of their connections and their effects on each other. To this end, besides describing the properties of connected neuronal pairs, it also necessary to estimate the convergence and divergence of the connections established by different IN types to be able to predict their impact at the network level. In the BLA networks, many basic fundamental questions regarding the build-up of the network are still unanswered. How many PCs are controlled by single INs? How many INs converge on single PCs? What is the ratio of the inhibitory inputs on single PCs originating from the different IN types? How effectively can INs control PC firing? During my PhD studies, I described the basic electrophysiological and anatomical properties of the perisomatic inhibitory inputs of BLA PCs, the functional effects of the inhibition on their firing, and the organization of the different perisomatic inputs in the BLA networks.

2. Objectives

The main goal of our studies was to investigate the organization and impact of the perisomatic inputs on the PC spiking in the BLA. Therefore, we focused on three main topics with the following specific questions:

I. To uncover the sources of the perisomatic inputs and the ratio of the innervation emerging from different cell types.

- What is the extent of the perisomatic region along the dendrites of BLA PCs?
- What is the density of inhibitory inputs arriving to this region?
- Which IN types give rise to the perisomatic GABAergic inputs and what is the ratio of their innervation?
- How many PCs are controlled by single INs? How many INs converge on individual PCs?

II. To determine the electrophysiological and morphological properties of the AAC inputs on the AIS and its effects on PC firing activity.

- What are the effects on the membrane potential of AAC inputs on BLA PCs?
- How efficiently can this input shape the spiking activity of PCs?
- What is the spatial distribution of the GABAergic inputs along the AIS and how it relates to the site of the action potential generation?

III. To compare the electrophysiological and morphological properties of the inputs of PCs originating from basket cells and their effects on PC firing activity.

- What electrophysiological properties characterize the connections established by CCK/CB_1BCs and PVBCs?
- Is there any difference in the impact of their inputs on PC spike generation?
- What is the distribution of the basket cell synapses along the somato-dendritic axis of PCs?

3. Methods

3.1. Electrophysiological experiments

3.1.1. Experimental animals and slice preparation

All experiments were approved by the Committee for the Scientific Ethics of Animal Research (22.1/360/3/2011) and were carried out according to the guidelines of the institutional ethical code and the Hungarian Act of Animal Care and Experimentation (1998. XXVIII. section 243/1998, renewed in 40/2013.). For recording AACs and PVBCs, transgenic mice of both sex (P18-24) expressing enhanced green fluorescent protein (eGFP) under the control of the PV promoter (Meyer et al., 2002) were used. For targeted patching of CCK/CB_1BCs, transgenic mice expressing red fluorescent protein under the control of cholecystokinin (CCK) promoter were used (BAC-CCK-DsRed) (Mate et al., 2013). Mice were deeply anaesthetised with isoflurane and decapitated. The brain was quickly removed and placed into ice-cold cutting solution containing (in mM): 252 sucrose, 2.5 KCl, 26 $NaHCO_3$, 0.5 $CaCl_2$, 5 $MgCl_2$, 1.25 NaH_2PO_4, 10 glucose, bubbled with 95% O_2/5 % CO_2 (carbogen gas). Horizontal slices of 200 μm thickness containing the basolateral amygdala were prepared with a Leica VT1000S or VT1200S Vibratome (Wetzlar, Germany), and kept in an interface-type holding chamber containing artificial cerebrospinal fluid (ACSF) at 36 ºC that gradually cooled down to room temperature. ACSF contained (in mM) 126 NaCl, 2.5 KCl, 1.25 NaH_2PO_4, 2 $MgCl_2$, 2 $CaCl_2$, 26 $NaHCO_3$, and 10 glucose, bubbled with carbogen gas.

3.1.2. Whole-cell recordings

After at least one hour of incubation, slices were transferred individually into a submerged type of recording chamber perfused with ACSF at 32±2 ºC with a flow rate of 2-3 ml/min. Recordings were performed under visual guidance using differential interference contrast microscopy (Olympus BX61W). EGFP or DsRed in cells was excited by a UV lamp, and the fluorescence was visualized by a CCD camera (Hamamatsu Photonics, Japan). Patch pipettes were pulled from borosilicate glass capillaries with inner filament (Hilgenberg, Germany) using a DMZ-Universal Puller

(Zeitz-Instrumente GmbH, Germany). For somatic whole-cell recordings, pipettes with 0.188 mm wall thickness were used and had a resistance of around 3-5 MΩ when filled with the intrapipette solution. K-gluconate-based intrapipette solution used in all recordings contained (in mM): 110 K-gluconate, 4 NaCl, 2 Mg-ATP, 20 HEPES, 0,1 EGTA, 0.3 GTP (sodium salt) and 10 phosphocreatine adjusted to pH 7.3 using KOH and with an osmolarity of 290 mOsm/L. For recording the presynaptic interneurons 10 mM GABA and 0.2% biocytin were added, whereas for the postsynaptic PC 100 μM Alexa Fluor 488 hydrazide sodium salt (Invitrogen) was included. Recordings were made with a Multiclamp 700B amplifier (Molecular Devices, Foster City, CA, USA), low-pass filtered at 2 kHz, digitized at 10 kHz and recorded with in-house data acquisition and stimulus software (Stimulog, courtesy of Prof. Zoltán Nusser, Institute of Experimental Medicine, Hungarian Academy of Sciences, Budapest, Hungary). Recordings were analyzed with EVAN 1.3 (courtesy of Prof. Istvan Mody, Department of Neurology and Physiology, UCLA, CA), the in-house analysis software SPIN 1.0.1 (courtesy of Prof. Zoltán Nusser) and Origin 8.6 and 9.2 (Northampton, MA). Recordings were not corrected for junction potential. To record the firing characteristics, cells were injected with 800-ms-long hyperpolarizing and depolarizing square current pulses with increasing amplitudes from 10 to 600 pA. PC identity was characterized by the broad action potential waveform, accommodating firing pattern and slow afterhyperpolarzing current as well as the post hoc morphological analysis of their spiny dendrites. For recording postsynaptic inhibitory currents (IPSCs), the presynaptic IN was held around a membrane potential of -65 mV in current clamp mode, and stimulated by brief square current pulses (2 ms, 1.5–2 nA) to evoke action potentials, and the PC was clamped at a holding potential of -40 mV. Series resistance was monitored (range: 6-20 MΩ) and compensated by 65%. To record postsynaptic inhibitory potentials (IPSPs), the presynaptic cell was stimulated in the same way, and the postsynaptic PC was held in current clamp mode around -55 mV. Bridge balance was adjusted throughout the recordings. The kinetic properties of IPSCs and IPSPs were analysed on averaged events that were calculated with excluding the transmission failures. The latency of synaptic transmission was calculated by subtracting the time of the action potential peaks from the onset of the postsynaptic currents.

To test the ability of INs to inhibit PC firing, theta frequency (3.53 Hz) sinusoidal current pulses with peak-to-peak amplitudes of 30 pA and 50 pA were injected into the postsynaptic PC. The membrane potential of PCs was set (approximately around -55 mV) such to evoke a spike at the peak of the sinusoidal current pulses with the amplitude of 50 pA, but not of 30 pA. This adjustment maintained the membrane potential of PCs near the spiking threshold. One trial consisted of 7 sinusoidal waves (5x50pA and 2x30pA), repeated 10-20 times in each pair. Three action potentials at 30 Hz were evoked in the interneuron by brief square current pulses (2 ms, 1.5–2 nA) before the 4th sinusoidal wave (50 pA) in each trial. To calculate the reduction in firing probability, the firing probability of PCs under control conditions was calculated from the average of the responses to 50 pA currents (1st, 3rd, 5th and 6th sinusoidal wave), which was compared to that obtained during the 4th cycle. To evoke firing in PCs by synaptic input, electrical stimulation of external capsule fibers was delivered via a theta glass electrode filled with ACSF using a Supertech timer and isolator (Supertech Ltd., Pécs, Hungary).

3.1.3. Perforated patch recordings

For perforated patch recordings 100 mg/ml gramicidin (Sigma) stock solution was prepared in DMSO daily and kept at 4 ºC. Before the recordings gramicidin stock solution was diluted to the concentration of 100 μg/ml in the same K-gluconate based intrapipette solution as used for whole-cell recordings, containing (in mM): 110 K-gluconate, 4 NaCl, 2 Mg-ATP, 20 HEPES, 0,1 EGTA, 0.3 GTP (sodium salt) and 10 phosphocreatine adjusted to pH 7.3 using KOH and with an osmolarity of 290 mOsm/L. In addition, the solution contained 100 μM Alexa 488 hydrazide sodium salt and 1 mM QX-314 (Sigma). The solution was sonicated for a short period of time in an ultrasound bath several times before use. Pipettes with 0.188 mm wall thickness were used and had a resistance of around 3-5 MΩ when filled with the intrapipette solution. The tip of the pipette was filled with gramicidin free solution and then backfilled with the gramicidin containing intrapipette solution. The series resistance was monitored throughout the experiment, and recordings were started when the resistance fell below 100 MΩ. Pipette capacitance was neutralized and bridge balance was carefully adjusted throughout the recordings. Patch rupture was detected by i) the inability to evoke action potentials with

depolarizing current steps (the consequence of the Na+/K+ channel blocker QX-314 diffusion into the cell), ii) with the penetration of Alexa 488 dye into the cell, or iii) sudden drop in the access resistance, and in such cases the experiment was terminated (Fig. 2).

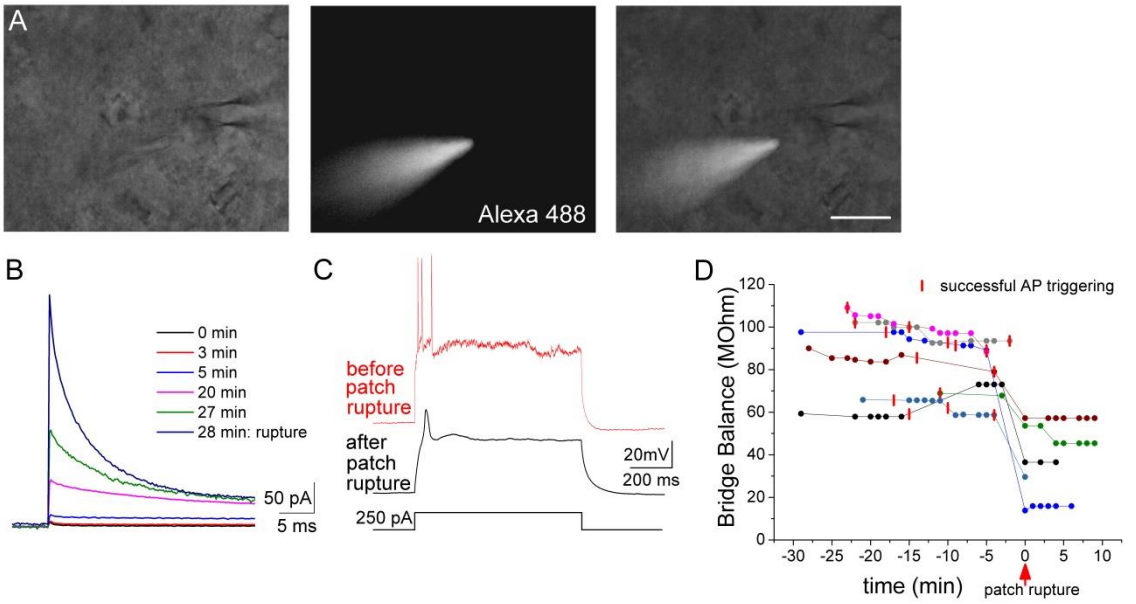

Figure 2: *The three approaches to test the integrity of the perforated patch configuration* A, Presence of the Alexa 488 in the recording pipette but not inside the cell was monitored throughout the recordings. B, The current changes in response to a depolarizing 5mV pulse (seal test) during a representative recording. Note the sudden increase in the current after the rupture of the perforated patch induced by negative pressure application. C, The cell capability to produce action potential in response to an intracellular current pulse injection was also tested throughout the recordings. Note the inability to evoke firing after the rupture of the patch, in a consequence of the QX-314 diffusion into the cell, a drug, which blocks voltage gated sodium and potassium channels applied in the intrapipette solution for the perforated patch recordings. D, Changes in the bridge balance values during the recordings, indicating the series resistance in current clamp mode. Each color represents a recorded pair (n=7), each dot represents a current clamp recording preceded by an Alexa 488 test (see A). Red vertical lines represent a successful test for the firing ability of the recorded cell (see C). In two cases (magenta and grey) the cell didn't survive the rupture of the patch by negative pressure application. Scale (A): 20 µm

To estimate the reversal potential of the evoked postsynaptic responses (Fig.7 E-G and Fig. 12 E-G), we plotted the area (integral) of IPSPs as a function of membrane potential and obtained the value, where the second order polynomial fit crossed the x

axis. For comparing the reversal potential of IPSPs in perforated patch and whole-cell mode, we compared the responses from the same presynaptic IN onto a PC recorded in perforated patch mode and a neighboring PC recorded in whole-cell mode.

3.1.4. Extracellular axon and whole-cell axon bleb recordings

In experiments, which aimed to define the action potential initiation site, PCs were recorded at the soma with K-gluconate based intrapipette solution containing 100 μM Alexa 488 and the dye filled axon was visualized with a CCD camera. If the axon was cut, the identified axon bleb was patched with a pipette filled with the same solution (0.315 mm wall thickness, ~12 MΩ open tip resistance). Access resistance was 10-25 MΩ for somatic recordings and 30-60 MΩ for bleb recordings. Pipette capacitance was neutralized and bridge balance was adjusted throughout the recordings. If the axon of the dye filled cell was intact and accessible for recordings, an Alexa 488-coated pipette (0.315 mm wall thickness, ~7 MΩ open tip resistance, coating achieved with heating) was filled with ACSF for extracellular action potential recordings in loose-patch mode visually guided by the Alexa 488 signal. Action potentials were evoked by somatic square current pulse injections (10 ms long, 0.5-2 nA at 0.5 Hz). Recordings were low-pass filtered at 20 kHz, digitally sampled at 100 kHz and analyzed with EVAN 1.3 and Clampfit software. For the comparison of the action potential timing at two recording sites, the peak time of the first order derivative was calculated for the action potentials recorded in whole-cell mode (both for somatic and bleb recordings), and the peak time of the voltage deflection was calculated for the action potentials recorded extracellularly. Axonal recording distances were calculated based on the CCD camera images and post hoc 3D reconstruction of the biocytin and Alexa dye-labeled cells with the aid of the Neurolucida 10.53 software (MBF Bioscience). To determine the site of the action potential generation, the nadir point of the maximal delay between the two recording sites was calculated using a bilinear fit with 95% confidence intervals (Matlab software, MathWorks Natick, MA, USA).

3.1.5. Morphological analysis of the recorded pairs

After recordings slices were fixed in 4 % paraformaldehyde (PFA) in 0.1 M phosphate buffer (PB; pH 7.4) overnight. For those slices which were processed for

electron microscopy the fixative solution contained in addition 0.05% glutaraldehyde and 15% picric acid. Slices were then washed out with PB several times, and incubated in cryoprotective solution (30% sucrose in 0.1 M PB) for 2 hrs, and then freeze-thawed three times above liquid nitrogen. INs were visualized using Alexa 594 or Alexa 647-conjugated streptavidin (1:1000, Invitrogen, Carlsbad, CA, USA), whereas PCs were labeled using rabbit anti-Alexa 488 primary antibody (1:1000, Invitrogen) and Alexa 488-conjugated goat anti-rabbit secondary antibody (1:200, Invitrogen). Confocal images were collected using a Nikon A1R microscope fitted with an oil immersion apochromatic lens (CFI Plan Apo VC60X Oil, N.A. 1.40; z step size: 0.8 μm, xy: 0.42 μm/pixel). For the analysis of the connectivity rate between the cells, only those pairs were included, where the axonal arbors of the presynaptic cells were relatively intact. Based on the confocal images the postsynaptic PC was fully reconstructed in 3D with the Neurolucida 10.53 software and the putative synaptic sites from the presynaptic IN were marked. For the detailed analysis of the contacts, higher magnification images were taken with the same microscope (z step size: 0.13 μm, xy: 0.08 μm/pixel). Only those recordings were used for morphological analysis where a single presynaptic interneuron was labeled in the slice. The distribution analysis of the synapses was performed with the Neurolucida Explorer software. Values were corrected for shrinkage and flattening of the tissue (x and y axis: no correction, z axis: 1.7). Four AAC-PC, three PVBC-PC and four CCK/CB_1BC-PC pairs were further processed for electron microscopic studies to confirm the presence of synaptic contacts. Biocytin in INs was visualized using avidin-biotinylated horseradish peroxidase complex reaction (ABC; Vector Laboratories, Burlingame, CA, USA) with nickel-intensified 3,3-diaminobenzidine (DAB-Ni) giving a dark brown reaction product. Alexa 488 in PCs was revealed with biotin-conjugated goat anti-rabbit antibody, with ABC reaction visualized by (3,3-diaminobenzidine) DAB producing a brown end-product. Sections were then postfixed in 0.5% OsO_4, treated in 10% uranyl acetate, dehydrated in a graded series of ethanol, and embedded in epoxy resin (Durcupan; Sigma). Ultrathin sections of a 60 nm thickness were cut, and contact sites, where the presynaptic axon made close appositions with the identified PC or with randomly sampled targets, were analysed in serial sections.

In those experiments where the Alexa 488 labeling in PCs was insufficient for contact site analysis, cell type identity of PV cells (AAC vs. PVBC) was confirmed with ankyrin G staining (Gulyás et al., 2010). Briefly, slices were re-sectioned to 40 μm thickness, and incubated in mouse anti-ankyrin G (1:100-1:500 Santa Cruz Biotechnology, Santa Cruz, CA) primary antibody followed by incubation in Alexa 594-conjugated goat anti-mouse secondary antibody (1:200, Invitrogen) after several washing steps.

3.2. Anatomical experiments

3.2.1. Principal cell reconstructions and analysis of the inputs on the perisomatic region in vitro

Whole-cell recordings using K-gluconate based intrapipette solution containing biocytin were obtained in PCs to visualize them for anatomical investigations. Similarly to interneurons, Alexa 647-coupled streptavidin was used to make visible the fine details of the neurons in the entire slice. To quantify excitatory inputs VGLUT1, VGLUT2 and bassoon immunostainings were carried out using a mixture of rabbit anti-VGLUT1 (1:10.000, Synaptic systems), guinea pig anti-VGLUT2 (1:1000, Sysy) and mouse anti-bassoon (1:3000, Abcam) primary antibodies visualized by donkey anti-rabbit IgG coupled with DyLight 405, donkey anti-guinea pig IgG-A488 and donkey anti-mouse-Cy3 secondary antibodies (all 1:500, Jackson ImmunoResearch Laboratories Inc., West Grove, PA). To assess the GABAergic inputs of these cells, we carried out immunostainings using guinea pig anti-VGAT IgG (Frontier Institute Co.Ltd 1:1000) and goat anti-panGAD IgG (Frontier Institute Co.Ltd 1:500) primary antibodies, visualized by Cy3 (donkey anti-guinea pig and donkey anti-goat, 1:200, Jackson). To label Kv2.1 we used mouse anti-Kv2.1 (1: 1000, 75-014, Neuromab), which was visualized with an Alexa 488-conjugated donkey anti-mouse antibody (1:500, Jackson). Using the 3D confocal images taken from the labeled cells, the soma surface of recorded cells and their dendritic trees decorated with spines were reconstructed with Neurolucida 10.53 software. The putative GABAergic inputs onto the cells were reconstructed by labeling the sites where the presynaptic boutons (i.e. panGAD/VGAT-containing profiles) faced the soma or dendrite of the biocytin filled

cell. The border of the Kv2.1 staining on the dendrites of biocytin filled PCs was also marked. In the same material, GABAergic inputs of the additional cells immunostained for Kv2.1 were also reconstructed. Values were corrected for shrinkage and flattening of the tissue (x,y: no correction, z:1.7). Shrinkage correction factors in the x and y axes were calculated by comparing the distance between characteristic landmarks in the slice (e.g., external capsule, anterior commissure, optic tract, alveus) immediately after slice preparation and after mounting the slices (n=10) using an epifluorescent microscope (Zeiss, AxioImager Z1). Z-axis shrinkage correction factor was calculated by comparing the vibratome-cut slice thickness and the thickness measured with a confocal microscope (A1R, Nikon) after mounting.

3.2.2. Evaluation of GABAergic inputs on the perisomatic region of principal cells in vivo

C57Bl/6J mice were deeply anesthetized and transcardially perfused with either 2.5% acrolein in 4% PFA (pH 6.8) in 0.1M PB for 10min followed by post-perfusion fixation in 4% PFA in 0.1M PB for 1.5 hours (3 mice) or with 2% PFA in 0.2MNa-acetate buffer (pH 6.0) for 20min without postfixation (2 mice). For all cases, the part of the brain containing the amygdala was sectioned into 40μm-thick sections, which were soaked in 30% sucrose overnight and the sections were kept in cryoprotectant anti-freeze solution consisting of sucrose, ethylene glycol, distilled H_2O, and phosphate-buffered saline (3:3:3.1 volume ratio) at –20°C until further processing was initiated (Watson et al., 1986). Prior to immunostaining the cryoprotectant was washed out in 0.1 M PB. Brains of three additional C57Bl/6J mice were quickly removed from the skull under deep anesthesia and a block containing the amygdala region was dissected followed by immersion into a fixative containing 2% PFA in 0.1 M PB for 2 hours. After fixation the blocks were rinsed several times in 0.1 M PB and re-sectioned to 40 μm thickness.

For the analysis of the GABAergic inputs onto the soma and proximal dendrites, the sections were blocked in 10% Normal Donkey Serum (NDS, Vector Laboratories, Burlingame, CA) in Tris-buffered saline (TBS, pH 7.4) followed by incubation in a mixture of primary antisera of rabbit anti-CB_1 (1:1000, Cayman Chemical Company, Ann Arbor, MI), guinea pig anti-VGAT (1:1000, Frontier Institute Co. Ltd., Sapporo,

Japan), goat anti-PV (1:5000) and mouse anti-Kv2.1 (1:1000, 75-014, Neuromab) diluted in Tris-Buffered Saline (TBS) containing 1% NDS and 0.1% Triton X-100 for three days at 4ºC. Following several washes in TBS, the sections were incubated in a mixture of secondary antisera of DyLight 405-conjugated donkey anti-rabbit, Alexa 488-conjugated donkey anti-guinea pig, Cy3-conjugated donkey anti-mouse, and Alexa 647-conjugated donkey anti-goat (all 1:500, Jackson ImmunoResearch Laboratories Inc.). To determine the calbindin content of PV- and CB_1-immunoreactive varicosities on the perisomatic region, sections were incubated in a mixture of primary antisera of guinea pig anti-CB_1 (1:1000, Frontier Institute Co. Ltd), rabbit anti-Calb (1:5000, CB-38a, Swant) and mouse anti-Kv2.1 or in a mixture of antisera of guinea pig anti-PV (1:10000, Sysy), rabbit anti-Calb (1:5000, CB-38a, Swant) and mouse anti-Kv2.1 diluted in Tris-Buffered Saline (TBS) containing 1% NDS and 0.1% Triton X-100 for three days at 4ºC. Following several washes in TBS, the sections were incubated in a mixture of secondary antisera of Alexa 488-conjugated donkey anti-rabbit (1:500, Invitrogen, Carlsbad, CA), Alexa 647-conjugated donkey anti-guinea pig (1:500, Invitrogen) and Cy3-conjugated donkey anti-mouse (1:500, Invitrogen) diluted in TBS for 2 hours. Following several washes in TBS, sections were mounted on glass slides in Vectashield (Vector Laboratories). For quantitative analysis, high resolution (60 nm/pixel) z-stack images (z-step size: 130 nm) were taken from the upper 3 μm of the slices using an A1R confocal laser scanning microscope (Nikon Europe, Amsterdam, The Netherlands, objective: CFI Plan Apo VC 60X Oil N.A. 1.4).

For the evaluation of Calb inputs onto the AISs the sections were incubated in 10% NDS containing 0.05% Triton-X 100 in 0.1 M PB for 45 min. followed by the incubation in a mixture of antisera mouse anti-ankyrin G IgG (Santa Cruz 1:200) and rabbit anti-Calb (1:5000) incubated at 4 C°. The primary antibodies were visualized by the incubation of donkey anti-mouse IgG conjugated Cy3 and donkey anti-rabbit conjugated Alexa 647 for 2 hours at room temperature. In a separate experiment, sections were incubated in a mixture of antisera mouse anti-ankyrin G (Santa Cruz 1:200) and rabbit anti-CB_1 (1:1000, Cayman). These primary antisera were visualized with Cy3-conjugated donkey anti-mouse and Alexa 488-conjugated donkey anti-rabbit secondary antibodies (all 1:500, Jackson). In both cases, sections were washed and mounted on slides in Vectashield (Vector Laboratories). Confocal images were

collected using a Nikon A1R microscope fitted with an oil immersion apochromatic lens (z step size: 0.13 μm, xy: 0.06 μm/pixel). Based on the 3D confocal images, the AISs of cells were delineated with the Neurolucida 10.53 software and the sites, where the presynaptic boutons (i.e. Calb/CB_1-containing profiles) made close apposition with ankyrin G-immunostained profiles were labeled as contact sites along the AISs. For the analysis of the obtained data the Neurolucida Explorer software was used. Values were corrected for shrinkage of the tissue (x, y, z axis correction: 1.08).

3.2.3. Neurochemical marker detection in biocytin filled INs

In those cases, when the Calb content of PV+ INs was evaluated, the sections containing the soma of recorded cells were first incubated in guinea pig anti-Calb (1:5000, Synaptic Systems) diluted in 0.1 M PB containing 1% NDS and 0.1% Triton X-100 for three days at 4ºC. Then the sections were incubated in DyLight 649-conjugated donkey anti-guinea pig secondary antibody (1:300, Millipore) diluted in 0.1 M PB for 2 hours. The Calb content of PV+ INs was investigated in the varicosities and, in most cases, in the soma and dendrites of biocytin-filled cells using confocal microscopy.

To determine the CB_1 content of interneurons sampled in slices prepared from CCK-DsRed mice, sections after re-sectioning of slices were first blocked in NGS (10%, Vector Laboratories) made up in TBS (pH 7.4) containing 0.1% Triton X-100 followed by incubation in rabbit anti-CB_1 (Cayman Chemical Company, Ann Arbor, MI) diluted 1:1000 in TBS containing 2% NGS and 0.1%. Following several washes in TBS, CB_1 expression was visualized using DyLight 405 (goat anti-rabbit, 1:500, Invitrogen). The CB_1 content of recorded interneurons was investigated in the varicosities of biocytin-filled cells.

3.2.4. Target distribution analysis of biocytin filled INs

To estimate the target distribution of BCs using light microscopy, sections were incubated in mouse anti-Kv2.1 (1: 1000, 75-014, Neuromab), which was visualized with Cy3-conjugated goat anti-mouse antibody. In case of CCKBCs, sections were incubated in a mixture of mouse anti-Kv2.1 and rabbit anti-CB_1 primary antibodies visualized with Alexa 488 (donkey antimouse, 1:200, Molecular Probes) and DyLight 405 (donkey

anti-rabbit, 1:200, Jackson ImmunoResearch Laboratories Inc.). Following several washes in TBS, sections were mounted on glass slides in Vectashield (Vector Laboratories). Images were taken using an A1R or a C2 confocal laser scanning microscope (Nikon Europe, Amsterdam, The Netherlands) using a 60× (NA = 1.4) apochromatic objective.

3.2.5. Reconstruction of in vivo *labeled AISs*

To get sparse labeling of PCs *in vivo,* biotinylated-dextran amine (BDA 3kDa) was bilaterally injected with iontophoresis for 2 min into the BLA (anteroposterior: -1.8 ; mediolateral: 3.2 ; dorsoventral: 4.0 mm from Bregma). After 2 days of recovery mice were perfused with 2.5% acrolein in 4% PFA (pH 6.8) in 0.1M PB for 10 min, the brain was removed and postfixed in 4% PFA in 0.1M PB for 1.5 hours. The areas containing the BLA were sectioned into 40 μm thick sections soaked in 30% sucrose overnight and the sections were kept in cryoprotectant anti-freeze solution consisting of sucrose, ethylene glycol, distilled H_2O and phosphate-buffered saline (3:3:3:1 volume ratio) at -20^{o}C until further processing was initiated (Watson et al., 1986). Prior to immunostaining the cryoprotectant was washed out in 0.1 M PB. The sections were treated with 0.1 mg/ml pepsin (Cat. No. S3002; Dako, Glostrup, Denmark) in 1 N HCl at 37^{o}C for 15 min and washed in 0.1 M PB several times, followed by incubation in 10% NDS containing 0.05% Triton-X 100 in 0.1 M PB for 45 min. Then, the sections were incubated in the sequentially applied primary antibodies in 0.1 M PB for four days. On the first day mouse anti-gephyrin IgG (Synaptic System 1:1000) and rabbit anti-ankyrin G IgG (Santa Cruz 1:200) were applied, incubated at 4 °C, then on the third day guinea pig anti-VGAT IgG (Frontier Institute Co.Ltd 1:1000) and goat anti-panGAD IgG (Frontier Institute Co.Ltd 1:500) were added to the solution, and further incubated at room temperature for 24 hours. The primary antibodies were visualized by the incubation of the following secondary antibodies for 2 hours at room temperature: donkey anti-mouse IgG conjugated Alexa 647, donkey anti-rabbit conjugated DyLight 405, donkey anti-guinea pig conjugated Alexa 594, donkey anti-goat conjugated Alexa 594 and Alexa 488 conjugated streptavidin. Sections were washed and mounted on slides in Vectashield (Vector Laboratories). Confocal images of the labeled cells in the BLA were collected using a Nikon A1R microscope fitted with an oil immersion

apochromatic lens (z step size: 0.13 μm, xy: 0.06 μm/pixel). The obtained pictures were deconvolved with the aid of the Huygens software (SVI, Hilversum, The Netherlands). Based on the 3D confocal image, the AISs of the BDA labeled cells were reconstructed with the Neurolucida 10.3 software and the sites where the presynaptic boutons (i.e. panGAD/VGAT-containing profiles) faced the postsynaptic marker gephyrin, were labeled as synaptic contacts along the AISs. For the analysis of the obtained data the Neurolucida Explorer software was used. Values were corrected for shrinkage of the tissue (x, y, z axis correction: 1.08).

3.2.6. Nav 1.6 and ankyrin G staining of AISs

Two mice were transcardially perfused with 2% PFA in 0.2 M Na-acetate buffer (pH 6.0) for 20 min, the brain was removed and sectioned into 40 μm thick sections. Nav 1.6 was revealed using a polyclonal rabbit anti-Nav 1.6 (1:500, Alomone Labs) primary antibody and Alexa 488-conjugated goat anti-rabbit secondary antibody; ankyrin G was labeled as described above. Confocal images were collected with a Nikon A1R microscope (z step size: 0.13 μm, xy: 0.1 μm/pixel). For the intensity analysis of the labeling, those AISs were analyzed that run parallel to the slice surface and could be traced from the soma to the end of the labeled profile. Intensity distributions of the immunolabelings were analyzed with the intensity profile function of Nikon Imaging System software using maximum z intensity projection pictures.

3.3. Statistical analysis

For comparison of data with normal distribution according to the Shapiro-Wilk test, the Two sample T-test and ANOVA were used. For data with non-normal distribution the Mann-Whitney U test (M-W test), Wilcoxon Signed Rank test and Kruskal-Wallis ANOVA (K-W ANOVA) was used. For the comparison of distributions, the two sample Kolmogorov-Smirnov test was used (K-S test). All statistics were performed using Origin 8.6 or 9.2 (Northampton, MA). Data are presented as mean ± s.e.m. unless indicated.

3.4. Personal contribution to the results

All electrophysiological experiments in the study were perfomed and analyzed by me. Also all the anatomical experiments were done and analyzed by me, except data presented in Fig. 3 F and K, Fig 4, Fig. 5 and Fig. 6 N-P, and all the electron microscopic investigations were performed by other members of the lab.

4. Results

4.1. Part I: Sources and organization of the GABAergic inputs onto the perisomatic region of principal cells in the BLA

4.1.1. The extent of the perisomatic region along the dendrites of principal cells

As in most, if not all cortical structures (Megias et al., 2001), the perisomatic region of PCs in the BLA is exclusively innervated by GABAergic synapses, while glutamatergic synaptic inputs arrive predominantly on their spines or thin dendritic shafts and avoid the soma (McDonald et al., 2002). To confirm this, we performed immunostaining against type 1 and type 2 vesicular glutamate transporters (VGLUT1 and VGLUT2) together with bassoon staining on biocytin-filled PCs. The former two markers are known to visualize the excitatory inputs (Takamori et al., 2000, 2001) 2001), while the presence of bassoon helps to identify the release sites in the boutons (Papp et al., 2013). The analysis of this immunostained material revealed no VGLUT1- or VGLUT2-immunoreactive bouton, which bassoon immunolabeled portion opposed toward the soma of biocytin filled PCs (n=7), while such terminals could be readily observed to contact PV-expressing cell bodies (n=3, unpublished observations). This latter observation is in accord with earlier studies describing that these interneurons receive excitatory synapses on their cell bodies and verify the previous results that the perisomatic region of PCs in the BLA receive only an insignificant number of excitatory inputs (Gulyas et al., 1999, McDonald et al., 2005).

To quantify the GABAergic inputs of the perisomatic region, first it was necessary to define its spatial extent along the proximal dendrites. We took a functional approach by estimating the amount and the ratio of excitatory and inhibitory inputs along the proximal dendritic branches started form soma. We first determined the spine distribution along the dendrites of intracellularly labeled neurons (Fig. 3A-C). Using high resolution 3D confocal images, the results of 11 reconstructed PCs showed that the spine number along the dendrites increased gradually (n=68), reaching the maximum in the density between 50-70 μm from the soma. Fitting a Boltzmann sigmoid function onto the spine distribution gave an inflection point at 30.5±0.85 μm, indicating a

distance from the soma where the steepest rise of spine density along the dendrites changes into a modest increase (Fig. 3B). This characteristic appearance of the spine distribution along the proximal dendrites of PC was rather distance than dendritic branching pattern-dependent, as the spine density along the 1st and 2nd order dendrites changed similarly (Fig. 3C).

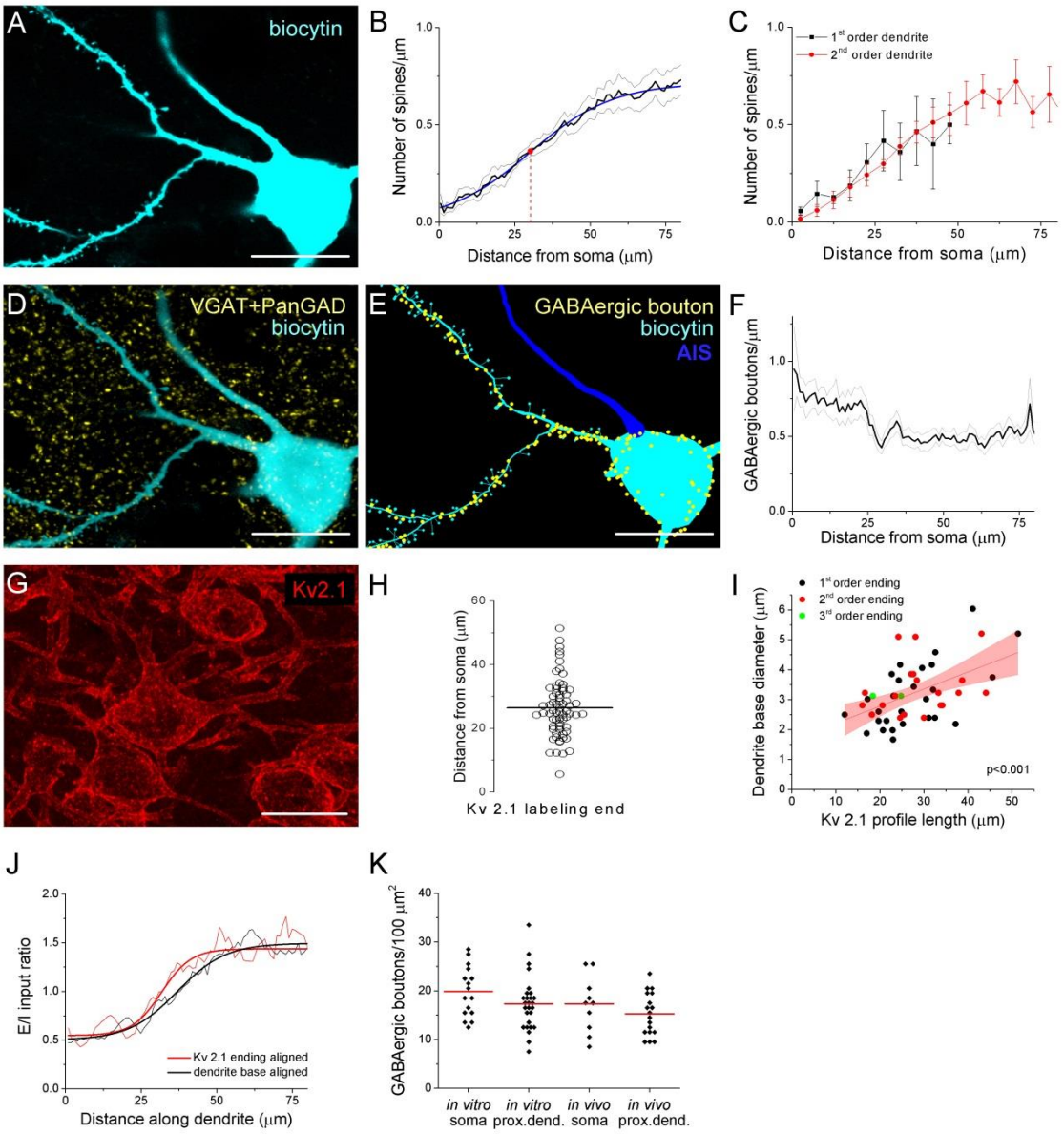

Figure 3. *Immunostaining against Kv2.1 channel protein visualizes the extent of the perisomatic region, which functional domain receives predominantly GABAergic inputs*. A, A biocytin-filled PC in the BLA. B, Relationship between the spine number and the distance from the soma. Boltzmann sigmoid function (blue line) fitted onto the spine distribution gave an inflection point at 30.5±0.85 µm (red dot). Pooled

data obtained from 68 dendrites of 11 PCs. C, The same as in B, but the dendrites were subgrouped according to their order. D, The same PC as in A is shown together with GABAergic boutons visualized with immunostaining against VGAT and PanGAD. E, GABAergic boutons at close apposition with the PC are indicated in a Neurolucida reconstruction. (AIS, axon initial segment) F, The distribution of GABAergic boutons along the dendrites as a function of the distance from soma (68 dendrites of 11 PCs). Grey lines: SEM. G, Representative Kv2.1 immunostaining in the BLA. H, The variance in the length of Kv2.1-immunopositive dendrites. Horizontal line indicates the mean of 26.43 μm (n=68). I, The length of the Kv2.1-labeling correlated with the diameter of biocytin filled dendrites at their somatic origin, but it was independent from the dendritic branching pattern (e.g. the order of the dendrites). Red area indicates 95% confidence interval of the linear fit. J, Excitatory and inhibitory (E/I) ratio on PCs calculated from data in B and F are shown aligned by dendrite base or the end of Kv2.1-immunostained profiles. Note the steeper change in E/I ratio, when the alignment was conducted by the end of Kv2.1-immunolabeled dendrites. (See the text for details). K, The density of GABAergic boutons on the PC somata and their Kv2.1-immunostained dendrites is similar determined both in vitro and in vivo. (Black dots, individual soma or dendrites, red lines, mean of the distributions). Scale bars (in μm): A, D, E, G: 20.

To investigate the distribution of GABAergic inputs along the proximal dendrites of biocytin-filled PCs, we visualized the GABAergic varicosities on the membrane surface by VGAT and PanGAD immunoreaction. The analysis revealed a decrease in the number of immunopositive boutons from the soma to the extent of ~ 30 μm, from where the density of GABAergic boutons showed no further change along the dendrites (n=19 dendrites from 4 PCs, Fig. 3D-F).

Earlier works showed that immunostaining against the voltage-gated K^+ channel type Kv2.1 (or KCNB1) visualizes the perisomatic membrane of neurons (Lim et al., 2000). This raised the possibility that Kv2.1-immunostained segments of the proximal dendrites might actually correspond to those membrane surfaces, which belong to the perisomatic region. Indeed, the average length of Kv2.1-immunostained parts of the dendrites (26.43±8.96 μm, n=68, Fig. 3G, H) showed a good correspondence with the inflection point determined with spine distribution (Fig. 3B) or with the dendritic length, from where the density of GABAergic inputs reached steady state, i.e., no further decrease along the dendrites could be observed (Fig. 3F). Moreover, there was a wide variability in the length of the individual Kv2.1-labeled dendritic segments (ranging from 5.6 to 51.4μm, Figure 3H). Importantly, there was a tight correlation between the length of the Kv2.1-immunostained dendritic segments and the diameter of

the dendrites at their somatic origin, which relationship was independent of dendritic order (Fig. 3I). These observations prompted us to examine the length of individual Kv2.1-immunostained profiles on those biocytin-filled dendrites where the distribution of the spines and VGAT/PanGAD-immunopositive boutons had been evaluated. Using this approach, we could calculate the ratio of excitatory/inhibitory (E/I) inputs for each individual proximal dendrite by dividing the number of spines with the number of GABAergic boutons along the given dendrite. We hypothesized if there is no relationship between the extent of the Kv2.1 immunoreactivity along the dendrites and the functional boundary of the perisomatic region, then the increase in the E/I input ratio along individual dendrites starting from either the soma or from the distal-most extent of Kv2.1 labeling should have a similar slope. Alternatively, if the extent of the Kv2.1-immunostained dendritic segments corresponds to the border of the perisomatic region, then the increase in the E/I ratio along individual dendrites starting from the distal-most extent the Kv2.1 labeling should have a steeper slope compared to a plot obtained for the E/I ratio along dendrites starting from the base of the dendrites. As shown in Fig. 3J, there was a steeper change in E/I input ratio after aligning the data obtained for individual dendrites by the end of Kv2.1-stained profiles in comparison to that determined with aligning these data to the base of the dendrites (max. derivative peak: 0.0454 vs. 0.0310 ΔE/I / Δ μm, Fig. 3J). These results together suggest that the extent of the perisomatic region along the individual dendrites of amygdalar PCs shows high variability, which can be predicted by the diameter of the dendrite at their somatic origin, and importantly, the perisomatic region of PCs can be visualized by immunostaining against Kv2.1. Therefore, in the following parts of the study, Kv2.1-immunostained dendrites will be considered as a part of the perisomatic region in addition to the soma and AIS.

4.1.2. Quantification of GABAergic inputs onto the soma and the proximal dendrites of amygdalar principal cells

In the next set of experiments, we aimed to reveal the density of GABAergic boutons received by the soma and proximal dendrites of PCs to determine the quantity of GABAergic inputs contacting the perisomatic region. To this end, we counted the number of VGAT-immunoreactive boutons forming close appositions with the soma

and Kv2.1-immunostained dendrites of biocytin-filled PCs (Fig. 3K). To validate these data obtained in *in vitro* slices, we similarly determined the number of GABAergic inputs onto the perisomatic regions of PCs in perfused tissue. The results showed that approximately 17-20 boutons/100 μm^2 could be found on the surface of the soma both *in vitro* and *in vivo* (19.87±5.18/100 μm^2 and 17.32±5.81/100 μm^2, n= 16 and 10, respectively), while the density of GABAergic inputs was slightly less on the proximal dendrites (*in vitro*: 17.34±5.56/100 μm^2 and *in vivo*: 15.25±4.36/100 μm^2, n= 27 and 18, respectively, Fig. 3K). The GABAergic coverage of the distinct membrane domains *in vitro* and *in vivo* did not differ ($p>0.1$, ANOVA). As the total soma surface of a PC was found to be 881.4 ± 83.4 μm^2 on average (n=10, range: 735.1 – 1030.7 μm^2), while the surface of its proximal dendrites is 439.8±128.2 μm^2 (49 dendrites of 8 PCs), we have estimated that approximately 158 and 71 GABAergic boutons form close contacts with the soma and proximal, Kv2.1-immunostained dendritic segments of amygdalar PCs, respectively.

4.1.3. Distribution of GABAergic boutons along the AIS

Having determined the number of GABAergic contacts on the somatic and proximal dendritic segments, we next determined the GABAergic boutons along the AISs to reveal the total inhibitory inputs terminating on the perisomatic region of PCs. Using quadruple immunostaining we analyzed the distribution of synaptic inputs along the AISs of PCs by confocal microscopy. PCs in the BLA were labeled in vivo with a tracer, biotinylated dextran amine (3 kDa BDA), while their AISs were identified with immunostaining for ankyrin G (Fig. 4A). GABAergic inputs were visualized with a mixture of antibodies against both isoforms of the GABA synthetizing enzyme GAD (GAD65 and GAD67, panGAD) and the vesicular GABA transporter, VGAT; whereas a scaffolding protein, gephyrin, expressed specifically at inhibitory synapses, was used to label functional synaptic junctions (Fig. 4B). In high resolution confocal images of the *in vivo* labeled PCs, we reconstructed AISs together with GABAergic terminals that were apposed to gephyrin labeling (Fig. 4C). In this material, the length of the ankyrin G-labeled segments was found to be 58.4±1.9 μm (n=7), which corresponds to the length of the AIS. The analysis showed that single AISs received 52.4 ± 7.8 inhibitory inputs on average (range: 31-86; n=7). Interestingly, we noticed that the GABAergic

innervation along the AISs is not evenly distributed, but tends to concentrate on a restricted region between 20 and 40 µm measured from the PC somata (Fig. 4D).

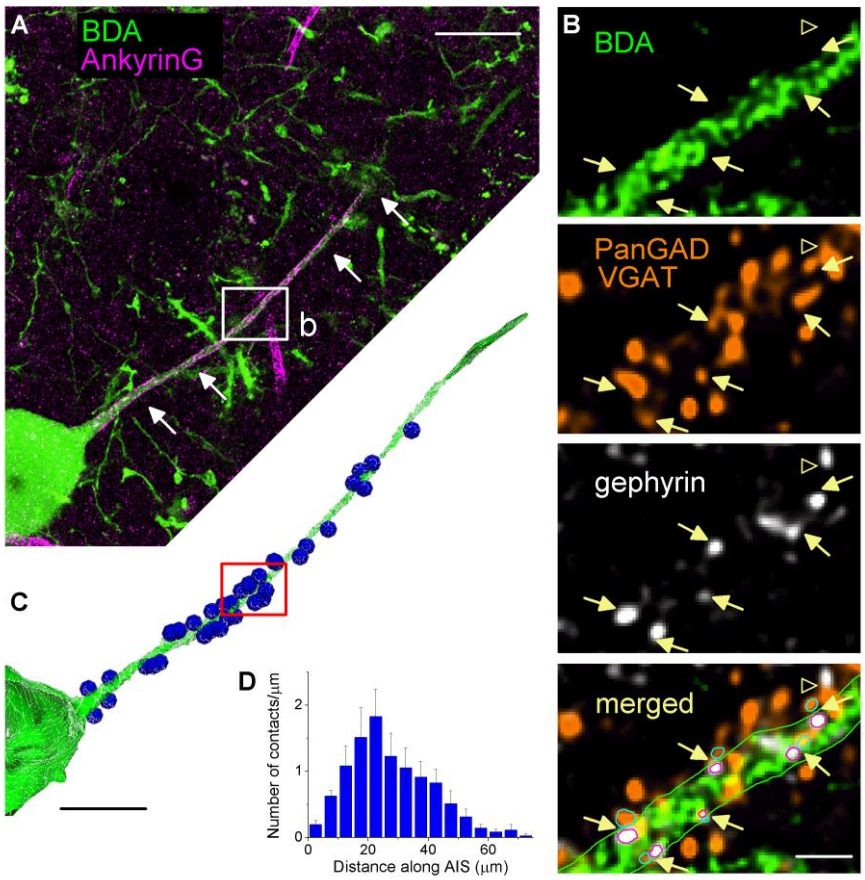

Figure 4. *Spatial distribution of GABAergic inputs along the proximal part of PC axons* A, Representative BDA-labeled PC (green). The AIS was identified with immunostaining against ankyrin G (magenta). B, Along the BDA-labeled axon, GABAergic terminals were visualized with antibodies detecting both isoforms of the GAD enzyme (GAD65 and GAD67) and the vesicular GABA transporter, VGAT. Functional contacts were revealed based on the presence of a scaffolding synaptic protein, gephyrin. Bottom panel; superimposed neurolucida reconstruction of GABAergic inputs along the given axonal segment. Arrows show the synaptic sites along the AIS, and the open arrowhead indicates a GABAergic bouton that did not target this BDA-labeled AIS. Images were taken from a single focal plane. C, 3D Neurolucida reconstruction of the proximal part of the axon and a part of the soma shown in A (green) and the GABAergic inputs where gephyrin was present (blue spheres) forming close apposition with the axon. D, Spatial distribution of GABAergic inputs along axons labeled in vivo (n=7 reconstructed axons, 5 µm bin size). Data represent mean±s.e.m. Scale bars (in µm): A, C 25; B 2.

4.1.4. The vast majority of GABAergic inputs onto the soma and proximal dendrites of amygdalar principal cells originates from two distinct types of GABAergic interneurons

In the next set of experiments, we intended to reveal the interneuron types contributing to the GABAergic inputs received by the soma and proximal dendrites of amygdalar PCs. As earlier work elucidated, GABAergic axon terminals expressing PV, Calb or CB_1 formed synaptic contacts with the perisomatic membrane of PCs (Smith et al., 1998, Katona et al., 2001, McDonald et al., 2005). Therefore, using multicolor immunofluorescent stainings we first examined the ratio of PV and CB_1 immunoreactive boutons among VGAT-immunolabeled varicosities, which were in close apposition to the perisomatic membranes of PCs (Fig. 5A). We found that i) 67% of VGAT-immunostained boutons both on the soma and the Kv2.1-immunolabeled dendrites was immunopositive for PV or CB_1 (n=498 boutons on 10 soma and 234 boutons on 18 dendrites) and ii) more PV- than CB_1-immunoreactive boutons contacting this membrane regions could be observed (p=0.007, M-W test, Fig. 5B).

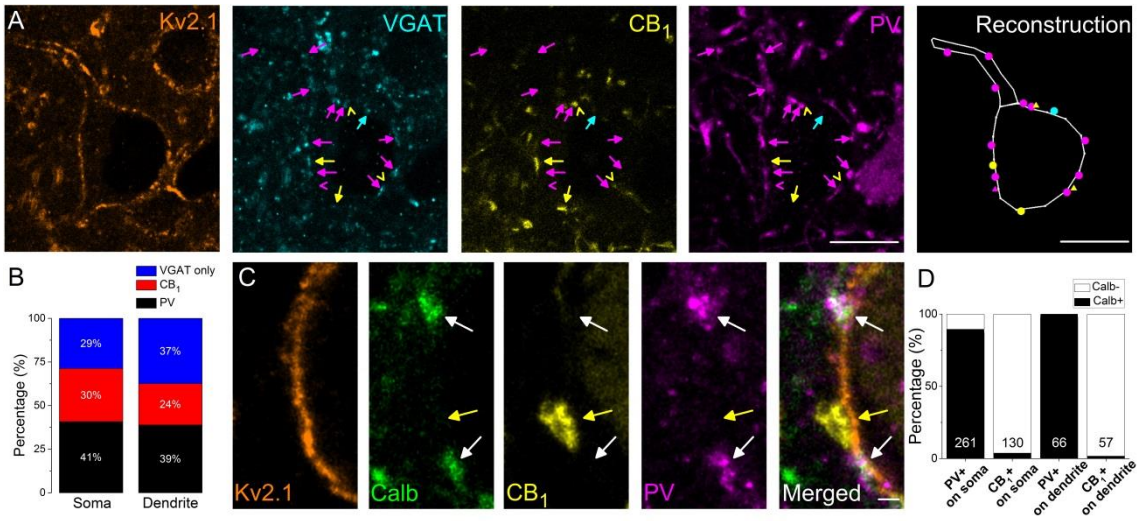

Figure 5. *The vast majority of perisomatic GABAergic inputs onto the principal cells originate from boutons co- expressing parvalbumin (PV) and calbindin (Calb) or CB_1 cannabinoid receptors*. A, Multicolor single plane confocal images taken from immunostaining against Kv2.1 (to delineate the perisomatic region of PCs), VGAT, CB_1 and PV. Far right: the reconstruction of a Kv2.1-immunostained neuron receiving GABAergic inputs. Arrows and dots in magenta point to VGAT/PV-immunostained boutons, an arrowhead and a triangle in magenta mark a PV-containing bouton, arrows and dots in yellow indicate VGAT/CB_1-immunopositive varicosities, arrowheads and triangles in yellow mark CB_1-immunoreactive boutons and an arrow and a dot in blue show a VGAT-immunolabeled bouton forming

close appositions with a Kv2.1-immunostained neuron. B, Ratio of boutons expressing PV, CB_1 and VGAT only on the Kv2.1-immunostained somata and dendrites. C, Multicolor single plane confocal images taken from immunostaining against Kv2.1, Calb, CB_1 and PV. White arrows point to boutons co-expressing Calb and PV forming close appositions with a Kv2.1 immunonustained soma membrane segment, while yellow arrow indicates a CB_1-immunoreactive varicosity lacking Calb immunolabeling. D, Ratio of PV- or CB_1-expressing boutons immunoreactive for Calb on soma or proximal dendrites. Numbers in the columns indicate the amount of boutons evaluated. Scale bars (in μm): A: 10, C: 1

Next, we examined the Calb content of PV or CB_1 immunostained boutons, because previous studies in the amygdala have shown that Calb-immunoreactive axon terminals could also form symmetrical synapses with the perisomatic membranes of PCs (Muller et al., 2003). Using multicolor immunofluorescent stainings, we clarified that Calb immunoreactivity was present predominantly in PV-immunostained varicosities (91.7% of all PV-immunopositive boutons contained also Calb, n=300/327 boutons), but was negligible (2.7%, n= 5/187 boutons) in CB_1-expressing boutons apposing the membrane surface of the perisomatic region (Fig. 5C, D). These data show that most of the GABAergic inputs onto the perisomatic region of PCs originates from two interneuron populations, i.e. from two distinct types of BCs, which differ in their Calb content.

4.1.5. Interneurons innervating the perisomatic region of amygdalar principal cells are neurochemically distinct

Next, we wanted to compare and contrast the morphological, neurochemical and single-cell properties of all major interneuron types innervating the perisomatic region. To this end, PV-containing and CB_1-expressing interneurons, which were shown to give the majority of GABAergic inputs onto the perisomatic membrane surface of PCs (Fig. 5), were intracellularly labeled in slices prepared from PV-eGFP and CCK-DsRed mice, respectively. In PV-eGFP mice both AACs and PVBCs were sampled, which cell types were separated *post hoc* at light microscopic level using double immunofluorescent staining against biocytin and ankyrin G (PVBC, n=69; AAC, n=47). In case of interneurons sampled in CCK-DsRed mouse slices, expression of CB_1 on the axon terminals of each recorded cell was verified using immunostaining (n=40) to

unequivocally identify this interneuron type. In all cases, the interneurons labeled with biocytin had spine-free or rarely spiny dendrites and dense local, often ramified axon collaterals bearing large boutons (Fig. 6A-C). Both the dendritic and axonal branches of intracellularly filled interneurons were mainly restricted to the amygdala, rarely penetrating into the capsules surrounding this cortical area.

Using multicolor immunofluorescent stainings, we first examined the Calb content of anatomically identified interneurons innervating the perisomatic region. We found that Calb content clearly distinguished PV-expressing interneurons. Namely, PVBCs expressed Calb both in their boutons and cell bodies (n=25 and 16, respectively, Fig. 6G), while the soma of all but one AAC was found to be immunonegative (n=14), and no immunolabeling for Calb in the axon terminals of examined AACs could be detected (n=18, Fig. 6H). The CB_1-immunostained varicosities of biocytin-filled interneurons were also found to be Calb immunonegative (n=11, data not shown). These results confirmed and extended our data obtained in perfused tissue (Fig. 5), showing that among interneurons targeting the perisomatic region PVBCs express Calb.

4.1.6. Target distribution of the two types of basket cells in the BLA

In the next part of the study, we first aimed to get a deeper insight into the target distribution of individual BCs innervating the perisomatic region of PCs. The potential targets of both types of BCs were investigated by revealing the somata and proximal dendrites of PCs using Kv2.1 immunostaining in addition to the biocytin-labeled axon varicosities (Fig. 6D, F). If the labeled bouton formed a close apposition with a Kv2.1-immunostained soma or a dendritic segment, then this bouton has been considered to target the perisomatic region. If no Kv2.1-immunostained profile could be seen in the close vicinity of a biocytin-containing bouton, then a non-perisomatic/unidentified target was marked. To reveal whether those boutons contacting non-Kv2.1-immunostained profiles could form synaptic contacts presumably on distal dendrites, electron microscopic examination of biocytin-filled varicosities has been carried out.

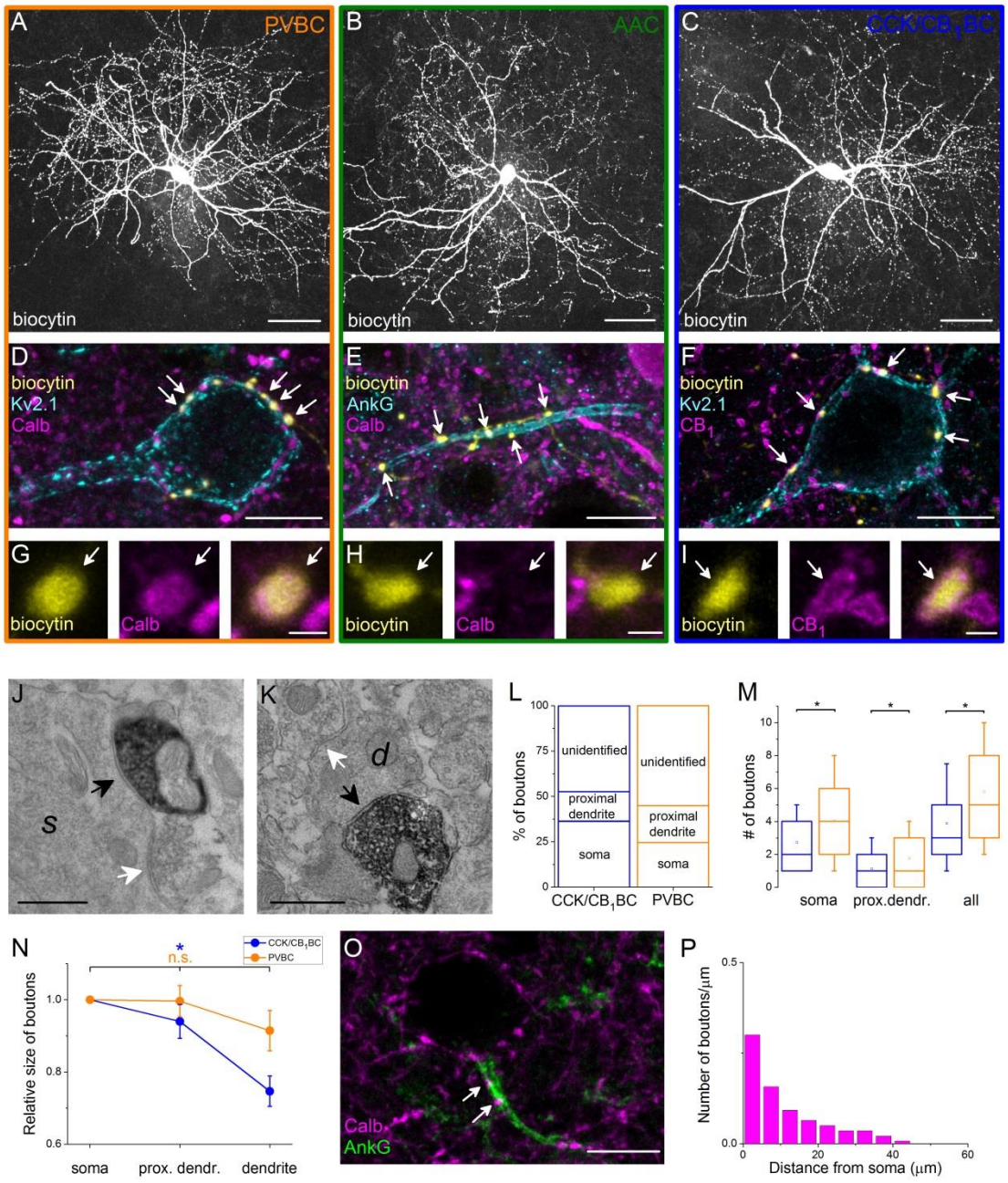

Figure 6. *Output features of three interneurons targeting the perisomatic region of the principal cells in the BLA.* Maximum z intensity projection images taken of an in vitro biocytin-filled PVBC (A), an AAC (B) and a CCK/CB_1BC (C). D, The biocytin-containing boutons expressing Calb (G) of the same cell as in A form close contacts with the perisomatic region of a PC. E, Varicosities of the AAC in B lacks Calb immunoreactivity (H) contact with an AIS visualized by ankyrin G staining. F, The boutons of the interneuron in C expressing CB_1 (I) form close appositions with the Kv2.1-immunostained membranes of a PC. J and K, Electron micrographs showing biocytin-labeled axon terminals of a PVBC forming symmetrical synapses on a soma (s) and on a small caliber dendrite (d)(black arrows). The same postsynaptic elements also received symmetrical synapses from unlabeled axon endings (white arrows).

L, Ratio of boutons of PVBCs (n=12) and CCK/CB_1BCs (n=12) forming close contacts with Kv2.1-immunostained somata and proximal dendrites, or which did not appose any Kv2.1-immunostained profiles (unidentified). Note that the high ratio of boutons contacting the perisomatic region of PCs defines the cells as BCs. M, Larger number of boutons from a PVBC than a CCK/CB_1BC contact the perisomatic region of individual PCs. Asterisks mark significant differences (for values see the text). Here, and in Fig. 4, the mean (open square), the median (midline of the box), the interquartile range (box) and the 5/95% values (whiskers) are shown on the charts. N, The relative size of CCK/CB_1BC boutons on the soma or proximal dendrites of PCs is significantly larger than those contacting non-Kv2.1-immunostained profiles ($p<0.05$). No difference was found in the PVBC bouton size. Data are shown as mean±SEM. O, A confocal image taken from immunostaining for Calb and ankyrin G. Arrows indicate Calb-containing boutons on an AIS. P, The number of Calb-immunoreactive boutons shows a steep decrease from the soma towards the end of the anykrin G-immunolabeled AISs. Scale bars (in μm): A-C: 50, D-F: 10, G-I: 1, J-K: 0.5, O: 10.

We verified that small caliber dendrites in addition to somata and proximal dendrites were among the targets of biocytin-filled boutons (PVBC: 23/57 synapses on dendrites (40%), CCK/CB_1BC:32/54 synapses on dendrites (59.2%), n=6 and 5 cells, respectively). The diameter of dendrites targeted by the BCs was similar (0.69±0.411 μm for PVBCs, 0.745±0.489 μm for CCK/CB_1BCs, $p=0.65$). These data indicate that those boutons, which did not contact Kv2.1-immunostained segments at light microscopic level, they could target indeed more distal dendrites of PCs. Having this in mind, we estimated the distribution of potential targets for BCs. Using this light microscopic approach, we found that the boutons of PVBCs (2529 boutons, n=12 cells) and CCK/CB_1BCs (2642 boutons, n=12 cells) innervated the perisomatic region of PCs with similar probability ($p=0.25$, Fig. 6L), although the ratio of those varicosities, which targeted only somata was significantly larger for CCK/CB_1 PCs than for PVBCs ($p=0.02$).

In addition to the target distribution, this approach allowed us to estimate the convergence of GABAergic inputs onto single PCs from the two types of BCs. By counting the number of boutons originating from individually labeled interneurons, which varicosities formed close appositions with soma and proximal dendrites of single Kv2.1-immunolabeled PCs, we found that individual PVBCs contacted single PC somata by 32% more boutons than CCK/CB_1BCs (PVBC: 4.04±2.90 boutons/individual

soma, totally 481 boutons on 119 PC cell bodies; CCK/CB_1BC: 2.76±1.96 boutons/individual soma, totally 357 boutons on 129 PC somata , n=8-8 IN, p<0.0001, Fig. 6M). In addition, the difference in number of bouton contacting Kv2.1-immunoreactive dendritic profiles was lower, but still statistically significant (PVBC: 1.76±1.80 boutons/proximal dendrites of individual cell, totally 210 boutons on 119 PCs; CCK/CB_1BC: 1.14±1.29 boutons/proximal dendrites of individual cell, totally 148 boutons 129 PCs was observed, n=8-8 IN, p=0.0005, Fig. 6M). Merging these data showed that the perisomatic region of single PCs received 33% more boutons from individual PVBCs than from individual CCK/CB_1BCs (PVBC: 5.80±3.33, CCK/CB_1BC: 3.91±2.66, p<0.0001, Fig. 6M).

4.1.7. Boutons of CCK/CB_1BCs targeting the perisomatic region are larger than those targeting the distal dendrites

Previous work obtained in the hippocampus showed that the size of the CB_1-immunolabeled boutons innervating the somata or the dendritic shafts of PCs was significantly different (Klausberger et al., 2005, Lenkey et al., 2015). To assess whether the CB_1-expressing boutons targeting functionally distinct membrane domains of amygdalar PCs have distinct sizes, we measured the perimeter of boutons originating from CCK/CB_1BCs. We found that the size of CB_1-expressing varicosities forming close appositions with Kv2.1-immunostained profiles was significantly larger than those ones, which avoided the cell bodies or proximal dendrites of PCs (ANOVA, p<0.005, *post hoc* Fisher test, p<0.05 for both comparison, n=16 cells, 20-30 bouton/cell in each category, Fig. 6N). Importantly, there was no difference in size between those CB_1-expressing boutons that were in close vicinity of somata or Kv2.1-immunoreactive dendritic segments (*post hoc* Fisher test, p=0.9, Fig. 6N). The former results point out that the volume of CB_1-expressing varicosities indicate the nature of postsynaptic targets, similarly to that described first in the hippocampus, while the latter findings support the idea that the perisomatic region, as a functional domain can be identical to Kv2.1-immunostained membrane surface. In a similar manner, we measured the volume of boutons along the axon collaterals of PVBCs. There was no significant difference in size of varicosities targeting perisomatic or non-perisomatic regions of PCs (ANOVA, p=0.69, n=15 cells, Fig. 6N). These data show that the difference in bouton size is

characteristic of CCK/CB_1BCs, but not of PVBCs, and, notably, this difference in CB_1-expressing bouton volume can have biological significance.

4.1.8. PVBCs target the proximal part of the AISs

Previous studies have raised the possibility that BCs could occasionally target the AISs of PCs (Kisvarday et al., 1985, Halasy et al., 1996), but neither the ratio of BC boutons among GABAergic inputs contacting AISs nor their spatial occurrence along the AISs are known. Therefore, we intended to estimate the number and the distribution of BC boutons along the AISs by exploiting the fact that Calb content of axon endings originating from PVBCs distinguishes them from those that belong to AACs (Fig. 6G,H). By examining the distribution of Calb-immunoreactive boutons along the ankyrin G-stained profiles in perfused tissue samples, we found that the majority of varicosities of PVBCs contacted the proximal part of the AISs and the number of Calb-immunoreactive boutons decreased sharply toward the end of the AISs (3.8 ± 1.9 Calb-positive bouton/AIS, n = 28 AISs, Fig. 6O,P). In separate double immunostained materials we found no close appositions between CB_1-expressing boutons and ankyrin G-stained profiles (n=10 AIS was evaluated, data not shown), indicating that the output of CCK/CB_1BCs contributes negligibly to the GABAergic innervations of AISs. These data indicates that besides the input from AACs, the proximal part of the axon is targeted mainly by PVBCs.

In the next part of the studies, we investigated the electrophysiological and morphological properties of the connections between AACs and PCs in details and the functional effects of this IN type on PC spiking.

4.2. Part II: Electrophysiological and morphological properties of the output synapses of AACs

4.2.1. Axo-axonic cells innervate the axon initial segments of principal cells in the BLA

In order to study the properties of AACs in the BLA, we obtained visually-guided, targeted recordings in amygdalar slices prepared from the brains of transgenic mice expressing eGFP under the control of PV promoter (Meyer et al., 2002). After recordings, each cell was morphologically identified (Fig. 7A). Briefly, we analyzed the bouton distribution of the recorded interneurons relative to the AIS of PCs at the light microscopic level. If the boutons of an interneuron formed close appositions with the AIS of the intracellularly-labeled PC in a monosynaptically-connected pair or with immunostained profiles visualized with ankyrin G (Fig. 7B), we identified the cell to be an AAC (Gulyás et al., 2010). In this part of the study, 45 AACs were included after separation from other types of PV-expressing interneurons. In the case of 3 AACs, we confirmed by electron microscopy that their axon terminals formed symmetrical synapses on AISs (n= 25 out of 28 boutons, Fig. 7C). Perikarya or dendrites were not among the postsynaptic targets of examined boutons. Thus, in the BLA, similarly to other cortical regions (Buhl et al., 1994b, Tamas and Szabadics, 2004), AACs can be separated from additional types of PV-expressing interneurons based on clear structural criteria.

4.2.2. Fast and large synaptic inhibition characterizes the connections between axo-axonic cells and PCs

First, we determined the spiking features of AACs and their basic membrane properties. Upon intracellular current injection, these interneurons had a fast spiking phenotype (max. firing frequency: 153.8±8.9 Hz, n=15), characterized by a firing with moderate accommodation (last/first inter-spike interval ratio: 2.03±0.10) and narrow spike width at half maximum amplitude (0.35±0.01 ms), as well as low input resistance (133.4±8.6 MΩ, Fig. 7D).

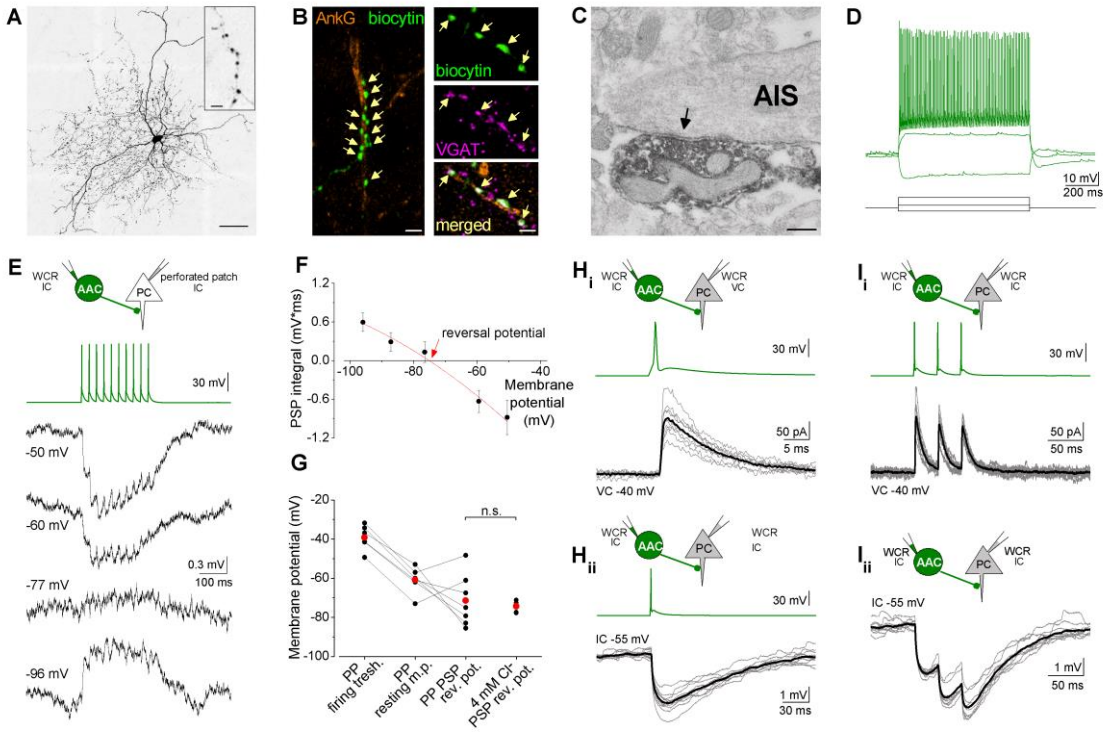

Figure 7. *Axo-axonic cells (AAC) in the BLA make synapses on the axon initial segments (AIS) and hyperpolarize their postsynaptic targets*. A, Maximum z intensity projection image of an in vitro biocytin-filled AAC. Inset: a characteristic cartridge formed by axon terminals. B, Biocytin-containing boutons of an AAC (green) make close appositions (arrows) with an AIS visualized with immunofluorescent staining against ankyrin G (orange). Vesicular GABA transporter (VGAT) content in axon varicosities of an AAC is indicative of a GABAergic phenotype. C, Representative axon terminal of a biocytin-filled AAC forms a symmetric synapse (black arrow) on an AIS. D, AACs have fast spiking characteristics revealed by step current injection (70, 300, -100 pA). E, Postsynaptic potentials (PSPs) recorded in a PC at different membrane potentials in gramicidin-perforated patch recordings upon a train of 10 action potentials evoked at 40 Hz in a presynaptic AAC. F, The integral of the summed PSPs was calculated at each membrane potential and fitted with a second order polynomial curve to determine the reversal potential of the response. G, Comparison of the firing threshold and the resting membrane potential of PCs with the reversal potential of the PSPs recorded in perforated patch mode revealed the inhibitory nature of AACs. A similar reversal potential of PSPs was obtained in whole-cell mode using an intrapipette solution containing 4 mM Cl^- (M-W test p=0.94). H-I, Representative recordings from an AAC-PC pair in whole-cell mode using 4 mM Cl-. Ten superimposed consecutive traces in gray, average in black. I, IPSCs and IPSPs in response to 3 action potentials evoked at 30 Hz show short-term depression. PP: perforated patch, WCR: whole cell recording, VC: voltage clamp, IC: current clamp. Scale bars (in μm): A 50, inset 5; B 5, 1; C 0.5.

Next, we aimed to reveal the synaptic effects of AACs onto PCs. To minimize the disturbance of the ionic milieu in PCs, we carried out recordings between monosynaptically connected AAC-PC pairs when the postsynaptic PC was recorded in perforated patch mode using gramicidin in the recording pipette. A train of action potentials was evoked in the presynaptic AAC, while the resulting monosynaptic PSPs were recorded in the PC at different membrane potentials (Fig. 7E). When we compared the estimated reversal potential of PSPs and the resting membrane potential of PCs (Fig. 7F), we found that in the majority of cases (5 out of 7) AACs hyperpolarized their postsynaptic partner at resting membrane potential (Fig. 7G). In the two remaining cases, although the PSP reversal was above the resting membrane potential, these values were still below the firing threshold of PCs. These data suggest that the synaptic effect of AACs onto PCs at resting membrane potential is inhibitory under our recording conditions (Fig. 7G). When we compared the reversal potential of IPSPs recorded in perforated patch mode to that obtained in whole-cell mode with an intrapipette solution containing 4 mM Cl^-, we found no significant difference (Fig. 7G, M-W test p=0.94). Therefore, in the following part of the study, the postsynaptic responses were recorded in whole-cell mode with an intrapipette solution containing 4 mM Cl^- concentration.

To reveal the basic characteristics of synaptic inhibition originating from AACs, AAC-PC cell pairs were recorded using the voltage-clamp configuration (Fig. 7H, I). We found that the probability of finding a connected AAC-PC pair was high (84%; n=45/54). Notably, in half of the connected pairs, PCs reciprocally innervated AACs (52%; n=17/33). Spikes in the presynaptic AACs triggered responses in the PCs with very low failure rate (probability of failure: 0.05±0.02) and fixed, short latency (1.01±0.03 ms, n=20), indicative of monosynaptic connections (Fig. 7H). The unitary postsynaptic currents recorded at a membrane potential of -40 mV had an amplitude of 100.5±13.5 pA on average, fast rise and decay kinetics (10-90% rise time: 0.83±0.07 ms; decay time constant: 6.27±0.53 ms), and were mediated via $GABA_A$ receptors, since a specific antagonist of $GABA_A$ receptors (10 μM gabazine) eliminated the action potential-evoked postsynaptic currents (n=3, data not shown). When we evoked three action potentials in AACs at 30 Hz, the amplitude of IPSCs showed a modest short-term depression (peak 3/peak 1, 0.80±0.03; n=20, Fig. 7I). In current clamp mode, IPSPs recorded in PCs at -55 mV upon evoking action potentials in AACs had large amplitude

(1.23±0.19 mV, n=16). When three action potentials were evoked in AACs, the IPSP amplitudes showed a pronounced short-term depression (peak3/peak1, 0.49±0.04). These data show that PCs receive large and reliable synaptic inputs from AACs that are inhibitory in nature and show short-term depression.

4.2.3. Axo-axonic cells potently regulate principal cell spiking

In the next set of experiments, we explored how inhibitory input from an AAC can control action potential generation in a PC. PCs in the BLA display intrinsic membrane potential oscillations at theta frequencies *in vivo*, a rhythm that can facilitate periodic firing at these frequencies (Pape et al., 1998). To mimic this intrinsic oscillation, we injected a sinusoidal current at low theta frequency (3.53 Hz) and adjusted the membrane potential of the PC to spike single action potentials at the peak of the sinusoidal inputs (see Materials and methods for details). To test the effect of the synaptic inhibition onto PC firing probability, three action potentials at 30 Hz were evoked in the presynaptic AAC before the positive peak of the sinusoidal current (Fig. 8A). In these experiments trains of action potentials were used instead of single spikes, since AACs tend to fire multiple spikes in vivo when they become active (Klausberger et al., 2003, Bienvenu et al., 2012). The stimulation of the interneuron was timed to provide the maximal inhibitory effect at the peak of the sinusoidal current, where the PC spiked with the highest probability. We found that under these conditions AACs could significantly reduce the firing probability of PCs compared to those sinusoidal cycles when the interneuron was silent (79.4±5.9% reduction, n=22 cells, K-W ANOVA $p<0.001$, Fig. 8B). The analysis showed that there was a strong positive correlation (Hill fit, $p<0.001$) between the magnitude of the synaptic inhibition (assessed as the IPSP integral, area of the IPSP under the baseline membrane potential) and the reduction in the firing probability of PCs, i.e. larger IPSPs from AACs more effectively reduced the PC spiking (Fig. 8C). We have estimated that an IPSP integral about 1 mV*ms is needed to achieve a 95% reduction in the PC firing probability under these conditions.

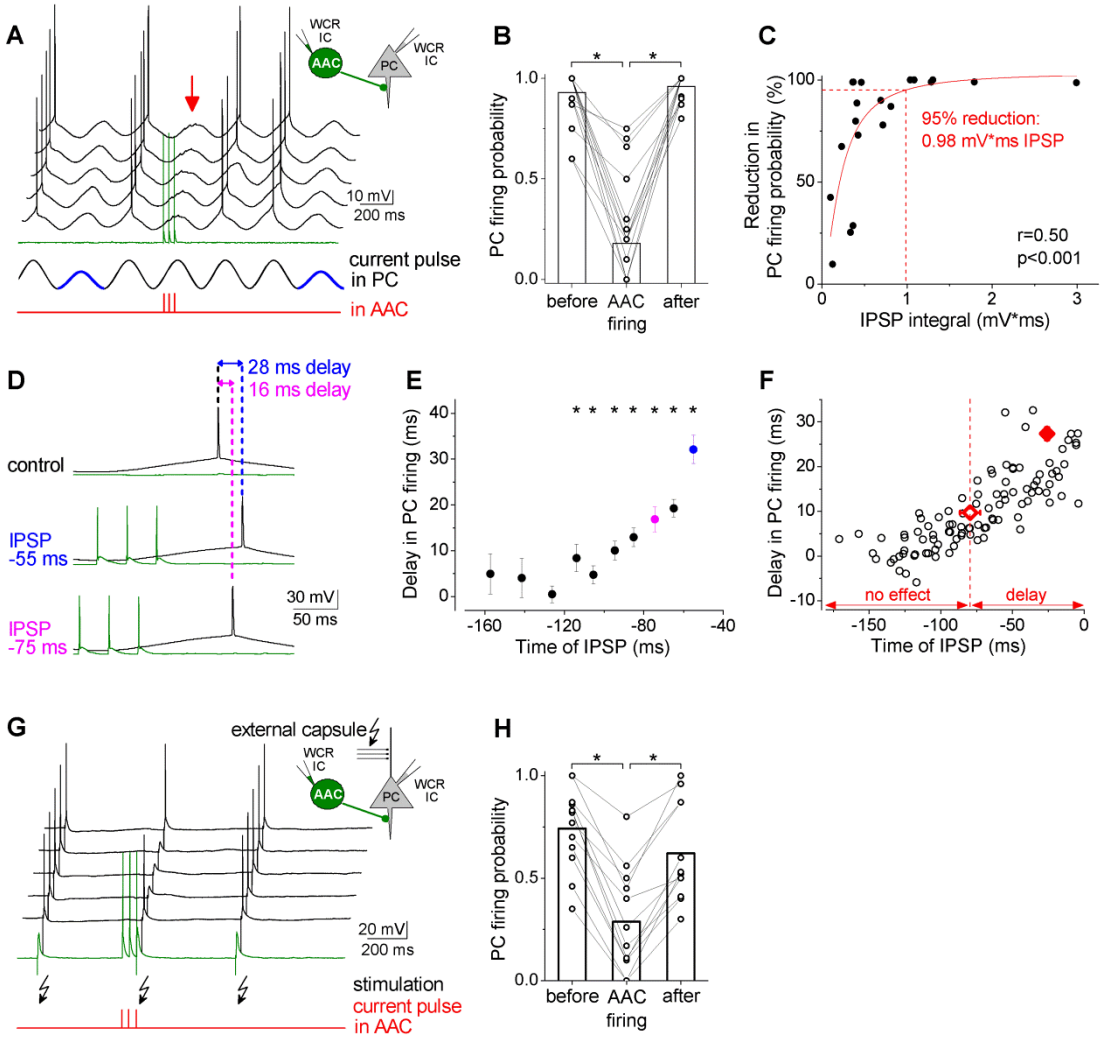

Figure 8. *AACs effectively control action potential generation in PCs.* A, Representative experiment testing the capability of AACs to inhibit spike generation in PCs. Sinusoidal current trains were injected into a PC to initiate firing and three action potentials were evoked at 30 Hz in the AAC 30-40 ms before the peak of the 4th cycle (for details see Materials and methods). Red arrow points to the IPSPs in the PC evoked by AAC spike trains. Voltage traces are offset for clarity. B, The firing probability of PCs evoked by current injection was significantly suppressed in the presence of the action potential train evoked in AACs (n=22, K-W ANOVA $p<0.001$). Columns represent mean. C, The relationship between the reduction in firing probability of PCs and the size of IPSPs (Hill function fit). D, Representative experiment testing AAC ability to postpone PC firing. The timing of the evoked action potential in an AAC was systematically shifted relative to the peak of the sinusoidal current injected into the PC. Note that a shorter interval between the presynaptic action potential train and the peak of the sinusoidal input caused a larger delay in PC spiking. E, The delay in PC firing as a function of the timing of synaptic inhibition in the pair shown in D. Asterisks indicate significant delay in firing compared to the peak of the cycle during the control period (paired sample Wilcoxon signed rank test $p<0.05$). F, Pooled data from 8 pairs. Filled and open diamonds show the average maximal delay and the average last time point with

significant delay in PC firing, respectively. G, Representative experiment testing the capability of AACs to suppress PC firing driven by excitatory postsynaptic potentials (EPSPs), which were evoked by electrical stimulation of fibers in the external capsule. Voltage traces are offset for clarity. H, The firing probability of PCs driven by EPSPs was significantly suppressed in the presence of the action potential train evoked in AACs (n=12, K-W ANOVA $p<0.001$). Columns represent mean.

Experimental and theoretical studies show that in addition to the spiking probability, inhibitory inputs can also prominently control the timing of action potential generation, which might play an important role in cortical network functions (Cobb et al., 1995, Kwag and Paulsen, 2009). To investigate how an AAC can affect the timing of PC firing and to determine the time window, in which this interneuron type can control the spike generation, IPSPs were evoked at different phases of the sinusoidal current injected into PCs (Fig. 8D, E). These experiments uncovered that depending on the timing of the inhibition, AACs could delay the generation of spikes in PCs with a minimum and maximum delay of 9.69±1.37 ms and 27.3±1.45 ms (n=8), respectively, defining a significant spike timing control within a time window of 20 ms. A controlling effect on PC firing by AACs was detected even if the peak of IPSPs was 79.5±7.03 ms before the peak of the sinusoidal current (Fig. 8F). Thus AACs in the BLA, in addition to their veto of action potential generation in PCs, can substantially control the timing of PC firing.

Although the sinusoidal current protocol is a reliable and controllable method to generate action potentials in PCs, spikes during physiological operation are evoked mainly by incoming integrated synaptic inputs (Epsztein et al., 2010; Svoboda et al., 1997). To test if AACs are also able to inhibit excitatory postsynaptic potential-evoked action potentials, we stimulated the fibers in the external capsule of the amygdala to induce synaptic input-driven single spikes in PCs (Fig. 8G). In the absence of AAC activity, the electrical stimulation of fibers readily evoked spikes in PCs, which was significantly reduced, when three action potentials were evoked in a single presynaptic AAC at 30 Hz (63.6±7.9% reduction, ANOVA $p<0.001$, n=12, Fig. 8H). These results imply that, depending on the timing of AAC activity, when AACs fire multiple action potentials, they can potently inhibit PC firing or delay their discharge.

4.2.4. Higher efficacy of inhibition is promoted by multiple synapses

To get deeper insights into the properties of synaptic organization underlying the potent inhibition between AACs and PCs, we first determined the number of putative synaptic sites between the recorded pairs using multichannel high resolution confocal microscopy. Specifically, we counted the number of AAC boutons that formed close appositions with the AIS of the recorded PC (visualized in red and green, respectively; Fig. 9A-D, see Materials and methods). This analysis uncovered that single AACs formed 8.4 ± 0.7 putative synapses on average with their postsynaptic partners (range: 2-16 boutons/AIS, total number of boutons: 201, n=24 pairs; Fig. 9J). We applied two approaches to confirm that the putative synaptic sites identified with confocal microscopy were synaptic junctions. First, for 6 cell pairs we visualized a cell adhesion molecule, neuroligin 2, which is present at GABAergic synapses, (Varoqueaux et al., 2004) to identify the functional contacts at the confocal microscopic level (Fig. 9E). This analysis revealed that in most instances (92%, n=44/48 boutons) immunolabeling for neuroligin 2 could be identified at the close appositions formed by AAC boutons with AISs of PCs. Second, we performed correlated light and electron microscopy in four cell pairs (Fig. 9F-I). We found that at the vast majority of boutons (96%, 28 out of 29 boutons), synapses could be unequivocally identified. These two approaches verified that in the overwhelming majority of cases, synaptic junctions underlie the contacts between AACs and PCs identified by light microscopy. Having determined the number of synaptic contacts at AAC-PC pairs, we next correlated this parameter with the physiological properties of these connections. We observed that the number of the contacting boutons correlated with the integral of the recorded IPSPs (Fig. 9K). Moreover, those AACs which contacted their partner with more synapses could inhibit the action potential generation more efficiently (tested in the protocol using sinusoidal current injection; Fig. 9L). We calculated that to achieve a 95% reduction in PC firing probability, simultaneous input from approximately 12 boutons was needed (Hill fit $p<0.001$, Fig. 9L). These results revealed the high efficacy of synaptic inhibition provided by AACs and showed that it substantially depends on the number of synaptic contacts targeting the AIS of PCs.

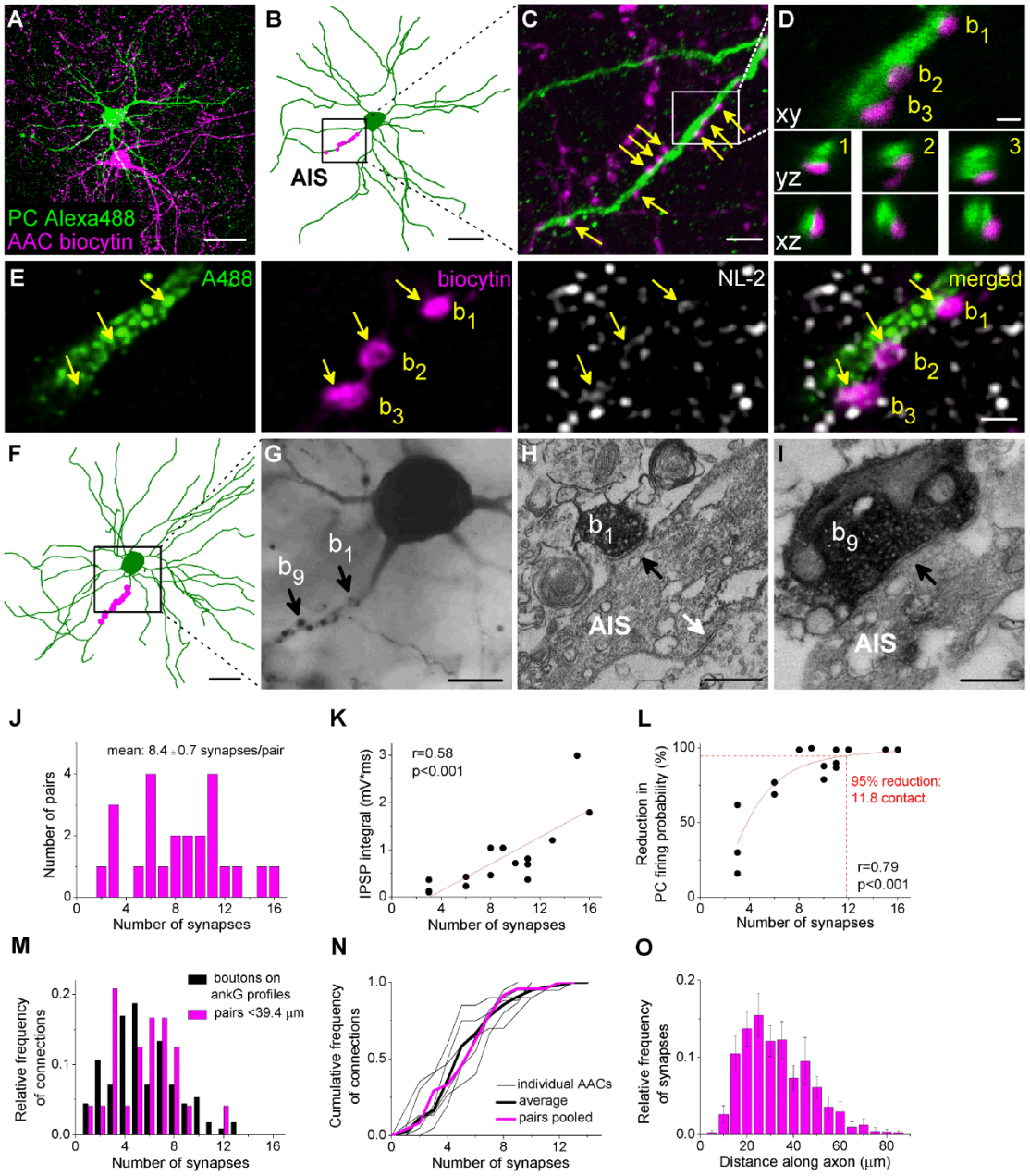

Figure 9. *AACs innervate PC AISs via multiple synaptic contacts*. A, Maximum z intensity projection of 3D confocal image of a representative pair. Biocytin in the AAC was visualized with streptavidin-conjugated Alexa 594 (magenta) and Alexa 488 in the PC (green). B, Neurolucida reconstruction of the postsynaptic PC (green) with the putative synaptic sites marked in magenta. C, High power magnification of the maximum z intensity projection image of the region indicated in B, showing a part of the AIS of the postsynaptic PC (green), which receives multiple boutons (arrows) from the presynaptic AAC (magenta). D, 3D analysis of confocal images of three boutons enclosed in the box in panel C shows close appositions of the pre- and postsynaptic structures. E, Verification of the functional synapses at the light microscopic level using neuroligin-2 staining. F-I, Analysis of the presence of synaptic contacts between the recorded pairs using correlative light and electron microscopy. F, Neurolucida reconstruction of

another AAC-PC pair. G, Light micrograph of the boxed region in panel F. H-I, Electron micrographs of two boutons of the presynaptic AAC indicated in panel G are shown, both of which form synaptic contacts with the AIS of the postsynaptic PC. The white arrow in H indicates an unlabelled bouton synapsing on the biocytin-labeled AIS. J, Distribution of the number of the boutons obtained by light microscopy (201 putative synaptic contacts from 24 pairs). In 28 cases, the presence of a synapse was verified using electron microscopy. K, Relationship between the integral of the summed IPSPs evoked by 3 action potentials and the number of synapses made by the AAC. L, Correlation between the effect of AACs on PC firing tested with a sinusoidal protocol (see Fig. 8A-C) and the number of axon-AIS synapses (Hill fit $p<0.001$). M, Distribution of the number of boutons from *in vitro* filled AACs on ankyrin G-labeled profiles (n=6 AACs, 616 contact sites on 112 ankyrin G-immunostained profiles, black) and AAC-PC pairs. The analysis of the varicosities was restricted to the average length obtained from the ankyrin G staining (39.4 μm) (n=24 pairs, 134 boutons, magenta). N, Cumulative distributions of bouton numbers on randomly-sampled individual ankyrin G-immunostained profiles taken from 6 filled AACs (each thin black line represent data from single AACs). The average of these distributions (thick black line) compared with the pooled data of the paired recordings shows no difference (K-S test $p=0.76$). O, Spatial distribution of the synapses along the axon obtained in paired recordings (n=24 pairs, 201 boutons). 0 μm marks the origin of the axon at the soma, data represent mean±s.e.m. Scale bars (in μm): A, B and F 30; C 5; D, E 1; G 10; H, I 0.25.

The variability in the bouton number from a single AAC to a single PC (2-16 contacts, coefficient of variation, CV=0.45) raises the question of whether there are AACs that preferentially target their postsynaptic partners via numerous synapses, while others only make a few contacts. This would imply that some AACs might have more profound effects on PC spiking during network operation than others. Or, alternatively, the large variability in the number of boutons contacting AISs characterizes the output of each AAC. To address this question, we counted the number of boutons of in vitro labeled AACs forming close appositions on 10-20 individual, randomly-sampled ankyrin G-stained AISs. We found that each AAC contacted different AISs with a variable number of varicosities ranging from 2 to 14 (5.5±0.25, n=616 boutons from 6 AACs onto 112 AISs, Fig. 9M), with similar variance in the bouton number (CV range: 0.36-0.67). Since the length of the ankyrin G-labeled profiles in slices was 39.4±0.7 μm (n=112), we re-analyzed the data obtained in pairs by restricting the analysis to those boutons present at the proximal part of the axon no further than 39.4 μm from the soma. This measurement allowed us to compare directly the variance in the number of boutons

targeting single AISs found in ankyrin G-labeled material with those obtained in paired recordings. We found no difference in the distributions of the bouton numbers at AISs using these two methods (K-S test p=0.76, Fig. 9N). Thus, we confirmed that our paired recordings reliably characterize the population of AAC outputs and, more importantly, AACs form a homogenous population regarding the manner in which they contact PCs, innervating their targets via a variable number of boutons.

We also observed that the AAC boutons along the AISs were not evenly distributed. Approximately 60% of all varicosities were found between 20 and 40 μm from the soma (Fig. 9O). Importantly, the spatial distribution of boutons of AACs was indistinguishable from that we found with the reconstruction of the GABAergic input *in vivo* (Fig. 4D; K-S test, p=0.57). This observation suggests that a specific region along the AIS is preferentially innervated by AACs.

4.2.5. GABAergic innervation of AISs overlaps with the site of the action potential generation in PCs

Our *in vitro* and *in vivo* observations that GABAergic inputs onto AISs of PCs prefer a specific area along the axon close to the soma raise the question of how this inhibitory input relates to the site of action potential generation. If the innervated region overlaps with the site, where the threshold for action potential generation is the lowest, then AACs could have a role primarily in the control of PC spiking. However, if the area along the AIS receiving the majority of GABAergic innervation is different from the site, where the threshold for action potential generation is the lowest, then AACs may rectify PC spiking by blocking action potential propagation either towards the soma or towards the distal axon depending on the spatial relationships of the two sites. To distinguish between these possibilities, we determined where the action potentials are generated either by simultaneous whole-cell recordings from the soma and axonal bleb of the same PCs (Shu et al., 2006) or by simultaneous recordings from the soma in whole-cell mode and along the intact axon in loose patch mode (Clark et al., 2005, Palmer et al., 2010). We evoked an action potential in the cell by injecting a square current pulse (0.5-1.5 nA, 10 ms) via the somatic electrode and measured the evoked action potentials at both recording sites (Fig. 10A, B). After the recordings the cell was

visualized and reconstructed in 3D and the distance of the bleb or the axonal recording sites from the soma was measured (see Materials and methods).

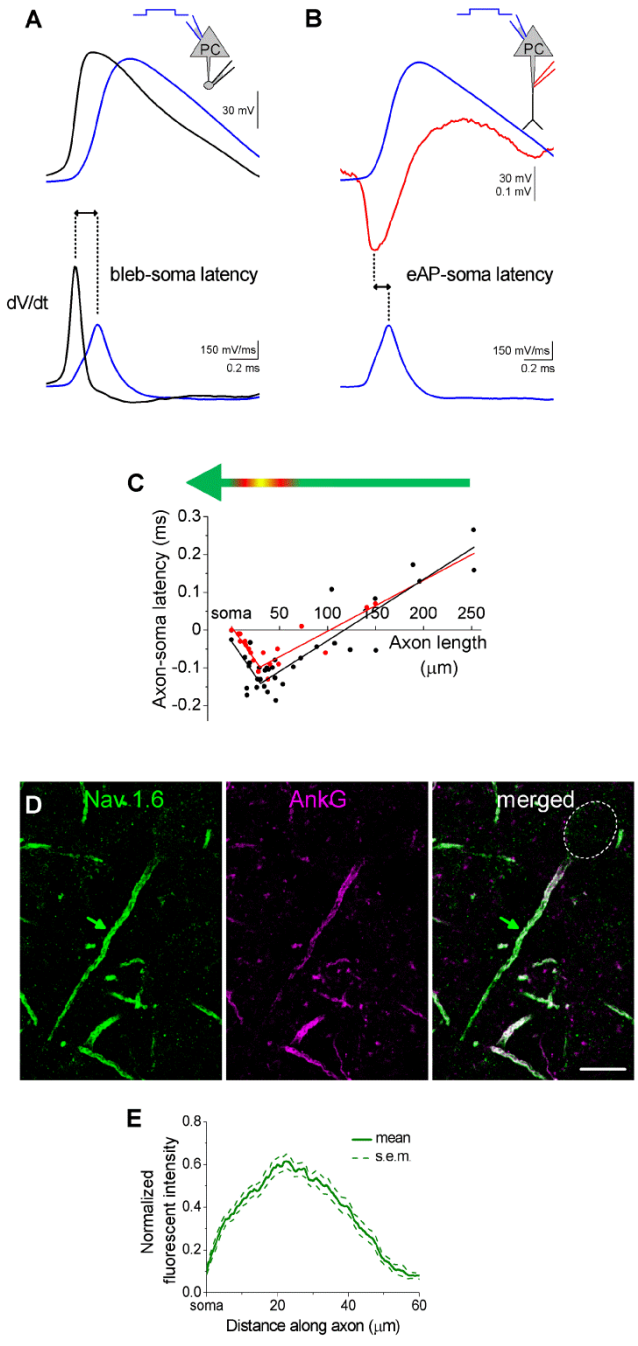

Figure 10. *Initiation zone for action potentials in PCs in the BLA*. A, Representative recordings obtained simultaneously at the soma and the axonal bleb in whole cell mode. Top: raw data; bottom: first order derivative. The peaks of the first order derivatives were used to calculate the delay between the action potentials recorded at the two sites. B, Representative traces of an action potential recorded at the soma in

whole cell mode and simultaneously at the axon in loose patch mode. Top: raw data; bottom: first order derivative of the somatic action potential. The peak of the first order derivative and the peak of action potential detected extracellularly were used to calculate the delay between the action potentials recorded at the two sites. C, The latency difference of the action potentials recorded at the two sites plotted as a function of the distance between the corresponding recording sites. Bilinear fit minimum point obtained in the bleb recordings and in extracellular detection of action potentials was 30.5±10.9 μm (black) and 29.5±8.5 μm (red), respectively. D, Double staining for Nav 1.6 and ankyrin G in the BLA. E, Normalized fluorescence intensity of the Nav 1.6 immunostaining as a function of the distance along the axon (n=20 AIS). Scale bar: B, D, 10 μm.

We compared the timing of the action potentials at the two recording sites and found that the difference in the spike timing was dependent on the distance of the axonal recording site from the soma (Fig. 10C). A bilinear fit to the data showed that the maximum difference in the axon-soma latency, which corresponds to the site of action potential generation, was at ~30 μm from the soma along the AIS (in bleb recordings: 30.5±10.9 μm, in experiments recorded action potentials extracellularly: 29.5±8.5, Fig. 10C).

To test this result obtained using dual patch recordings and have an independent estimate for the site of action potential generation, we investigated the distribution of the Nav 1.6 subtype of voltage-gated Na^+ channel, which is critical for the initiation of action potentials (Hu et al., 2009). Using confocal microscopy, we measured the fluorescence intensity of the immunolabeling for Nav 1.6 along the AIS as defined by ankyrin G-labeling (Fig. 10D, E, n=20 AIS, profile length: 61.6±1.6 μm). We found that the most intense labeling for Nav 1.6 along the AISs (20% of the highest intensity) was between 16.2-31.9 μm from the soma, which corresponds to the action potential generation site determined by the electrophysiological recordings.

As the site of the action potential generation in PCs in the BLA closely matches the area preferentially targeted by AACs, we propose that AAC output synapses are optimized to control Na^+ channel opening and thus PC firing.

4.2.6. AACs strategically position their synapses at the site of action potential generation

Our morphological analysis of the connectivity between AACs and PCs showed that there was a great variability in the number of synaptic contacts, ranging from 2 to up to 16 connections (Fig. 9J). This raises the question of whether the synapses originating from individual AAC-PC connections with different bouton numbers distribute evenly along the entire AIS, or, alternatively, tend to target the site of action potential generation, i.e. optimizing the efficacy of their synaptic inhibition.

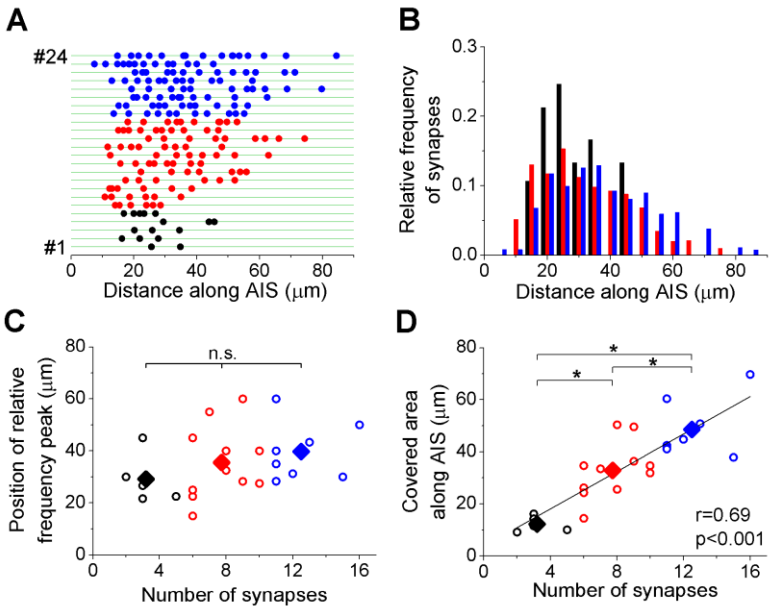

Figure 11. *AACs in the BLA preferentially target the action potential initiation zone.* A, Spatial distribution of the boutons along the AISs obtained in individual AAC-PC pairs. Each row represents a single AIS taken from AAC-PC pairs (n=24) that are arranged as a function of increasing bouton number. Each bouton is shown as a colored dot on each AIS (green). The pairs were categorized into three groups according to the number of contacts (black dots, 1-5 contacts; red dots, 6-10; blue dots, 11-16). B, The relative frequency distributions of boutons obtained in the three groups show a large correspondence. C, The position of peak values of the relative frequency distributions showed no difference among the three groups (p=0.34, ANOVA). D, The number of the boutons and the covered area along the AIS (e.g. the distance between the first and last boutons) significantly differed between the three groups (p<0.001, ANOVA).

To address this question, we examined the bouton distribution along the AIS as a function of the number of synapses. We divided the pairs into three groups based on the number of the boutons on single AISs (1-5, 6-10 or 10-16 contacts), and compared the spatial distribution of the boutons along the AISs among the groups (Fig. 11A). The analysis showed that all groups tended to concentrate their synapses at the action potential generation zone (Fig. 11B, C). Importantly, those cells contacting their partners with a few boutons restricted their output synapses to the estimated spike generation area. In contrast, the innervations of those AACs, which gave rise to more boutons, outreached the site of action potential generation, covering a significantly broader axonal area (Fig. 11D, ANOVA $p<0.001$). These data imply that AACs maximize their inhibitory efficacy by strategically positioning their synapses on the site of the action potential generation.

In the next part of the study we extended our investigations to the other two interneuron types targeting the perisomatic region of PCs and compared the electrophysiological and morphological properties of the inhibition provided by CCK/CB_1BCs and PVBCs in the BLA.

4.3. Part III: Comparison of the physiological and morphological properties of the output synapses of CCK/CB_1BCs and PVBCs

4.3.1. CCK/CB_1BCs and PVBCs provide inhibitory input onto PCs with similar properties

To compare the basic properties of inhibitory connections provided by the two BC types, IN-PC paired recordings were carried out using slices prepared from CCK-DsRed or PV-eGFP mouse lines. First, the firing characteristics of the presynaptic IN was tested using positive and negative square current pulses with increasing amplitude. CCK/CB_1BCs showed accommodating firing pattern (accommodation ratio: 5.37±0.57) having 33.51±3.54 Hz maximal firing rate, slow afterhyperpolarizing potentials (AHP 50% decay: 88.71±14.32 ms) and marked sag in the voltage responses evoked at negative potentials (relative sag amplitude: 0.21±0.05) (n=14, Fig. 12A). In contrast, PVBCs had fast spiking phenotype (113.91±6.22 Hz) with only a slight accommodation in their firing (1.55±0.08). They were characterised by a marked fast afterhyperpolarizing potentials (AHP 50% decay: 20.55±1.91 ms) and no or only moderate sag in their voltage responses at negative potentials (relative sag amplitude: 0.11±0.01) (Fig. 12C). The synaptic coupling between the IN and PC was tested by evoking three action potentials in the IN and measuring the spike-locked responses in the postsynaptic PC (Fig. 12B and D). The probability to find a synaptically connected neighbouring (<200 μm) PC was high in both cases (85% for CCK/CB_1BCs and 81% for PVBCs, respectively, n=40 CCK/CB_1BC and n=37 PVBC).

To test the effect of INs on the firing of PCs, it was essential to use an intrapipette solution with a Cl^- concentration close to the physiological values. To determine the actual reversal potential for Cl^- in the PCs at the output synapses of BCs, we first measured monosynaptic PSPs at different membrane potentials in the postsynaptic neuron using perforated patch mode. Then, we made the same measurements in whole-cell mode using 4 mM Cl^- containing intrapipette solution (Fig. 12E and F, for details see Materials and Methods). By plotting the postsynaptic response magnitudes as a function of the holding potential values, we could not find significant difference between the estimated reversal potentials of the PSPs recorded in perforated patch and whole-cell mode (CCK/CB_1BC p=0.296, PVBC p=0.403, Fig.

12G). Therefore, in the further experiments, we used the 4 mM Cl^- containing intrapipette solution. Furthermore, we found that the reversal potential of the PSPs arriving from both IN types were at more hyperpolarized values than the resting membrane potential of the PCs. Based on this observation, we concluded that the net effect of these INs on their postsynaptic PC is inhibitory ($p<0.001$, Fig. 12G).

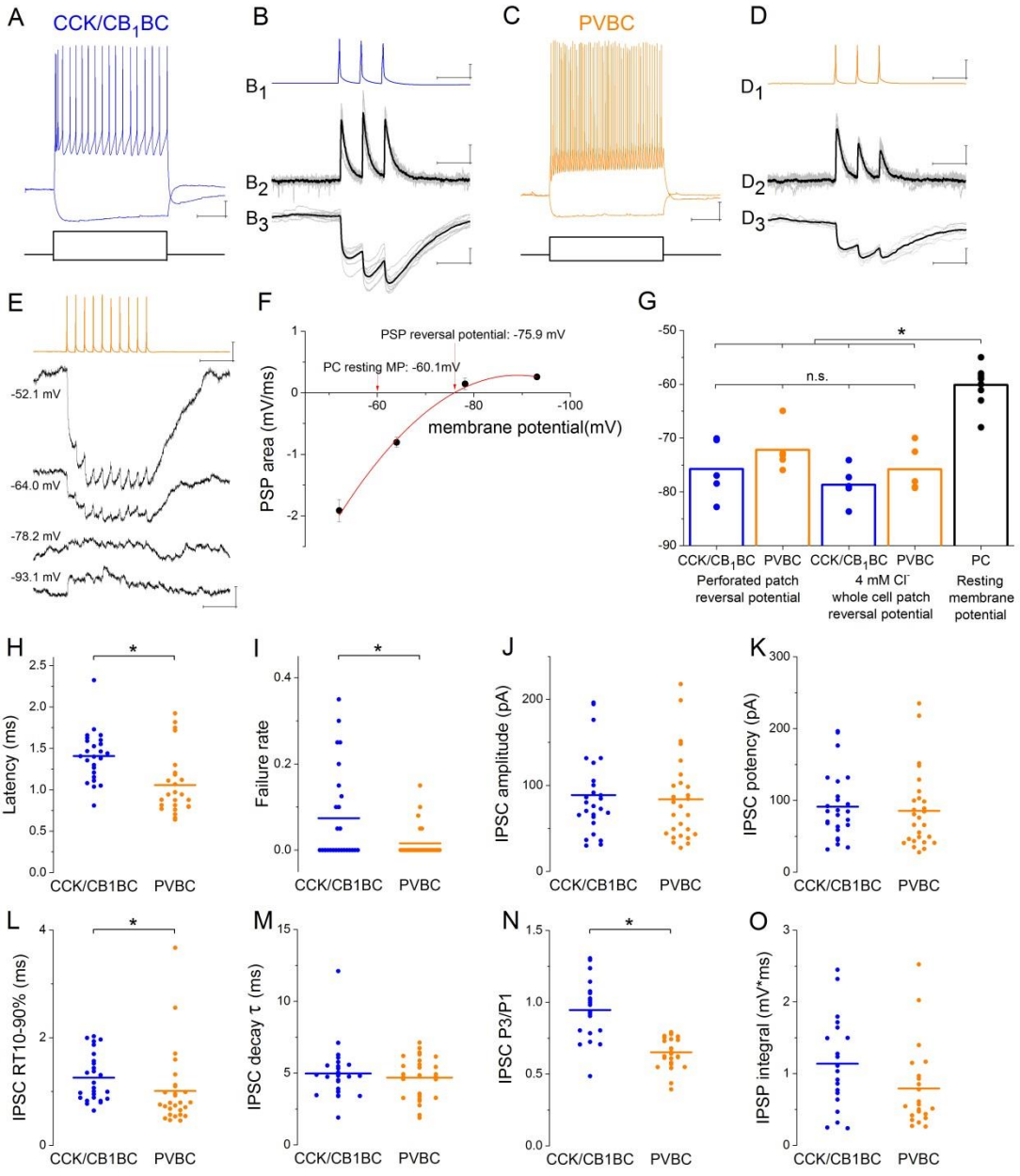

Figure 12. *Similar basic electrophysiological properties characterize the inhibitory connections in CCK/CB1BC- and PVBC-PC pairs.* Representative firing pattern of a CCK/CB_1BC (A, 400, -100 pA) or a

PVBC (C, 300, -100 pA) upon step current injections. Representative postsynaptic current (PSC, B_1, D_1) and postsynaptic potential (PSP, B_2, D_2) recordings in a CCK/CB_1BC-PC (B) or in a PVBC-PC pair (D) in response to 3 action potentials evoked at 30 Hz. Ten superimposed consecutive traces in grey, average in black. E, PSPs recorded in a PC at different membrane potentials in gramicidin-based perforated patch recordings upon a train of 10 action potentials evoked at 40 Hz in a presynaptic IN. F, The integral of the summed PSPs was calculated at each membrane potential and fitted with a second order polynomial curve to determine the reversal potential of the responses. G, Comparison of the estimated reversal potential of PSP recorded in perforated patch and whole-cell patch clamp mode using 4 mM Cl^- intrapipette solution and the resting membrane potential of PCs revealed the inhibitory nature of the connection. Comparison of the basic properties of IPSCs (H-N) and IPSPs (O) at the output synapses of CCK/CB_1BCs and PVBCs recorded in whole-cell mode. Scales: A and C: 10 mV, 200 ms; B and D x: 50ms, B_1 and D_1 y: 30 mV, B_2 and D_2 y: 50pA, B_3 and D_3 y: 1 mV , E: 0.5 mV (PC), 30 mV (IN) and 100 ms.

Next, we compared the kinetics of IPSCs and IPSPs of the output synapses of the two IN types recorded in whole-cell mode (Table 1, Fig. 12H-O). Importantly, the latency of the signals indicated the monosynaptic nature of the connections from both cell types, however, IPSCs from PVBCs arrived with significantly shorter latencies than those from CCK/CB_1BCs onto PCs (Fig. 12H). Moreover, the failure rate of the events was also significantly higher in the case of CCK/CB_1BCs (Fig. 12I). Interestingly, the potency and -despite the significant difference in the failure rate- the amplitude of IPSCs were not different (Fig. 12J, K). The events arriving from PVBCs had faster rise time but similar decay time constant (Fig. 12L, M). There was a significant difference in the short-term plasticity of the signals: IPSCs arriving from PVBCs onto PCs showed a marked depression, while those originating from CCK/CB_1BCs showed sometimes marked facilitation, and only a very slight depression on average (Fig. 12N). Importantly, the area of IPSPs evoked by the two BCs in response to 3 action potentials at 30 Hz was not significantly different (Fig. 12O). These data revealed that the basic properties of the inhibitory connections originating from CCK/CB_1BCs and PVBCs are similar and may have the same potency to inhibit the postsynaptic PC spiking.

Table 1. Comparison of the basic properties of postsynaptic responses at CCK/CB_1BC-PC and PVBC-PC connections. Data presented as median, minimum and maximum values. Significant differences are shown in bold.

	CCK/CB_1BC-PC	n	PVBC-PC	n	p (Mann-Whitney U test)
IPSC latency (ms)	1.40 (0.81-2.32)	26	0.94 (0.64-1.92)	27	**<0.001**
IPSC failure rate	0 (0-0.35)	26	0 (0-0.15)	27	**0.031**
IPSC amplitude (pA)	78.19 (30.07-196.39)	26	75.79 (27.56-217.89)	27	0.624
IPSC potency (pA)	84.51 (31.61-196.39)	25	75.79 (27.56-235.00)	27	0.486
IPSC rise time 10-90% (ms)	1.11 (0.65-2.03)	26	0.79 (0.46-3.67)	27	**0.002**
IPSC decay τ (ms)	4.81 (1.90-12.10)	25	4.85 (1.88-7.12)	25	0.851
IPSC P3/P1	0.95 (0.49-1.31)	20	0.64 (0.39-0.79)	25	**<0.001**
IPSP integral (mV*ms)	1.07 (0.24-2.45)	20	0.56 (0.26-2.52)	22	0.071

4.3.2. CCK/CB_1BCs and PVBCs inhibit PC spiking with similar efficacy

To compare how efficiently these two IN types can control the firing of their postsynaptic partners, the same experimental protocol was carried out as in case of AACs (shown in Fig. 8A, for details see Materials and Methods). Briefly, firing in PCs was evoked by injecting sinusoidal currents into the cell body, and the firing probability of the PC was measured with and without the presence of inhibitory input from a presynaptic IN (Fig. 13A, B). When we compared the inhibitory efficacy of CCK/CB_1BCs and PVBCs, e.g. the probability that they can prevent PC firing, we could not find any significant difference: both IN types could silence their postsynaptic partners with ~75% probability on average (CCK/CB_1BC: 76.2±5.8%, n=25, PVBC: 74.3±5.8%, n=25, p=0.785, M-W test, Fig. 13 C). However, in both cell types there were INs, which could veto PC firing with very high probability (>95% inhibitory efficacy, 44% of CCK/CB_1BCs and 44% of PVBCs, n=11 and 11, respectively), whereas others had only a weak inhibitory efficacy (< 50% inhibitory efficacy, 24% of CCKCB_1/BCs and 24% of PVBCs, n=6 and 6, respectively).

In addition, we observed that IPSPs, which failed to veto PC firing, could alter the timing of the spike, delaying it with up to 38.5 ms (Fig. 13D-F). The maximal delay caused by the two IN types was not significantly different (CCK/CB$_1$BC: 22.40±4.14 ms, n=7, PVBC: 23.76±3.16 ms, n=6, p=0.720, M-W test, Fig. 13F).

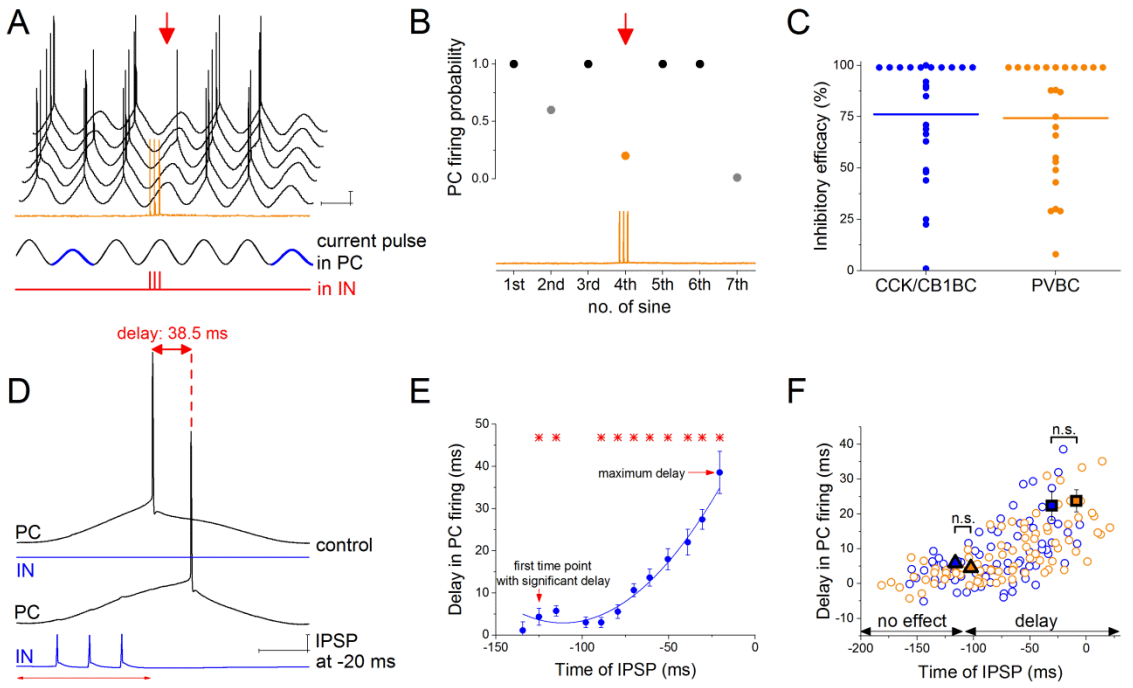

Figure 13. *CCK/CB$_1$BCs and PVBCs inhibit PC firing with similar efficacy*. A, Representative experiment for testing the capability of an IN to control spike generation in PCs. Sinusoidal current trains were injected into a PC to initiate firing and three action potentials were evoked at 30 Hz in the presynaptic IN 30-40 ms before the peak of the 4th cycle (for details see Materials and Methods). Red arrow points to the cycle, when the presynaptic IN was stimulated. Voltage traces are offset for clarity. B, Summary data of experiments shown in panel A: the firing probability of the PC was significantly suppressed within the cycle when the action potential train was evoked in the presynaptic IN. C, Comparison of the inhibitory efficacy of CCK/CB$_1$BCs and PVBCs. The inhibitory efficacy shows the probability of the suppression of action potential generation in the PC by IN firing (i.e.: 1- (PC firing probability during the control sinusoid cycles - firing probability when the IN is stimulated)). D, Representative experiment for testing INs ability to postpone PC firing. The timing of the evoked action potential in an IN was systematically shifted relative to the peak of the sinusoidal current injected into the PC. E, The delay in PC firing as a function of the timing of synaptic inhibition in the pair shown in D. Asterisks indicate significant delay in firing compared to the peak of the cycle during the control period (paired sample Wilcoxon signed rank test $p<0.05$). F, Pooled data from 7 CCK/CB$_1$BC and 6 PVBC pairs. Squares show the average maximal delay and triangles show the average last time point with

significant delay in PC firing. Color codes are the same as in panel C (blue: CCK/CB_1BCs, orange: PVBCs). Scales: A: 10 mV, 200 ms; D: 10 mV, 50ms.

We tested the importance of the timing of IPSPs by stimulating the IN at different time points relative to the peak of the sinusoid current evoking action potentials in the PC and measuring the caused delay in PC firing. We found that both cell types could control the firing of PCs in a ~110 ms time window (CCK/CB_1BC: -116.21±14.47 ms, PVBC: -102.41±18.58 ms, p=0.943, M-W test, Fig. 13F), with increased delaying effect in PC firing as the IPSP arrived closer to the sinusoid cycle peak (i.e. to the theoretical time of the spike).

These results together showed that inhibitory inputs from CCK/CB_1BCs and PVBCs had the same powerful potential to veto or control the timing of PC spiking.

4.3.3. PV and CCK/CB_1R+ INs target the same somato-dendritic compartments of PCs

To get an insight into the structural basis of the recorded IN-PC connections, the cells were loaded during the recordings with biocytin and a green Alexa dye (Alexa 488), respectively. With dual immunofluorescent labeling the pre- and postsynaptic cells were revealed in two different colors, enabling the detailed examination of the potential contact sites along the entire somato-dendritic surface using high resolution 3D confocal microscopy (Fig. 14A-D). Correlated light and electron microscopic investigations showed that 85.4% of the potential contact sites (based on the confocal microscopic analysis) formed symmetrical synaptic contacts on the soma (87.5%, n=18 terminals from 6 pairs, Fig. 14E and G) and dendrites (83.3%, n=16 terminals from 6 pairs, Fig. 14F and G) of the postsynaptic PCs. We found that the diameter of the targeted dendrites was variable: both cell types established synapses on thick (> 1 μm, CCK/CB_1BCs n=10, PVBCs n=6), presumably proximal and thin (< 0.5 μm, CCK/CB_1BCs n=12, PVBCs n=10), presumably distal dendritic segments as well (Fig. 14H, p=0.627, K-S test).

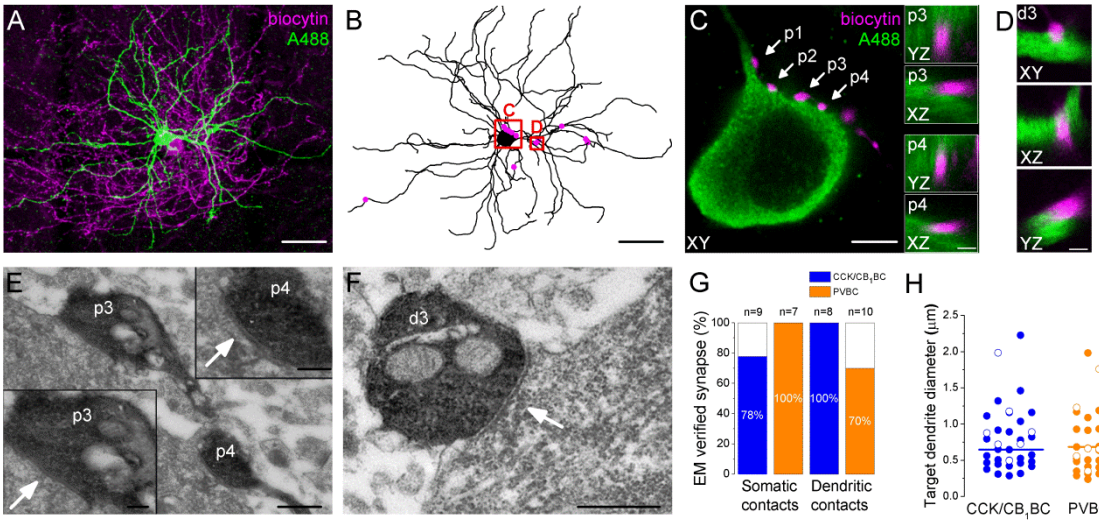

Figure 14. *Morphological analysis of the synaptic connections of recorded cell pair*. A, Maximum z intensity projection of a 3D confocal image of a representative pair. Biocytin in the PVBC was visualized with streptavidin-conjugated Alexa 594 (magenta), while Alexa 488 in the PC is shown in green. B, Neurolucida reconstruction of the postsynaptic PC with the contact sites originated from PVBC indicated by magenta. C, High power magnification of the perisomatic region shown in B, which receives multiple boutons (arrows, perisomatic contact #1-4: p1-p4) from the presynaptic PVBC (magenta). Insets: 3D analysis of confocal images of p3 and p4 boutons show close appositions of the pre- and postsynaptic structures. D, High power magnification 3D confocal images of the region indicated in panel B, showing a close apposition between a dendrite-targeting bouton (d3) and a PC dendrite. E, Electron micrographs of p3 and p4 shown in panel C. In both cases synaptic contacts with the soma of the postsynaptic PC (arrows) are visible. F, An electron micrograph of d3 shown in panel D, confirming the presence of synaptic contact on the dendrite of the postsynaptic PC (arrow). G, Ratio of close appositions observed at the confocal microscopic level forming synaptic contacts confirmed with electron microscopy. H, Analysis of the diameters of the target dendrites measured on the electron micrographs shows that both IN types form synapses on large diameter, probably proximal and small diameter, probably distal dendritic segments. Open circles show contacts on the recorded, postsynaptic PCs, filled dots represent synapses on random targets of the labeled INs in the sample. Scales (in µm): A and B: 50; C: 5, insets and D: 1; E: 0.5, insets: 0.2; F: 0.5.

The analysis of the bouton distribution of 39 CCK/CB_1BC-PC and 29 PVBC-PC pairs with confocal microscopy showed that the number of contacts is variable at the connections between the two IN types and PCs, ranging from 1 to 25 (Fig. 15, Table 2). To calculate the number of the boutons targeting the perisomatic region of the postsynaptic PC, we defined the border of the perisomatic region in each dendrite of the

postsynaptic PC indirectly with the following method. As the Kv2.1 immunostaining showed that the extent of the perisomatic region along the dendrites correlates with the base diameter of the given dendrite (Fig. 3I), we could categorize each contact as perisomatic region- or dendrite targeting terminals by measuring the distance of the bouton from the soma and the basal diameter of the targeted dendrite and using the 95% confidence intervals of the correlation shown in Fig.3I.

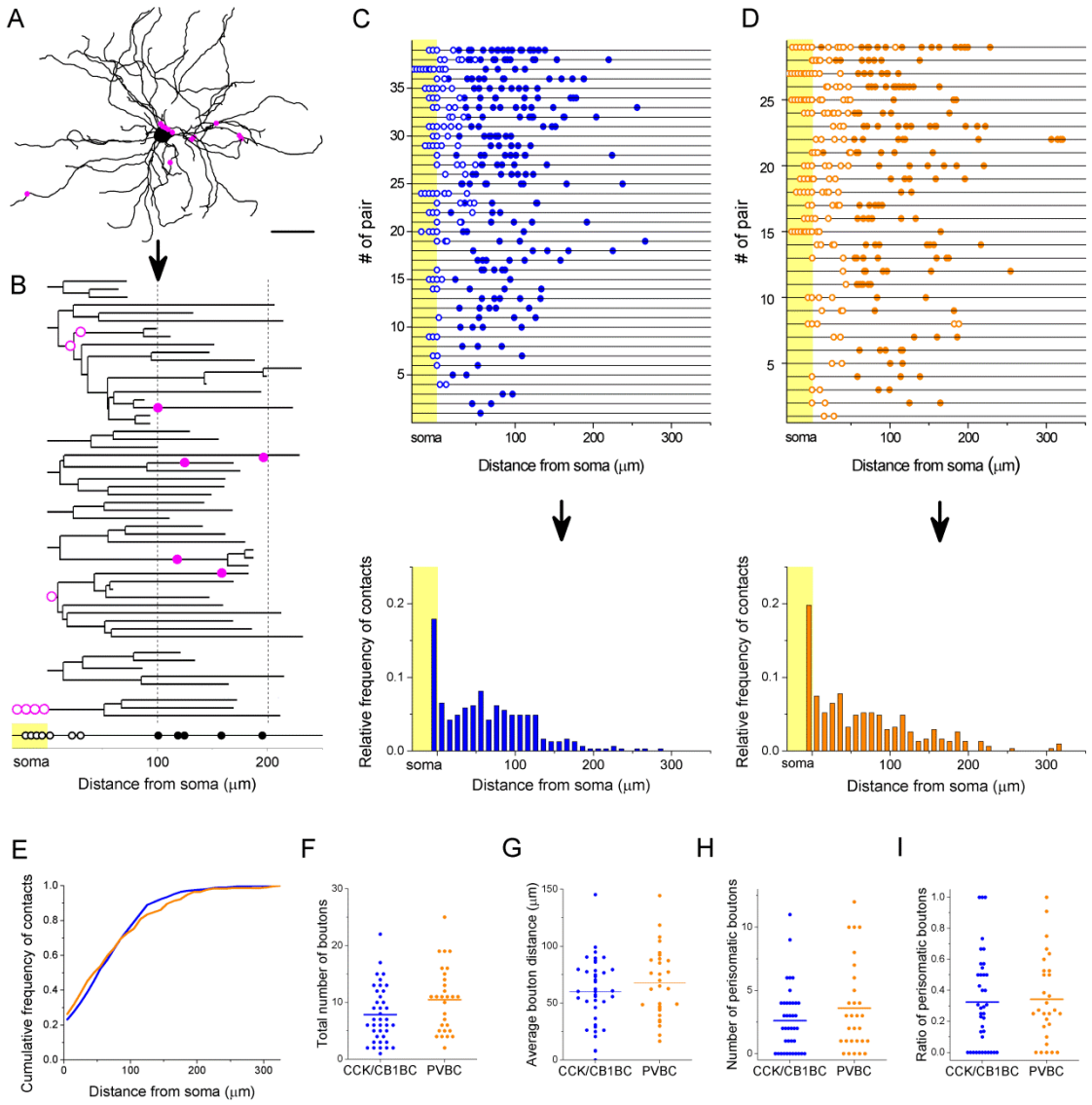

Figure 15. *Similar structural basis underlying the connections established by CCK/CB$_1$BCs and PVBCs.* A, Neurolucida reconstruction of the postsynaptic PC with the contact sites (same cell as in Figure 14 panel B). B, Dendrogram of the reconstructed postsynaptic PC (same as in panel A) showing the contact sites on the perisomatic region (open magenta dots) and along dendritic processes (filled magenta dots). Bottom: schematic visualization (dendrogram) of the innervation pattern compressed along a single

horizontal line showing somatic boutons in the yellow area and dendritic boutons along the line indicating their distance from the soma. Open dots mark perisomatic region targeting boutons, filled dots mark dendrite targeting terminals. C and D, Schematic innervation patterns of the reconstructed 39 CCK/CB_1BC-PC and 29 PVBC-PC pairs, respectively. Bottom: spatial distribution of the contacts, data from all pairs pooled together. E, Comparison of the cumulative distribution of the contacts on PCs from the two IN types show no difference in the innervation patterns (two sample K-S test p=0.453). F-I, Comparison of the properties of CCK/CB_1-PC and PVBC-PC connections revealed no difference. Scale in A: 50 μm

The comparison of the target distribution of the two BC types revealed no difference (Fig.15C,D,E, Table 2): CCK/CB_1BCs and PVBCs innervated their postsynaptic partners with similar number of boutons (Fig. 15F), moreover, the average distance of the innervation along the somato-dendritic tree (Fig.15G), the number of the contacts established on the perisomatic region (Fig.15H) and the ratio of perisomatic contacts in all boutons was also not different (Fig. 15I). There was only a small population of INs, which restricted their innervation exclusively to the perisomatic region (e.g. ratio of perisomatic contacts =1, 7.69% of CCK/CB_1BCs and 3.44% of PVBCs, n=3 and 1, respectively, Fig. 15I), but most of the cells also contacted the dendrites with several synapses (92.3% of CCK/CB_1BCs and 93.1% of PVBCs, n=36 and 27, respectively). Importantly, the ratio of the perisomatic boutons was variable and showed a continuous distribution across the populations of both cell types.

Table 2. Morphological properties of CCK/CB_1BC-PC and PVBC-PC connections. Data presented as median, minimum and maximum values.

	CCK/CB_1BC (n=35)	PVBC (n=25)	p (Mann-Whitney U test)
Total number of boutons	7 (1-22)	11 (2-25)	0.064
Average bouton distance (μm)	60.25 (0-145.31)	64.95 (16.48-144.43)	0.449
Number of perisomatic boutons	2 (0-11)	3 (0-12)	0.336
Ratio of perisomatic boutons	0.29 (0-1)	0.27 (0-1)	0.680

By analysing the potential relationships between the electrophysiological properties of inhibitory connections and their underlying structural features, we found that the potency of IPSCs is correlated with the number of the perisomatic boutons, and their average distance from the soma, but not with the total number of contacts (n=20-21 CCK/CB_1BC and PVBC pairs, Fig. 16 A-C). The area of the IPSPs was correlated with the number of the perisomatic contacts only in the case of PVBCs, although CCK/CB_1BCs also showed a strong tendency in this analysis (p=0.052, Fig.16D). Moreover, the inhibitory efficacy of both INs showed better correlation with the number of perisomatic synapses than the total number of synapses (Fig. 16 G-H). These results showed that CCK/CB_1BCs and PVBCs innervate their postsynaptic partner with similar pattern, targeting somatic, proximal- and distal dendritic compartments with multiple synapses. Importantly, the most determining factor of their inhibitory efficacy is the number of the contacts established on the perisomatic region of PCs.

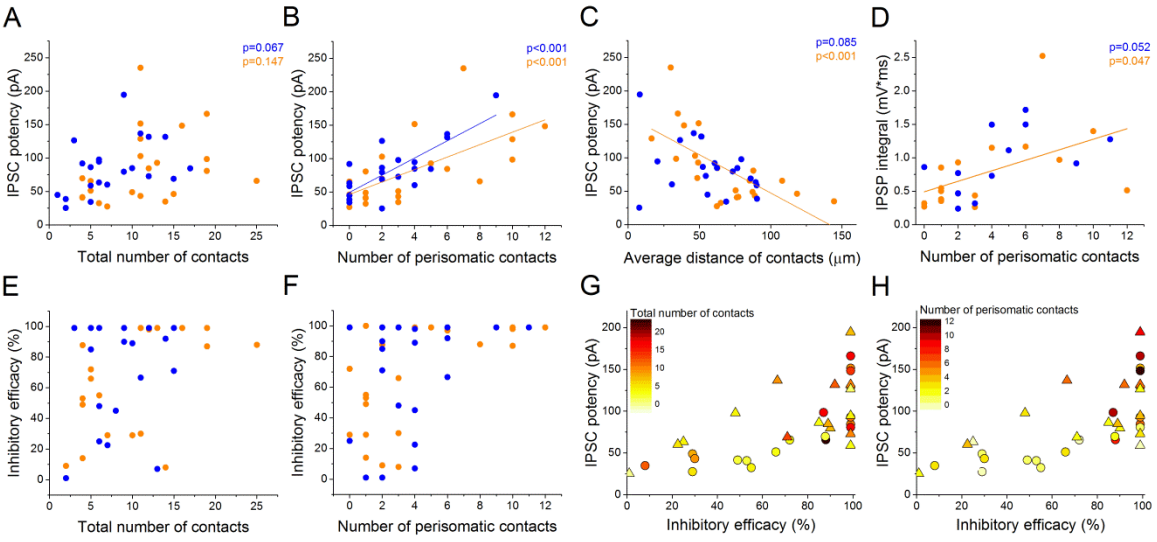

Figure 16. *The number of the perisomatic contacts is the main determinant of inhibitory efficacy in BC-PC pairs.* A-F, Relationship between the structural and electrophysiological properties of the output synaptic contacts recorded in CCK/CB_1BC-PC (blue) and PVBC-PC (orange) pairs. Linear correlation between data sets is labeled with a solid line. Significance levels of correlations are indicated in the top right corner of the plots. I-K, Relationship between the inhibitory efficacy and IPSC potency, plotted together with the total number (G) and number of perisomatic contacts (H) as a heat map. Note that the inhibitory efficacy and potency of the IPSCs show more dependence on the number of the perisomatic contacts than in the total number of boutons. Circles label PVBCs, triangles mark CCK/CB_1BCs.

4.3.4. Innervation pattern of single CCK/CB$_1$BCs and PVBCs is variable on different postsynaptic cells

The analysis of the innervation patterns of both types of perisomatic INs on single postsynaptic PCs showed that some cells tend to target the soma and proximal dendrites (cells with high ratio of perisomatic contacts), while others target rather the dendritic segments (cells with low ratio of perisomatic contacts) (Fig. 15I). This raises the question whether there are INs, which can be classified as perisomatic region-targeting cells, because they innervate predominantly the perisomatic region of their postsynaptic partners in most cases, and accordingly, other cells might be classified as dendrite-targeting interneurons innervating mostly the dendritic shafts of PCs. Or, alternatively, one IN innervates some of their partners mainly perisomatically, whereas other PCs receive inputs from the same cell mainly on the dendrites. To address this question, we analyzed the target distribution of single labeled INs on the whole somato-dendritic surface of three sequentially recorded and labeled postsynaptic PCs with the same method as used in the paired recordings (quadruplet recordings, Fig. 17).

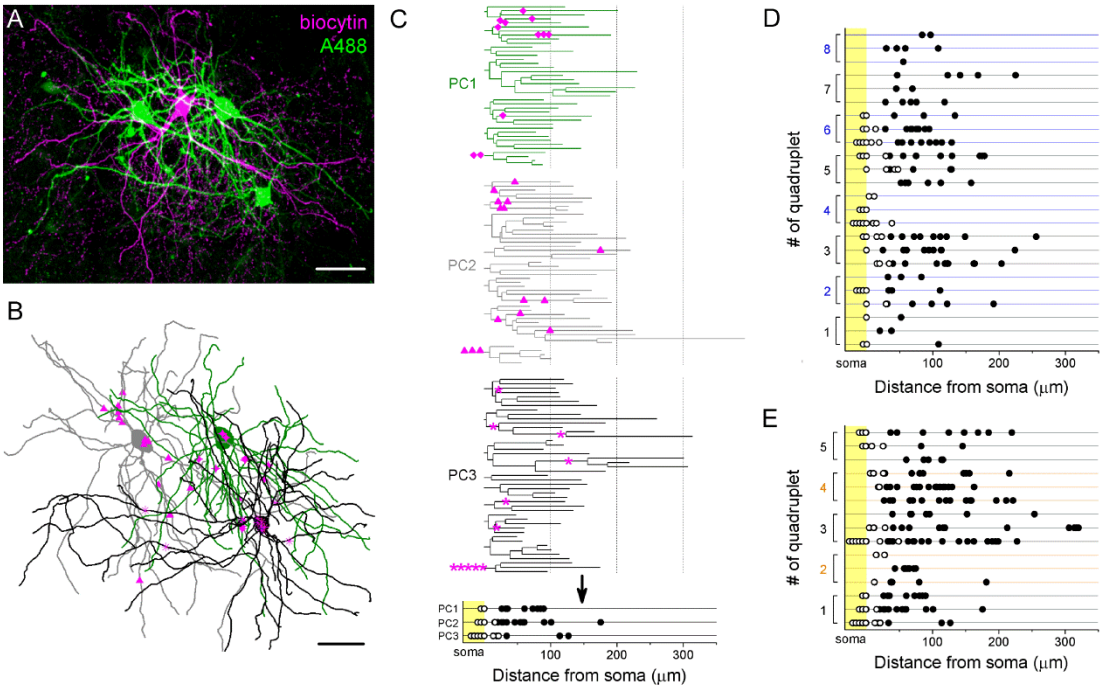

Figure 17. *Target distribution of CCK/CB$_1$BCs and PVBCs on multiple synaptic partners.* A, Maximum z intensity projection of 3D confocal image of a representative quadruplet. A single PVBC was filled with biocytin (visualized by Alexa 594, magenta) and three monosynaptically connected PCs (confirmed with

electrophysiology) were filled with Alexa 488 (green). B, Neurolucida reconstruction of the postsynaptic PCs (green) with the putative synaptic sites marked in magenta. Circles are contacts on PC1, triangles on PC2, stars on PC3. For the reconstructions the same method was used as in Fig. 13. C, On the dendrograms of the three reconstructed postsynaptic PCs the putative contact sites are marked. Bottom: innervation patterns of the presynaptic IN on the three postsynaptic PCs. D and E, Innervation patterns of the reconstructed quadruplets (n=8 CCK/CB_1BC-PCs and 5 PVBC-PC quadruplets). Scales (in μm): A and B: 50.

We found that in some cases the innervation patterns from one IN to three distinct PCs were similar: either mainly innervating the perisomatic region (e.g. quadruplet #4 in Fig. 17D) or more distal dendritic regions (e.g. quadruplet #8 in Fig. 15D). However, there were some cases, where the same IN innervated the soma of one postsynaptic PC with multiple contacts, whereas targeted only the dendrites of another PC (e.g. quadruplet #3 and 5 in Fig. 17E). This data indicated that the innervation pattern of both CCK/CB_1BCs and PVBCs can be variable and form a continuum if we evaluated the target distribution on the different postsynaptic partners.

To extend this investigation on a larger dataset, the samples from paired recordings were further processed for Kv2.1 immunolabeling. This allowed us to investigate the number and distribution of contacts from the presynaptic IN both on the single biocytin labelled PC from paired recordings and on the perisomatic region of 10-20 neighbouring Kv2.1 immunolabeled cells (Fig. 18A,B, n=15 CCK/CB_1BC-PC and 6 PVBC-PC pairs, see Kv2.1 method also in Fig. 6M). Since the analysis of paired recordings didn't show difference in the innervation patterns, data form CCK/CB_1BCs and PVBCs were pooled. We found that the number of the perisomatic contacts from individual INs was very variable on their different Kv2.1 labelled postsynaptic partners (ranging from 1 to 12, CV=0.54±0.03, Fig. 18C), and showed no correlation with the number of the perisomatic contacts on the intracellularly-labeled postsynaptic PC (Fig. 18D). Moreover, from these data we could also reveal the ratio of the boutons on Kv2.1-labeled perisomatic- and on unlabeled, presumably distal dendritic regions, thereby calculating the perisomatic target ratio of single INs at population level (see method also in Fig. 6L). We found no correlation in the ratio of perisomatic contacts obtained at the populational level and in pairs (Fig. 18E). However, there was a correlation between the average number of perisomatic contacts on Kv2.1-labeled

profiles and the ratio of perisomatic contacts at the populational level showing that those cells which tend to target the perisomatic region at higher ratio, they also form more contacts on this region of the individual target cells (Fig. 18F), which enables them to control the spiking activity of the postsynaptic cells more efficiently.

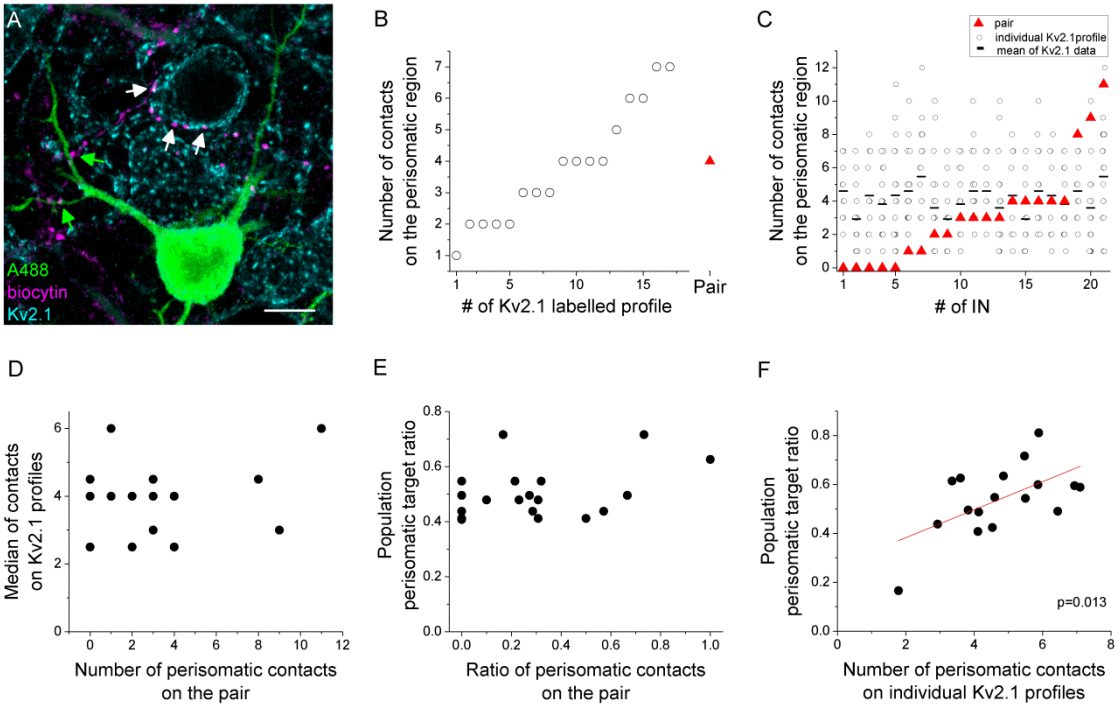

Figure 18. *Comparison of the innervation pattern of BCs at single cell and population levels.* A, Kv2.1 immunostaining (blue) was used to label the perisomatic region of cells in slices where IN-PC pairs were visualized (biocytin in IN (magenta), and Alexa 488 in PC (green)). Putative contact sites from the same labeled IN were identified on the labeled PC (green arrows) and on Kv2.1- expressing profiles (white arrows). B, Data from a representative IN: the number of the established contacts was calculated on 17 Kv 2.1 labeled profiles (open circles, arranged as a function of increasing contact number) and on the biocytin filled postsynaptic PC pair (red triangle). C, Data from 21 INs. Each column represents an individual IN, the number of the established contacts on Kv 2.1 labeled profiles are labelled with open circles, mean value with black line, and the number of the contacts on the biocytin filled postsynaptic PC pair with red triangle (data are arranged as a function of increasing contact number in the pair). D, Number of the contacts on the perisomatic region of the postsynaptic pair plotted together with the median of the contacts established on Kv2.1-labelled profiles from single INs. E, Ratio of the perisomatic contacts on the postsynaptic pair plotted together with the ratio of perisomatic region targeting boutons at the populaton level (calculated with Kv2.1 staining) from single INs. F, Correlation between the number of the perisomatic contacts and perisomatic target ratio at the population level. Scale: 10 µm.

These data together indicates that both CCK/CB_1BCs and PVBCs tend to target the perisomatic region of PCs as a population, however, there is a marked variability in the number and ratio of the perisomatic contacts originating from individual INs on the surface of different postsynaptic PCs. Therefore, it is not possible to determine the characteristic innervation pattern of a given IN based on the bouton distribution on a single postsynaptic partner, rather investigation of the target distribution at the population level is needed. In addition, these observations strengthen our previous notion that both types of INs expressing PV or CCK/CB_1 form a continuum in respect of their postsynaptic target distribution, cannot be objectively separated into perisomatic region- and dendrite-targeting IN types.

5. Discussion

We have examined the organization of GABAergic inputs received by the perisomatic region of PCs in the BLA, identified the interneuron types giving rise to perisomatic afferents, and revealed the properties and effects of these GABAergic cells on the firing of PCs. Our main findings are as follows: (1) The perisomatic region of BLA PCs receives the majority of its inputs from three main IN types, which differ in their electrophysiological properties and neurochemical content. (2) The proximal segment of the AIS is targeted by PVBCs, whereas AACs concentrate their synapses on the action potential generation site and provide an efficient control of PC spiking. (3) The soma and proximal dendrites of PCs are innervated mainly by CCK/CB_1BCs and PVBCs, which two cell types are equally capable to efficiently control the probability and timing of spike generation in PCs.

The perisomatic region of cortical principal cells receives mainly, if not exclusively GABAergic inputs (Somogyi et al., 1998, Megias et al., 2001, Freund and Katona, 2007). This functional domain is comprised of the axon initial segment, soma and the proximal dendrites, although the latter has not been defined accurately in the lack of proper markers visualizing its extent. Here, we showed that immunostaining for Kv2.1 can be a proper tool to reveal the extent of the proximal dendritic segments belonging to the perisomatic region (at least for the PCs in the BLA). First, a clear change in the ratio of excitatory and inhibitory inputs correlated well with the end of the Kv2.1-immunostaining along the dendrites. Second, boutons of CCK/CB_1BCs contacting soma and Kv2.1-immunostained profiles were similar in size, but were significantly larger than those varicosities that were not in the close proximity of Kv2.1-immunostained profiles. Therefore, we propose that Kv2.1-immunostaining can be used to visualize the perisomatic region of PCs in the BLA.

Our data regarding the spine distribution along the proximal dendrites obtained in the BLA are in agreement with those observed in the neocortex (Ballesteros-Yanez et al., 2006), suggesting that the perisomatic region of PCs in other cortical structures might have similar extent as we determined here. Previous studies in rats described that some of the BLA PCs have a prominent dendrite among the others, resembling apical

dendrites observed in the neocortex, whereas the dendritic arbor of other PCs showed more symmetrical, stellate-like appearance (Faber et al., 2001). In mice, we could not separate two PC populations based on different morphology, however, the extent of the perisomatic region along individual dendritic branches was very variable and also dependent on the diameter of the host dendrite measured at the soma. This implies that dendritic branches can be structurally and functionally different, having distinct extent of perisomatic region. Thus, different amount of inhibitory inputs can regulate the somatic propagation of excitatory inputs arriving from that particular dendritic branch. Whether this difference in GABAergic innervation between individual branches correlates with specific excitatory inputs has not been investigated yet.

5.1. GABAergic inputs onto the axon initial segments of PCs in the BLA

We found that the initial part of the axon receives inhibitory inputs from (at least) two cell types: PVBCs and AACs. As reported earlier in the hippocampus (Halasy et al., 1996) and in the neocortex (Somogyi et al., 1983a), we found that in addition to the soma and proximal dendrites, PVBCs also target the axon initial segments of neurons. Comparing Calb immunopositivity of boutons, which separate varicosities of PVBCs from AACs, we could estimate for the first time both the ratio of GABAergic inputs onto the axon initial segments derived from PVBCs and their spatial distribution along the proximal part of the axons. Our data showing that the majority of PVBC boutons contacted the soma-near region of the axon initial segments indicate that the initial part of the axon may be functionally segregated onto two portions. PVBCs target mainly the proximal 1-15 μm of the axon, which might be considered functionally as a soma-equivalent region, since the Nav1.6 density is low in this region and the action potential is generated further away along the AIS (Fig. 10). AACs on the other hand, which provide the vast majority of GABAergic inputs onto this region, cover the whole length of the AIS, with exception of the first 10 μm at the soma, and concentrate their synapses at the action potential initiation site (Fig. 19).

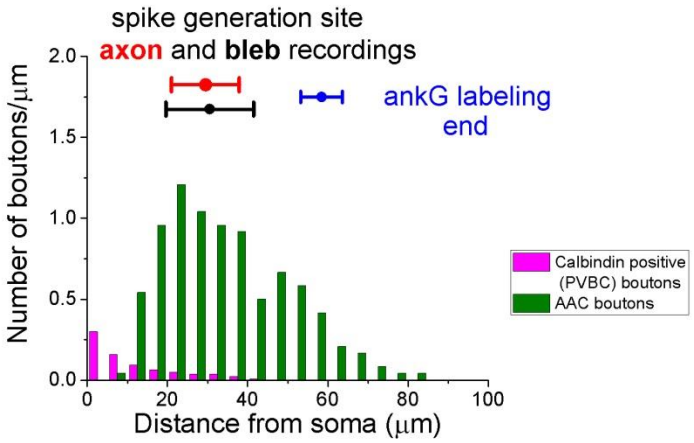

Figure 19. *Inhibitory inputs from PVBCs and AACs cover distinct regions along the AIS.* Merging data from Fig. 6P, Fig. 9O and Fig. 10C shows that GABAergic inputs at the proximal AIS derives from Calbindin-immunopositive PVBCs (magenta), while AACs (green) concentrate their boutons at 20-40 µm from the soma, where the action potentials are generated.

We have shown that AACs in the BLA act via a $GABA_A$ receptor-mediated Cl^- conductance and have confirmed the results of a recent in vivo study obtained in the BLA, showing that AACs innervated exclusively the AISs (Bienvenu et al., 2012). These observations are in agreement with those found earlier in the hippocampus and neocortex (Somogyi, 1977, Somogyi et al., 1982, Buhl et al., 1994a, Buhl et al., 1994b, Cobb et al., 1995, Szabadics et al., 2006). However, there is still a debate whether AACs inhibit or excite PCs, which may depend on several factors, including the resting membrane potential of postsynaptic neurons, the reversal potential for Cl^- in the AIS or on the HCO_3^- efflux from the AIS, which can activate Kv7/KCNQ channels (Buhl et al., 1994b, Szabadics et al., 2006, Woodruff et al., 2011, Jones et al., 2014). Using gramicidin-based perforated patch recordings, we found that in the majority of PCs the reversal potential of the postsynaptic responses from AACs was below both the resting membrane potential and the firing threshold of PCs. Thus, we concluded that under our experimental conditions AACs were inhibitory in the BLA, similar to the results obtained in the hippocampus (Buhl et al., 1994b, Cobb et al., 1995, Glickfeld et al., 2009). In the neocortex, AACs can excite some of their postsynaptic partners (Szabadics et al., 2006, Molnar et al., 2008), which could be dependent on the membrane potential of PCs (Woodruff et al., 2011). Similar $GABA_A$ receptor-mediated excitation of PCs was described in the BLA *in vitro*, but the type of PV-expressing

interneurons giving rise to this effect has not been clarified (Woodruff et al., 2006). Further studies should address the identity of those amygdalar interneurons that might excite PCs monosynaptically via $GABA_A$ receptors.

When the earliest studies described that AACs selectively target the AISs of PCs, it was proposed that this unique target distribution allows AACs to effectively control the activity of their postsynaptic partners (Somogyi, 1977, Somogyi et al., 1982). Indeed, we have found that AACs are well suited to regulate PC spiking, because their output synapses, regardless of the number of contacts, predominantly cover the part of the AISs, where the initiation of action potentials has the largest probability measured by electrophysiological methods and supported by immunocytochemical data (Fig. 20). Recent studies showed that both the length and the position of the AIS along the proximal part of the axon could be dynamically regulated as a function of neuronal excitability (Grubb and Burrone, 2010, Kuba et al., 2010, Kuba, 2012). During these plastic changes the position of the GABAergic AIS input has been proved to remain stable, which can result a significant lag in the action potential invasion into the soma (Wefelmeyer et al., 2015). These data indicate that AACs might be able to influence the induction of short and long-term forms of synaptic plasticity according to the PC excitability level.

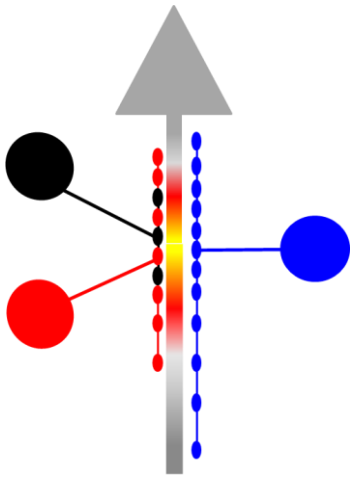

Figure 20. *AACs maximize their inhibitory efficacy by strategically positioning their synapses on the action potential generation site.* Summary scheme indicating that AACs preferentially target, and cluster at the site of the action potential generation along the PC axon indicated by yellow regardless of the number of synapses made by a given connection.

Our paired recordings revealed that an AAC innervated PCs via 8.4 synapses on average, which agrees remarkably well to the 8 synaptic contacts reported in the cat visual cortex (Somogyi et al., 1982). This value was higher by ~30% than that found by counting the number of varicosities of single AACs on the ankyrin G-immunopositive profiles (5.5 bouton/AIS). The reason for the higher number of boutons found on the intracellularly-labeled PCs is that the full targeted part of the axons is visualized including those that could not be labeled by immunostaining against ankyrin G. Thus, there might be a systematic underestimation of the number of GABAergic inputs from individual AACs onto PCs, if the counting is based on the visualization of AISs by immunostaining against e.g. ankyrin G. Reconstruction of *in vivo* labeled PCs showed that an AIS received 52.4 boutons on average, ranging from 31 to 86, which is comparable to an average of 43 in cat visual cortex (Somogyi et al., 1982), and 56 in CA1 of the monkey (Somogyi et al., 1983b), but lower than found in the CA3 area of the rat (150) (Kosaka, 1980). Our values in the BLA are higher compared to the 15-30 synapses contacting single AISs found earlier (McDonald and Betette, 2001, Muller et al., 2006). Similar studies in other cortical regions showed that the number of synapses on single AISs is quite variable, ranging from 1 to 150 depending on the area and cortical layer (Kosaka, 1980, Somogyi et al., 1982, Freund et al., 1983, Somogyi et al., 1983b, DeFelipe et al., 1985, Farinas and DeFelipe, 1991, Buhl et al., 1994a, Tamas and Szabadics, 2004). Comparative light microscopic studies also suggested substantial variability in the innervation density of AISs between different cortical areas and layers (Inda et al., 2007, 2009) and found that the cortical nuclei of the amygdala were among the regions having particularly dense AIS innervation. Because the vast majority of these GABAergic inputs originated from AACs (Howard et al., 2005), it is possible that single PCs receive innervation on their AIS from at least 4 to 10 AACs. These estimations are in accordance with those obtained in other cortical structures (Freund et al., 1983, Buhl et al., 1994b, Inan et al., 2013). Taking into account our calculation that approximately 12 synapses were needed for a 95% reduction in PC firing probability under our recording conditions, a simultaneous train of action potentials in 2-3 AACs could effectively block spike genesis. This implies that for the complete suppression of PC firing 20-50% of all AACs innervating individual PCs should discharge synchronously.

5.2. Synaptic inputs received by the soma and proximal dendrites of PCs in the BLA

Our results showing that synaptic inputs onto the somatic region of amygdalar PCs originated almost exclusively from GABAergic axon terminals are in agreement with previous studies obtained in the BLA (Carlsen, 1989, McDonald et al., 2002). This conclusion is supported by several lines of evidence. First, soma of amygdalar PCs receiving glutamatergic inputs is extremely rare in this region (present study, (Washburn and Moises, 1992, McDonald et al., 2002, Muller et al., 2006). Second, asymmetrical synapses characteristic for excitatory inputs in cortical regions do not target the perisomatic region of PCs, only boutons forming symmetrical synapses could be observed (Carlsen, 1989, McDonald et al., 2002).

Earlier work established that GABAergic boutons expressing PV, CB_1 or Calb formed symmetrical synapses with the perikarya and proximal dendrites of PCs in the amygdala (Sorvari et al., 1996, Smith et al., 1998, Katona et al., 2001, Muller et al., 2003, 2006). We confirmed these results and extended by showing that PV and Calb were colocalized in the same varicosities contacting the Kv2.1-immunostained profiles and these boutons originated from PVBCs. In addition, CB_1-expressing boutons contacting the perisomatic region derived from CCK/CB_1BCs and were found to lack Calb immunolabeling. These latter interneurons, at least in part could express type 3 vesicular glutamate transporter (VGLUT3) and/or vasoactive intestinal polypeptide (VIP), as VGLUT3 has been shown to be expressed in CB_1/CCK-expressing varicosities (Omiya et al., 2015) and VIP-expressing axon terminals contacting the somata of PCs were found to be distinct from Calb-expressing boutons (Muller et al., 2003). Thus, two main basket cell types with distinct neurochemical features are the main sources of the GABAergic inputs onto the soma and proximal dendrites of PCs in the BLA. However, in contrast to the hippocampus, where almost exclusively these two basket cell types gave rise to the innervations of perikarya of pyramidal cells (Takacs et al., 2015), we found that 30% of GABAergic boutons contacting the Kv2.1-immunostained profiles were immunonegative for both PV and CB_1. This observation might indicate that some of the boutons were false negative, i.e. we actually overestimated the number of boutons expressing neither PV nor CB_1. Alternatively, these boutons might originate from other GABAergic cell types. Indeed, a recent study

has provide evidence that GABAergic cells from the intercalated cell mass projected back to the BLA, where formed synapses, among other targets, on somata of PCs (Asede et al., 2015).

The use of transgenic mouse lines allowed us to selectively target different interneuron types in slices preparations and perform single-cell or paired recordings. In accordance with previous findings obtained in the amygdala (Rainnie et al., 2006, Woodruff and Sah, 2007b), our results indicated that PVBCs had a fast spiking character, narrow spike width and fast after-hyperpolarization, while CCK/CB_1BCs showed accommodation in firing, wider action potentials and slower after-hyperpolarization (Jasnow et al., 2009). These data are in full agreement with those found in other cortical areas (Glickfeld and Scanziani, 2006, Armstrong and Soltesz, 2012). The features of the output synapses of perisomatic region-targeting interneurons, however, were previously only studied for PV-expressing cells without separation of PVBCs and AACs (Woodruff et al., 2006, Woodruff and Sah, 2007b, a). Therefore, our study is the first to provide detailed comparative analysis of the synaptic properties of basket cells. As found in the hippocampus (Szabó et al., 2010), these cell types gave rise to synaptic currents with fast rise time indicating the perisomatic origin of the postsynaptic events recorded in the PCs, moreover the rise time of the events showed strong correlation with the location of the synapses along the somato-dendritic membrane surface. Interestingly, although the rise time of the events originated from the CCK/CB_1BCs was significantly slower, the location of their synapses was not distinct from those of PVBCs. This indicates that the differences rather might be in the spatiotemporal profile of neurotransmitter release, as it was described in the hippocampus (Bucurenciu et al., 2008, Lenkey et al., 2015). This might also be the explanation for the observed differences in the latency of the responses. Importantly, the short-term dynamics at the output synapses of BCs were distinct, implying that at a given activity pattern the three interneurons could provide quite a unique GABAergic input onto the perisomatic region of PCs.

The dual color labeling of the recorded pairs provided a powerful tool to analyze the arrangement of the connections along the somato-dendritic membrane surface of the postsynaptic cell(s). We found that both types of basket cells innervate the perisomatic and also the distal dendritic compartments up to 320 μm far from the soma (i.e. till the

end of PC dendrites). This innervation pattern resembles the properties of neocortical basket cells, because they could also innervate distal dendritic regions of PCs with several synapses (Kubota et al., 2015). On average ~30% of the synapses of both CCK/CB_1BCs and PVBCs was formed on the perisomatic region. We found with morphological analysis of the recorded pairs that the number of the contacts established on the perisomatic region is in correlation with the potency of the inputs and the inhibitory efficacy of an IN. When we counted the number of perisomatic contacts on multiple Kv2.1-labeled cells, we found that PVBCs contacted their partner with more synapses than CCK/CB_1BCs (Fig. 6M), however, this difference was not significant when we analyzed the established perisomatic contact number by the pairs, only a tendency could be observed (Fig. 15H). The reason for this discrepancy can be the different sample number used in the two methods (n=8 and 8 INs in Kv2.1 labeled target analysis vs. n=39 and 29 INs in paired recordings). Importantly, despite the slight difference in the number of the established contacts on the perisomatic region, the inhibitory efficacy of these two cell populations was similar, which can be, at least partially, explained by the fact that the axon terminals of CCK/CB_1BCs in the BLA (as in other cortical regions) establish multiple release sites on the same target (Katona et al., 2001). Unfortunately, the analysis of DAB/DABNi labeled pairs at the EM level we have applied in this study doesn't allow the recognition and separation of discrete release sites, therefore this difference in the transmitter release site number between CCK/CB_1BCs and PVBCs was not taken into account in our analysis. Nevertheless, the larger somatic bouton size we found in case of CCK/CB_1BCs also might indicate the presence of multiple release sites (Biro et al., 2006, Lenkey et al., 2015).

The ratio of the perisomatic contacts was variable in both BC types, e.g. there were cells, which completely avoided the perisomatic region and formed synapses only on more distal sites, whereas others innervated exclusively the perisomatic membrane surface. Between these two extremes, the innervation pattern of INs formed a continuum, therefore categorisation of the INs into perisomatic and dendrite-targeting cells is not possible in the BLA. When we analysed the target distribution of single INs on multiple postsynaptic cells, we found the same continuous innervation pattern: only a few percent of the INs formed synapses with the very same distribution on all of its postsynaptic partners. The functional implication of both somatic and dendritic

inhibitory inputs from the same cell requires more investigations, however, basket cells in the BLA -besides controlling action potential generation and somatic signal integration- might be able to influence local dendritic computations by innervating distal dendritic segments (Mullner et al., 2015).

Quantification of the perisomatic inputs showed that single PCs receive ~230 GABAergic boutons on their perisomatic region (Fig. 3K), of which 27% is CB_1+ and 40% is PV+ (Fig. 5B). Moreover, we have shown that single CCK/CB_1BCs and PVBCs give rise to 3.9 and 5.8 boutons on the perisomatic region of a PC, respectively (Fig. 6M). Collectively, these data indicate that approximately the same number of CCK/CB_1BCs and PVBCs (15-17) converges onto individual PCs in the BLA (Fig. 21).

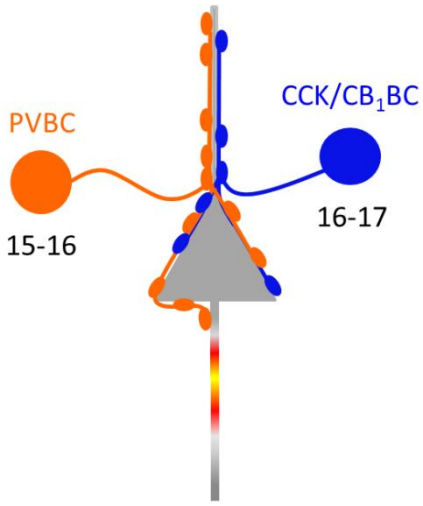

Figure 21. *Same number of CCK/CB_1BCs and PVBCs converges on PCs in the BLA.*. Quantification of the number of GABAergic boutons, the ratio of CB_1+ and PV+ boutons and the number of contacts emerging from individual BCs together show that individual PCs are innervated by same number of BCs from the two types.

5.3. Functional implications

Our results showed that there are three different perisomatic region-targeting interneurons, which can control PC firing with the same efficacy, thereby they are equally in the position to shape the output of the BLA. In cortical regions, individual

perisomatic region-targeting cells have been shown to veto PC spiking (Cobb et al., 1995, Miles et al., 1996, Tamas et al., 2004, Woodruff and Sah, 2007a). By affecting the spiking of several neurons simultaneously, perisomatic region-targeting interneurons are thus in a position to synchronize the neuronal activities at low frequencies, which might contribute to the generation of e.g. the theta rhythm (Buzsaki, 2002). In addition, the bulk stimulation of inhibitory fibers can not only delay, but also advance PC spiking in the CA1 hippocampal region (Kwag and Paulsen, 2009). Indeed, we found that single AACs, CCK/CB_1BCs and PVBCs all could significantly delay the spiking in amygdalar PCs in a similar way to that observed for CA1 PCs. However, we have not observed any advancement in PC spiking upon activation of these interneurons. The reason for this could be two-fold. First, PCs in the BLA express only a modest h-current (Faber et al., 2001, Park et al., 2007) which mediates the advancement in spiking in CA1 (Kwag and Paulsen, 2009). Second, GABAergic cells that make synapses on the distal dendrites of PCs might be more suitable to activate h-current, which is expressed predominantly in PC dendrites (Magee, 1999, Lorincz et al., 2002). Our result showing that single INs can delay PC spiking by 10 to 30 ms suggests that perisomatic region-targeting INs might have a role in regulating synaptic plasticity by restricting the precise timing of PC spiking to a time window, when the Hebbian forms of synaptic plasticity take place.

What can be the reason for the presence of three different IN types with the same powerful inhibitory effect on PC spiking? Several lines of evidence in the literature and recent findings from our lab suggest that these IN types might play remarkably different roles during BLA network activities and therefore in emotional information processing. For instance, how these IN types can be recruited by local PCs is markedly different. Morphological data (Smith et al., 2000) and unpublished observations from our lab showed that AACs and PVBCs are heavily innervated by local PCs, whereas CCK/CB_1BCs lack the strong local feedback excitation. These results imply that AACs and PVBCs might be involved in local feedback inhibitory circuits, and shape the firing of PCs even at moderate network activity levels. On the other hand, local PCs can recruit CCK/CB_1PCs to provide feedback inhibition only when the BLA network activity is elevated, or together with concomitant activation of subcortical afferents.

There are some evidence suggesting that single INs from the three IN types might control different amount of the local PC network. Data from our lab revealing the

axon and dendrite structures showed functionally relevant differences in both dendritic and axon arborizations among the examined interneurons (Vereczki et al., 2016). Dendrites and axons of both BC types occupied significantly larger area within the BLA than AACs. Moreover, the number of axon terminals formed by PVBCs was double as many as in the case of AACs or CCK/CB_1BCs (AACs: ~5500, CCK/CB_1BCs: ~7000, PVBCs: ~13000 varicosities). If we estimate the number of the contacted PCs by each IN types by taking into account the average number of the synapses established between IN-PC pairs (AACs: 8.4, CCK/CB_1BCs: 7.4, PVBCs: 12.8) we find that PVBCs innervate more PCs than AACs, and a slightly more than CCK/CB_1BCs (AACs: ~600-650, CCK/CB_1BCs: ~700-800, PVBCs: ~800-900, Fig. 22). This suggests that BCs, especially PVBCs are suited better to monitor and control the activity of larger local PC populations than AACs.

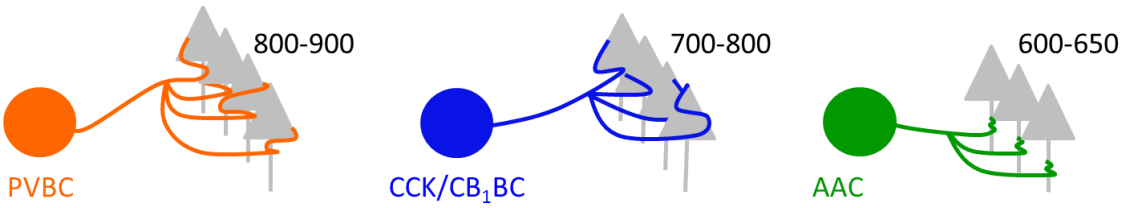

Figure 22. *BCs control the activity of a larger PC population than AACs.* Calculating the number of the target PCs of perisomatic region-targeting INs shows that both BC types innervate more PCs than AACs.

A recent *in vivo* study showed that there are distinct IN types in the BLA with cell type-specific firing modes during network activities, together with characteristic responsiveness to incoming noxious stimuli (Bienvenu et al., 2012). Particularly, AACs discharged with high fidelity to painful stimulation, which, in combination with our data, might explain the stimulus-induced GABAergic inhibition and silencing of PCs within the BLA (Windels et al., 2010). Although there is currently no published data how CCK/CB_1BCs in the BLA discharge *in vivo*, data obtained in the hippocampus imply (Klausberger et al., 2005) that this third type of perisomatic region-targeting INs could provide GABAergic inputs onto PCs at distinct temporal window than PV-expressing interneurons. As predicted from our paired recordings, each type of the three

interneurons targeting the perisomatic region might control the PC spiking with similar efficacy. Therefore, we assume that to maximize the efficacy of firing control in the PCs or to provide a flexible and brain state-dependent regulation of PC activities, the spiking behavior of three interneuron types should be combined or temporarily separated, respectively, depending on the functional demands regarding the amygdalar operation. Such synchronization or temporal segregation in firing of these interneurons can be achieved by intra- and/or extra-amygdalar afferents (Pare and Smith, 1998, McDonald et al., 2005), if these inputs can recruit distinctly the three interneuron types. Thus, to understand the function(s) of these GABAergic cells they fulfil in the amygdala, future studies should reveal the properties of cortical and subcortical inputs onto these interneurons in addition to their spiking behavior during distinct brain states.

6. Conclusions

The perisomatic region of PCs in the BLA is innervated by three main types of morphologically, neurochemically and electrophysiologically distinct INs.

The AISs of PCs are parceled out by PVBCs and AACs, as the majority of GABAergic inputs onto the very proximal part of the AISs is originated from PVBCs, while the largest portion of the AIS is innervated almost exclusively by AACs. Regarding their effects on PC spiking, AACs in the BLA hyperpolarize their postsynaptic partners at resting membrane potential or near the spike threshold. AACs can effectively inhibit the firing of PC and delay spike generation. The length of the AIS is ~60 μm as estimated from immunostainings, and AACs concentrate 60% of their output synapses to the segment between 20 and 40 μm from the soma, a region corresponding to the action potential initiation site. Thus, AACs maximize their inhibitory efficacy by strategically concentrating their synaptic junctions along the AISs to effectively counteract voltage-gated Na^+ channel activation and action potential generation in the PCs.

The soma and proximal dendrites of PCs are innervated primarily by two types of basket cells: CCK/CB_1BCs and PVBCs. Both types of basket cells in the BLA innervate the perisomatic region and also the more distal dendritic segments to varying extents. At population level, INs cannot be separated into perisomatic region- and dendrite-targeting cells, but instead their target preference shows a continuous distribution. The inhibitory efficacy of the two basket cell types is equal: they both can powerfully influence the probability and timing of action potential generation in the PCs. We found that the same number (15-17) of PVBCs and CCK/CB_1BCs converges onto single PCs.

Our results suggest that the three main interneuron types innervating the perisomatic region of PCs are able to powerfully modulate the firing of their postsynaptic partners with high temporal precision, a feature, which might endow them with crucial roles in amygdalar network operations. By being differently embedded into the amygdalar networks, these INs might fulfil specific function(s) during various brain states and fear memory processing.

7. Summary

Action potential generation is most effectively controlled by inhibitory inputs that target the perisomatic region of neurons. Despite the critical importance of this functional domain, very little is known about the organization of the GABAergic inputs contacting the perisomatic region and their functional effect on the activity of principal cells (PCs) in the basolateral amygdala, a brain region which plays key role in the formation and expression of fear memory traces. In this study, we determined the number and sources of inhibitory inputs on the perisomatic region and compared how efficiently perisomatic region targeting interneurons can control action potential generation in PCs.

We found that the perisomatic region of PCs was primarily innervated by three distinct interneuron types: the axon initial segment was innervated predominantly by axo-axonic cells while the soma and proximal dendrites were innervated primarily by two neurochemically distinct basket cell types expressing parvalbumin or cholecystokinin and type 1 endocannabinoid receptors. Axo-axonic cells powerfully inhibited or delayed the timing of PC by strategically positioning their synapses on the narrow portion of the axon initial segment where action potentials were generated with the highest likelihood. We calculated that 6-7 axo-axonic cells converged on the axon initial segment of a PC, of which 2-3 were necessary to be simultaneously active to veto PC firing under our recording conditions. We found that similar numbers (15-17) of the two basket cell types converge onto single PCs, and that individual interneurons from both types provided powerful inhibition of spike generation with similar electrophysiological and morphological properties. Besides the perisomatic region, both basket cell types innervated distal dendritic regions as well, however, the determining factor of their inhibitory efficacy was the number of the synapses established on the perisomatic region.

Our results collectively suggest that the three perisomatic region targeting interneuron types can effectively control the activity of PCs, therefore the output of the basolateral amygdala. By the spatiotemporally precisely regulated inhibition of PCs, these interneurons are in the position to powerfully contribute to the formation and expression of fear memories.

8. Összefoglalás

Az agykérgi fősejtek kisülése leghatékonyabban a periszomatikus régióra érkező gátlás által szabályozható. Kiemelkedő fontossága ellenére azonban nagyon keveset tudunk az ezen funkcionális régióra érkező gátló bemenetek szerveződéséről és hatásukról a bazolaterális amygdalában, mely agyterület fontos szerepet játszik a félelmi memórianyomok rögzülésében és előhívásában. Kutatásaink során meghatároztuk a fősejtek periszomatikus régiójára érkező gátló bemenetek számát és azok eredetét. Megvizsgáltuk, hogy az egyes gátlósejtek milyen hatékonysággal képesek szabályozni a fősejtek aktivitását, valamint összehasonlítottuk a különböző típusú gátlósejtek által biztosított bemenetek elektrofiziológiai és morfológiai tulajdonságait.

Eredményeink azt mutatták, hogy a periszomatikus régióra érkező bemenetek döntő többsége három gátlósejttípustól ered. Az axon kezdeti szakaszát legnagyobb arányban az axo-axonikus sejtek innerválják, míg a sejttesten és a proximális dendriteken két, neurokémiailag elkülöníthető kosársejttípus képez gátló szinapszisokat: az egyik típus parvalbumint, míg a másik kolecisztokinint és 1-es típusú kannabinoid receptort fejez ki. Azáltal, hogy az axo-axonikus sejtek az akciós potenciál keletkezésének helyét innerválják a legnagyobb sűrűséggel, képesek igen hatékonyan megakadályozni vagy időben eltolni a fősejtek kisülését. Eredményeink alapján 6-7 axo-axonikus sejt idegez be egy fősejt axon kezdeti szakaszát, melyek közül 2-3 sejt együttes aktivitása szükséges ahhoz, hogy a fősejt kisülését teljesen megakadályozzák. A fősejtek sejttestét és proximális dendritjét azonos számú (15-17) kosársejt innerválja mindkét típusból. Mindkét típusú kosársejt ugyanolyan hatékonyan képes szabályozni a fősejtek kisülését, és az általuk biztosított gátlás elektrofiziológiai és morfológiai tulajdonságai is hasonlóak. Mindkét kosársejttípus képez szinapszisokat távoli dendritszakaszokon is, ám gátló hatékonyságukat a periszomatikus régión létrehozott szinapszisok száma határozza meg a leginkább.

Eredményeink tehát azt mutatják, hogy a három fő periszomatikus régiót innerváló sejttípus az amygdalában igen hatékonyan képes befolyásolni a fősejtek aktivitását. A fősejtek térben és időben precízen szabályozott gátlásával ezen sejttípusok fontos szerepet játszhatnak a bazolaterális amygdala működésében a félelmi memórianyomok kialakulása során.

9. References

1. Acsády L, Görcs TJ, Freund TF (1996) Different populations of vasoactive intestinal polypeptide-immunoreactive interneurons are specialized to control pyramidal cells or interneurons in the hippocampus. Neuroscience 73:317-334.
2. Adolphs R (2010) What does the amygdala contribute to social cognition? Annals of the New York Academy of Sciences 1191:42-61.
3. Aggleton JP (1993) The contribution of the amygdala to normal and abnormal emotional states. Trends in neurosciences 16:328-333.
4. Ahmed MS, Siegelbaum SA (2009) Recruitment of N-Type Ca(2+) channels during LTP enhances low release efficacy of hippocampal CA1 perforant path synapses. Neuron 63:372-385.
5. Anglada-Figueroa D, Quirk GJ (2005) Lesions of the basal amygdala block expression of conditioned fear but not extinction. J Neurosci 25:9680-9685.
6. Ariav G, Polsky A, Schiller J (2003) Submillisecond precision of the input-output transformation function mediated by fast sodium dendritic spikes in basal dendrites of CA1 pyramidal neurons. J Neurosci 23:7750-7758.
7. Armony JL, Servan-Schreiber D, Cohen JD, LeDoux JE (1995) An anatomically constrained neural network model of fear conditioning. Behavioral neuroscience 109:246-257.
8. Armstrong C, Soltesz I (2012) Basket cell dichotomy in microcircuit function. J Physiol 590:683-694.
9. Asede D, Bosch D, Luthi A, Ferraguti F, Ehrlich I (2015) Sensory inputs to intercalated cells provide fear-learning modulated inhibition to the basolateral amygdala. Neuron 86:541-554.
10. Ballesteros-Yanez I, Benavides-Piccione R, Elston GN, Yuste R, DeFelipe J (2006) Density and morphology of dendritic spines in mouse neocortex. Neuroscience 138:403-409.
11. Ben-Ari Y (2002) Excitatory actions of gaba during development: the nature of the nurture. Nature reviews Neuroscience 3:728-739.

12. Bienvenu TC, Busti D, Magill PJ, Ferraguti F, Capogna M (2012) Cell-type-specific recruitment of amygdala interneurons to hippocampal theta rhythm and noxious stimuli in vivo. Neuron 74:1059-1074.
13. Biro AA, Holderith NB, Nusser Z (2006) Release probability-dependent scaling of the postsynaptic responses at single hippocampal GABAergic synapses. J Neurosci 26:12487-12496.
14. Bucurenciu I, Kulik A, Schwaller B, Frotscher M, Jonas P (2008) Nanodomain coupling between Ca2+ channels and Ca2+ sensors promotes fast and efficient transmitter release at a cortical GABAergic synapse. Neuron 57:536-545.
15. Buhl EH, Halasy K, Somogyi P (1994a) Diverse sources of hippocampal unitary inhibitory postsynaptic potentials and the number of synaptic release sites. Nature 368:823-828.
16. Buhl EH, Han ZS, Lőrinczi Z, Stezhka VV, Karnup SV, Somogyi P (1994b) Physiological properties of anatomically identified axo-axonic cells in the rat hippocampus. Journal of neurophysiology 71:1289-1307.
17. Busti D, Geracitano R, Whittle N, Dalezios Y, Manko M, Kaufmann W, Satzler K, Singewald N, Capogna M, Ferraguti F (2011) Different fear states engage distinct networks within the intercalated cell clusters of the amygdala. J Neurosci 31:5131-5144.
18. Buzsaki G (2002) Theta oscillations in the hippocampus. Neuron 33:325-340.
19. Buzsaki G, Chrobak JJ (1995) Temporal structure in spatially organized neuronal ensembles: a role for interneuronal networks. Current opinion in neurobiology 5:504-510.
20. Buzsaki G, Penttonen M, Nadasdy Z, Bragin A (1996) Pattern and inhibition-dependent invasion of pyramidal cell dendrites by fast spikes in the hippocampus in vivo. Proc Natl Acad Sci U S A 93:9921-9925.
21. Carlsen J (1988) Immunocytochemical localization of glutamate decarboxylase in the rat basolateral amygdaloid nucleus, with special reference to GABAergic innervation of amygdalostriatal projection neurons. J Comp Neurol 273:513-526.

22. Carlsen J (1989) New perspectives on the functional anatomical organization of the basolateral amygdala. Acta neurologica Scandinavica Supplementum 122:1-27.
23. Chhatwal JP, Gutman AR, Maguschak KA, Bowser ME, Yang Y, Davis M, Ressler KJ (2009) Functional interactions between endocannabinoid and CCK neurotransmitter systems may be critical for extinction learning. Neuropsychopharmacology : official publication of the American College of Neuropsychopharmacology 34:509-521.
24. Clark BA, Monsivais P, Branco T, London M, Hausser M (2005) The site of action potential initiation in cerebellar Purkinje neurons. Nat Neurosci 8:137-139.
25. Cobb SR, Buhl EH, Halasy K, Paulsen O, Somogyi P (1995) Synchronization of neuronal activity in hippocampus by individual GABAergic interneurons. Nature 378:75-78.
26. Cohen I, Navarro V, Clemenceau S, Baulac M, Miles R (2002) On the origin of interictal activity in human temporal lobe epilepsy in vitro. Science 298:1418-1421.
27. Cossart R, Bernard C, Ben-Ari Y (2005) Multiple facets of GABAergic neurons and synapses: multiple fates of GABA signalling in epilepsies. Trends in neurosciences 28:108-115.
28. David C, Schleicher A, Zuschratter W, Staiger JF (2007) The innervation of parvalbumin-containing interneurons by VIP-immunopositive interneurons in the primary somatosensory cortex of the adult rat. Eur J Neurosci 25:2329-2340.
29. DeFelipe J, Hendry SH, Jones EG, Schmechel D (1985) Variability in the terminations of GABAergic chandelier cell axons on initial segments of pyramidal cell axons in the monkey sensory-motor cortex. J Comp Neurol 231:364-384.
30. Douglas RJ, Martin KA (1991) A functional microcircuit for cat visual cortex. J Physiol 440:735-769.
31. Eggermann E, Jonas P (2012) How the 'slow' Ca(2+) buffer parvalbumin affects transmitter release in nanodomain-coupling regimes. Nat Neurosci 15:20-22.

32. Ehrlich I, Humeau Y, Grenier F, Ciocchi S, Herry C, Luthi A (2009) Amygdala inhibitory circuits and the control of fear memory. Neuron 62:757-771.
33. Engel AK, Fries P, Singer W (2001) Dynamic predictions: oscillations and synchrony in top-down processing. Nature reviews Neuroscience 2:704-716.
34. Faber ES, Callister RJ, Sah P (2001) Morphological and electrophysiological properties of principal neurons in the rat lateral amygdala in vitro. Journal of neurophysiology 85:714-723.
35. Farinas I, DeFelipe J (1991) Patterns of synaptic input on corticocortical and corticothalamic cells in the cat visual cortex. II. The axon initial segment. J Comp Neurol 304:70-77.
36. Foldy C, Lee SH, Morgan RJ, Soltesz I (2010) Regulation of fast-spiking basket cell synapses by the chloride channel ClC-2. Nat Neurosci 13:1047-1049.
37. Freund TF (2003) Interneuron Diversity series: Rhythm and mood in perisomatic inhibition. Trends in neurosciences 26:489-495.
38. Freund TF, Buzsáki G (1996) Interneurons of the hippocampus. Hippocampus 6:347-470.
39. Freund TF, Katona I (2007) Perisomatic inhibition. Neuron 56:33-42.
40. Freund TF, Martin KA, Smith AD, Somogyi P (1983) Glutamate decarboxylase-immunoreactive terminals of Golgi-impregnated axoaxonic cells and of presumed basket cells in synaptic contact with pyramidal neurons of the cat's visual cortex. J Comp Neurol 221:263-278.
41. Galarreta M, Hestrin S (2001) Spike transmission and synchrony detection in networks of GABAergic interneurons. Science 292:2295-2299.
42. Galarreta M, Hestrin S (2002) Electrical and chemical synapses among parvalbumin fast-spiking GABAergic interneurons in adult mouse neocortex. Proc Natl Acad Sci U S A 99:12438-12443.
43. Gaudreau H, Pare D (1996) Projection neurons of the lateral amygdaloid nucleus are virtually silent throughout the sleep--waking cycle. Journal of neurophysiology 75:1301-1305.
44. Gidon A, Segev I (2012) Principles governing the operation of synaptic inhibition in dendrites. Neuron 75:330-341.

45. Glickfeld LL, Roberts JD, Somogyi P, Scanziani M (2009) Interneurons hyperpolarize pyramidal cells along their entire somatodendritic axis. Nat Neurosci 12:21-23.
46. Glickfeld LL, Scanziani M (2006) Distinct timing in the activity of cannabinoid-sensitive and cannabinoid-insensitive basket cells. Nat Neurosci 9:807-815.
47. Golding NL, Spruston N (1998) Dendritic sodium spikes are variable triggers of axonal action potentials in hippocampal CA1 pyramidal neurons. Neuron 21:1189-1200.
48. Golding NL, Staff NP, Spruston N (2002) Dendritic spikes as a mechanism for cooperative long-term potentiation. Nature 418:326-331.
49. Gonzalez-Burgos G, Hashimoto T, Lewis DA (2010) Alterations of cortical GABA neurons and network oscillations in schizophrenia. Current psychiatry reports 12:335-344.
50. Grubb MS, Burrone J (2010) Activity-dependent relocation of the axon initial segment fine-tunes neuronal excitability. Nature 465:1070-1074.
51. Gulyas AI, Hajos N, Freund TF (1996) Interneurons containing calretinin are specialized to control other interneurons in the rat hippocampus. J Neurosci 16:3397-3411.
52. Gulyas AI, Hajos N, Katona I, Freund TF (2003) Interneurons are the local targets of hippocampal inhibitory cells which project to the medial septum. Eur J Neurosci 17:1861-1872.
53. Gulyas AI, Megias M, Emri Z, Freund TF (1999) Total number and ratio of excitatory and inhibitory synapses converging onto single interneurons of different types in the CA1 area of the rat hippocampus. J Neurosci 19:10082-10097.
54. Gulyás AI, Miles R, Hájos N, Freund TF (1993) Precision and variability in postsynaptic target selection of inhibitory cells in the hippocampal CA3 region. Eur J Neurosci 5:1729-1751.
55. Gulyás AI, Szabó GG, Ulbert I, Holderith N, Monyer H, Erdélyi F, Szabó G, Freund TF, Hájos N (2010) Parvalbumin-containing fast-spiking basket cells generate the field potential oscillations induced by cholinergic receptor activation in the hippocampus. J Neurosci 30:15134-15145.

56. Halasy K, Buhl EH, Lőrinczi Z, Tamás G, Somogyi P (1996) Synaptic target selectivity and input of GABAergic basket and bistratified interneurons in the CA1 area of the rat hippocampus. Hippocampus 6:306-329.
57. Han ZS, Buhl EH, Lorinczi Z, Somogyi P (1993) A high degree of spatial selectivity in the axonal and dendritic domains of physiologically identified local-circuit neurons in the dentate gyrus of the rat hippocampus. Eur J Neurosci 5:395-410.
58. Haubensak W, Kunwar PS, Cai H, Ciocchi S, Wall NR, Ponnusamy R, Biag J, Dong HW, Deisseroth K, Callaway EM, Fanselow MS, Luthi A, Anderson DJ (2010) Genetic dissection of an amygdala microcircuit that gates conditioned fear. Nature 468:270-276.
59. Hefft S, Jonas P (2005) Asynchronous GABA release generates long-lasting inhibition at a hippocampal interneuron-principal neuron synapse. Nat Neurosci 8:1319-1328.
60. Herry C, Ciocchi S, Senn V, Demmou L, Muller C, Luthi A (2008) Switching on and off fear by distinct neuronal circuits. Nature 454:600-606.
61. Herry C, Ferraguti F, Singewald N, Letzkus JJ, Ehrlich I, Luthi A (2010) Neuronal circuits of fear extinction. Eur J Neurosci 31:599-612.
62. Howard A, Tamas G, Soltesz I (2005) Lighting the chandelier: new vistas for axo-axonic cells. Trends in neurosciences 28:310-316.
63. Hu W, Tian C, Li T, Yang M, Hou H, Shu Y (2009) Distinct contributions of Na(v)1.6 and Na(v)1.2 in action potential initiation and backpropagation. Nat Neurosci 12:996-1002.
64. Inan M, Blazquez-Llorca L, Merchan-Perez A, Anderson SA, DeFelipe J, Yuste R (2013) Dense and overlapping innervation of pyramidal neurons by chandelier cells. J Neurosci 33:1907-1914.
65. Inda MC, Defelipe J, Munoz A (2007) The distribution of chandelier cell axon terminals that express the GABA plasma membrane transporter GAT-1 in the human neocortex. Cereb Cortex 17:2060-2071.
66. Inda MC, DeFelipe J, Munoz A (2009) Morphology and distribution of chandelier cell axon terminals in the mouse cerebral cortex and claustroamygdaloid complex. Cereb Cortex 19:41-54.

67. Isaacson JS, Scanziani M (2011) How inhibition shapes cortical activity. Neuron 72:231-243.
68. Jasnow AM, Ressler KJ, Hammack SE, Chhatwal JP, Rainnie DG (2009) Distinct subtypes of cholecystokinin (CCK)-containing interneurons of the basolateral amygdala identified using a CCK promoter-specific lentivirus. Journal of neurophysiology 101:1494-1506.
69. Jia H, Varga Z, Sakmann B, Konnerth A (2014) Linear integration of spine Ca2+ signals in layer 4 cortical neurons in vivo. Proc Natl Acad Sci U S A 111:9277-9282.
70. Jinno S, Klausberger T, Marton LF, Dalezios Y, Roberts JD, Fuentealba P, Bushong EA, Henze D, Buzsaki G, Somogyi P (2007) Neuronal diversity in GABAergic long-range projections from the hippocampus. J Neurosci 27:8790-8804.
71. Jones RT, Faas GC, Mody I (2014) Intracellular bicarbonate regulates action potential generation via KCNQ channel modulation. J Neurosci 34:4409-4417.
72. Katona I, Rancz EA, Acsady L, Ledent C, Mackie K, Hajos N, Freund TF (2001) Distribution of CB1 cannabinoid receptors in the amygdala and their role in the control of GABAergic transmission. J Neurosci 21:9506-9518.
73. Kemppainen S, Pitkanen A (2000) Distribution of parvalbumin, calretinin, and calbindin-D(28k) immunoreactivity in the rat amygdaloid complex and colocalization with gamma-aminobutyric acid. J Comp Neurol 426:441-467.
74. Kisvarday ZF, Martin KA, Whitteridge D, Somogyi P (1985) Synaptic connections of intracellularly filled clutch cells: a type of small basket cell in the visual cortex of the cat. J Comp Neurol 241:111-137.
75. Klausberger T, Magill PJ, Márton LF, Roberts JD, Cobden PM, Buzsáki G, Somogyi P (2003) Brain-state- and cell-type-specific firing of hippocampal interneurons in vivo. Nature 421:844-848.
76. Klausberger T, Marton LF, O'Neill J, Huck JH, Dalezios Y, Fuentealba P, Suen WY, Papp E, Kaneko T, Watanabe M, Csicsvari J, Somogyi P (2005) Complementary roles of cholecystokinin- and parvalbumin-expressing GABAergic neurons in hippocampal network oscillations. J Neurosci 25:9782-9793.

77. Kosaka T (1980) The axon initial segment as a synaptic site: ultrastructure and synaptology of the initial segment of the pyramidal cell in the rat hippocampus (CA3 region). Journal of neurocytology 9:861-882.
78. Kuba H (2012) Structural tuning and plasticity of the axon initial segment in auditory neurons. J Physiol 590:5571-5579.
79. Kuba H, Oichi Y, Ohmori H (2010) Presynaptic activity regulates Na+ channel distribution at the axon initial segment. Nature 465:1075-1078.
80. Kubota Y, Kondo S, Nomura M, Hatada S, Yamaguchi N, Mohamed AA, Karube F, Lubke J, Kawaguchi Y (2015) Functional effects of distinct innervation styles of pyramidal cells by fast spiking cortical interneurons. eLife 4.
81. Kwag J, Paulsen O (2009) Bidirectional control of spike timing by GABA(A) receptor-mediated inhibition during theta oscillation in CA1 pyramidal neurons. Neuroreport 20:1209-1213.
82. Lang EJ, Pare D (1997) Synaptic and synaptically activated intrinsic conductances underlie inhibitory potentials in cat lateral amygdaloid projection neurons in vivo. Journal of neurophysiology 77:353-363.
83. Larkum ME, Zhu JJ, Sakmann B (1999) A new cellular mechanism for coupling inputs arriving at different cortical layers. Nature 398:338-341.
84. Lavzin M, Rapoport S, Polsky A, Garion L, Schiller J (2012) Nonlinear dendritic processing determines angular tuning of barrel cortex neurons in vivo. Nature 490:397-401.
85. LeDoux JE (2000) Emotion circuits in the brain. Annual review of neuroscience 23:155-184.
86. Lenkey N, Kirizs T, Holderith N, Mate Z, Szabo G, Vizi ES, Hajos N, Nusser Z (2015) Tonic endocannabinoid-mediated modulation of GABA release is independent of the CB1 content of axon terminals. Nature communications 6:6557.
87. Li XF, Stutzmann GE, LeDoux JE (1996) Convergent but temporally separated inputs to lateral amygdala neurons from the auditory thalamus and auditory cortex use different postsynaptic receptors: in vivo intracellular and extracellular recordings in fear conditioning pathways. Learning & memory 3:229-242.

88. Likhtik E, Popa D, Apergis-Schoute J, Fidacaro GA, Pare D (2008) Amygdala intercalated neurons are required for expression of fear extinction. Nature 454:642-645.
89. Lim ST, Antonucci DE, Scannevin RH, Trimmer JS (2000) A novel targeting signal for proximal clustering of the Kv2.1 K+ channel in hippocampal neurons. Neuron 25:385-397.
90. Lorincz A, Notomi T, Tamas G, Shigemoto R, Nusser Z (2002) Polarized and compartment-dependent distribution of HCN1 in pyramidal cell dendrites. Nat Neurosci 5:1185-1193.
91. Losonczy A, Magee JC (2006) Integrative properties of radial oblique dendrites in hippocampal CA1 pyramidal neurons. Neuron 50:291-307.
92. Lovett-Barron M, Turi GF, Kaifosh P, Lee PH, Bolze F, Sun XH, Nicoud JF, Zemelman BV, Sternson SM, Losonczy A (2012) Regulation of neuronal input transformations by tunable dendritic inhibition. Nat Neurosci 15:423-430, S421-423.
93. Magee JC (1999) Dendritic Ih normalizes temporal summation in hippocampal CA1 neurons. Nat Neurosci 2:848.
94. Magee JC (2000) Dendritic integration of excitatory synaptic input. Nature reviews Neuroscience 1:181-190.
95. Magee JC, Cook EP (2000) Somatic EPSP amplitude is independent of synapse location in hippocampal pyramidal neurons. Nat Neurosci 3:895-903.
96. Manko M, Bienvenu TC, Dalezios Y, Capogna M (2012) Neurogliaform cells of amygdala: a source of slow phasic inhibition in the basolateral complex. J Physiol 590:5611-5627.
97. Marsicano G, Wotjak CT, Azad SC, Bisogno T, Rammes G, Cascio MG, Hermann H, Tang J, Hofmann C, Zieglgansberger W, Di Marzo V, Lutz B (2002) The endogenous cannabinoid system controls extinction of aversive memories. Nature 418:530-534.
98. Mascagni F, McDonald AJ (2003) Immunohistochemical characterization of cholecystokinin containing neurons in the rat basolateral amygdala. Brain research 976:171-184.

99. Mate Z, Poles MZ, Szabo G, Bagyanszki M, Talapka P, Fekete E, Bodi N (2013) Spatiotemporal expression pattern of DsRedT3/CCK gene construct during postnatal development of myenteric plexus in transgenic mice. Cell and tissue research 352:199-206.
100. McBain CJ, DiChiara TJ, Kauer JA (1994) Activation of metabotropic glutamate receptors differentially affects two classes of hippocampal interneurons and potentiates excitatory synaptic transmission. J Neurosci 14:4433-4445.
101. McDonald AJ (1982) Neurons of the lateral and basolateral amygdaloid nuclei: a Golgi study in the rat. J Comp Neurol 212:293-312.
102. McDonald AJ (1985) Immunohistochemical identification of gamma-aminobutyric acid-containing neurons in the rat basolateral amygdala. Neuroscience letters 53:203-207.
103. McDonald AJ (1992) Projection neurons of the basolateral amygdala: a correlative Golgi and retrograde tract tracing study. Brain research bulletin 28:179-185.
104. McDonald AJ, Augustine JR (1993) Localization of GABA-like immunoreactivity in the monkey amygdala. Neuroscience 52:281-294.
105. McDonald AJ, Betette RL (2001) Parvalbumin-containing neurons in the rat basolateral amygdala: morphology and co-localization of Calbindin-D(28k). Neuroscience 102:413-425.
106. McDonald AJ, Mascagni F (2001) Colocalization of calcium-binding proteins and GABA in neurons of the rat basolateral amygdala. Neuroscience 105:681-693.
107. McDonald AJ, Mascagni F (2002) Immunohistochemical characterization of somatostatin containing interneurons in the rat basolateral amygdala. Brain research 943:237-244.
108. McDonald AJ, Mascagni F, Mania I, Rainnie DG (2005) Evidence for a perisomatic innervation of parvalbumin-containing interneurons by individual pyramidal cells in the basolateral amygdala. Brain research 1035:32-40.

109. McDonald AJ, Muller JF, Mascagni F (2002) GABAergic innervation of alpha type II calcium/calmodulin-dependent protein kinase immunoreactive pyramidal neurons in the rat basolateral amygdala. J Comp Neurol 446:199-218.
110. McDonald AJ, Payne DR, Mascagni F (1993) Identification of putative nitric oxide producing neurons in the rat amygdala using NADPH-diaphorase histochemistry. Neuroscience 52:97-106.
111. McDonald AJ, Pearson JC (1989) Coexistence of GABA and peptide immunoreactivity in non-pyramidal neurons of the basolateral amygdala. Neuroscience letters 100:53-58.
112. Megias M, Emri Z, Freund TF, Gulyas AI (2001) Total number and distribution of inhibitory and excitatory synapses on hippocampal CA1 pyramidal cells. Neuroscience 102:527-540.
113. Meyer AH, Katona I, Blatow M, Rozov A, Monyer H (2002) In vivo labeling of parvalbumin-positive interneurons and analysis of electrical coupling in identified neurons. J Neurosci 22:7055-7064.
114. Miles R, Tóth K, Gulyás AI, Hájos N, Freund TF (1996) Differences between somatic and dendritic inhibition in the hippocampus. Neuron 16:815-823.
115. Mitchell SJ, Silver RA (2003) Shunting inhibition modulates neuronal gain during synaptic excitation. Neuron 38:433-445.
116. Molnar G, Olah S, Komlosi G, Fule M, Szabadics J, Varga C, Barzo P, Tamas G (2008) Complex events initiated by individual spikes in the human cerebral cortex. PLoS biology 6:e222.
117. Muller C, Beck H, Coulter D, Remy S (2012) Inhibitory control of linear and supralinear dendritic excitation in CA1 pyramidal neurons. Neuron 75:851-864.
118. Muller JF, Mascagni F, McDonald AJ (2003) Synaptic connections of distinct interneuronal subpopulations in the rat basolateral amygdalar nucleus. J Comp Neurol 456:217-236.
119. Muller JF, Mascagni F, McDonald AJ (2006) Pyramidal cells of the rat basolateral amygdala: synaptology and innervation by parvalbumin-immunoreactive interneurons. J Comp Neurol 494:635-650.

120. Muller JF, Mascagni F, McDonald AJ (2007a) Postsynaptic targets of somatostatin-containing interneurons in the rat basolateral amygdala. J Comp Neurol 500:513-529.
121. Muller JF, Mascagni F, McDonald AJ (2007b) Serotonin-immunoreactive axon terminals innervate pyramidal cells and interneurons in the rat basolateral amygdala. J Comp Neurol 505:314-335.
122. Mullner FE, Wierenga CJ, Bonhoeffer T (2015) Precision of Inhibition: Dendritic Inhibition by Individual GABAergic Synapses on Hippocampal Pyramidal Cells Is Confined in Space and Time. Neuron 87:576-589.
123. Omiya Y, Uchigashima M, Konno K, Yamasaki M, Miyazaki T, Yoshida T, Kusumi I, Watanabe M (2015) VGluT3-expressing CCK-positive basket cells construct invaginating synapses enriched with endocannabinoid signaling proteins in particular cortical and cortex-like amygdaloid regions of mouse brains. J Neurosci 35:4215-4228.
124. Palmer LM, Clark BA, Grundemann J, Roth A, Stuart GJ, Hausser M (2010) Initiation of simple and complex spikes in cerebellar Purkinje cells. J Physiol 588:1709-1717.
125. Pape HC, Driesang RB (1998) Ionic mechanisms of intrinsic oscillations in neurons of the basolateral amygdaloid complex. Journal of neurophysiology 79:217-226.
126. Pape HC, Pare D (2010) Plastic synaptic networks of the amygdala for the acquisition, expression, and extinction of conditioned fear. Physiological reviews 90:419-463.
127. Papp OI, Karlocai MR, Toth IE, Freund TF, Hajos N (2013) Different input and output properties characterize parvalbumin-positive basket and Axo-axonic cells in the hippocampal CA3 subfield. Hippocampus 23:903-918.
128. Pare D, Smith Y (1998) Intrinsic circuitry of the amygdaloid complex: common principles of organization in rats and cats. Trends in neurosciences 21:240-241.
129. Park K, Lee S, Kang SJ, Choi S, Shin KS (2007) Hyperpolarization-activated currents control the excitability of principal neurons in the basolateral amygdala. Biochemical and biophysical research communications 361:718-724.

130. Paulsen O, Moser EI (1998) A model of hippocampal memory encoding and retrieval: GABAergic control of synaptic plasticity. Trends in neurosciences 21:273-278.
131. Paxinos G FK (2001) The Mouse Brain in Stereotaxic Coordinates. San Diego: Academic press.
132. Pfeffer CK, Xue M, He M, Huang ZJ, Scanziani M (2013) Inhibition of inhibition in visual cortex: the logic of connections between molecularly distinct interneurons. Nat Neurosci 16:1068-1076.
133. Phelps EA, LeDoux JE (2005) Contributions of the amygdala to emotion processing: from animal models to human behavior. Neuron 48:175-187.
134. Pi HJ, Hangya B, Kvitsiani D, Sanders JI, Huang ZJ, Kepecs A (2013) Cortical interneurons that specialize in disinhibitory control. Nature 503:521-524.
135. Poncer JC, McKinney RA, Gahwiler BH, Thompson SM (1997) Either N- or P-type calcium channels mediate GABA release at distinct hippocampal inhibitory synapses. Neuron 18:463-472.
136. Popescu AT, Pare D (2011) Synaptic interactions underlying synchronized inhibition in the basal amygdala: evidence for existence of two types of projection cells. Journal of neurophysiology 105:687-696.
137. Povysheva NV, Zaitsev AV, Gonzalez-Burgos G, Lewis DA (2013) Electrophysiological heterogeneity of fast-spiking interneurons: chandelier versus basket cells. PloS one 8:e70553.
138. Rainnie DG, Mania I, Mascagni F, McDonald AJ (2006) Physiological and morphological characterization of parvalbumin-containing interneurons of the rat basolateral amygdala. J Comp Neurol 498:142-161.
139. Remy S, Spruston N (2007) Dendritic spikes induce single-burst long-term potentiation. Proc Natl Acad Sci U S A 104:17192-17197.
140. Rogan MT, Staubli UV, LeDoux JE (1997) Fear conditioning induces associative long-term potentiation in the amygdala. Nature 390:604-607.
141. Sah P, Faber ES, Lopez De Armentia M, Power J (2003) The amygdaloid complex: anatomy and physiology. Physiological reviews 83:803-834.

142. Schumann CM, Bauman MD, Amaral DG (2011) Abnormal structure or function of the amygdala is a common component of neurodevelopmental disorders. Neuropsychologia 49:745-759.
143. Scott SK, Young AW, Calder AJ, Hellawell DJ, Aggleton JP, Johnson M (1997) Impaired auditory recognition of fear and anger following bilateral amygdala lesions. Nature 385:254-257.
144. Seidenbecher T, Laxmi TR, Stork O, Pape HC (2003) Amygdalar and hippocampal theta rhythm synchronization during fear memory retrieval. Science 301:846-850.
145. Shu Y, Hasenstaub A, Duque A, Yu Y, McCormick DA (2006) Modulation of intracortical synaptic potentials by presynaptic somatic membrane potential. Nature 441:761-765.
146. Smith Y, Pare JF, Pare D (1998) Cat intraamygdaloid inhibitory network: ultrastructural organization of parvalbumin-immunoreactive elements. J Comp Neurol 391:164-179.
147. Smith Y, Pare JF, Pare D (2000) Differential innervation of parvalbumin-immunoreactive interneurons of the basolateral amygdaloid complex by cortical and intrinsic inputs. J Comp Neurol 416:496-508.
148. Somogyi P (1977) A specific 'axo-axonal' interneuron in the visual cortex of the rat. Brain research 136:345-350.
149. Somogyi P, Freund TF, Cowey A (1982) The axo-axonic interneuron in the cerebral cortex of the rat, cat and monkey. Neuroscience 7:2577-2607.
150. Somogyi P, Kisvárday ZF, Martin KA, Whitteridge D (1983a) Synaptic connections of morphologically identified and physiologically characterized large basket cells in the striate cortex of cat. Neuroscience 10:261-294.
151. Somogyi P, Klausberger T (2005) Defined types of cortical interneurone structure space and spike timing in the hippocampus. J Physiol 562:9-26.
152. Somogyi P, Nunzi MG, Gorio A, Smith AD (1983b) A new type of specific interneuron in the monkey hippocampus forming synapses exclusively with the axon initial segments of pyramidal cells. Brain research 259:137-142.

153. Somogyi P, Tamas G, Lujan R, Buhl EH (1998) Salient features of synaptic organisation in the cerebral cortex. Brain research Brain research reviews 26:113-135.
154. Soriano E, Nitsch R, Frotscher M (1990) Axo-axonic chandelier cells in the rat fascia dentata: Golgi-electron microscopy and immunocytochemical studies. J Comp Neurol 293:1-25.
155. Sorvari H, Miettinen R, Soininen H, Pitkanen A (1996) Parvalbumin-immunoreactive neurons make inhibitory synapses on pyramidal cells in the human amygdala: a light and electron microscopic study. Neuroscience letters 217:93-96.
156. Szabadics J, Varga C, Molnar G, Olah S, Barzo P, Tamas G (2006) Excitatory effect of GABAergic axo-axonic cells in cortical microcircuits. Science 311:233-235.
157. Szabó GG, Holderith N, Gulyás AI, Freund TF, Hájos N (2010) Distinct synaptic properties of perisomatic inhibitory cell types and their different modulation by cholinergic receptor activation in the CA3 region of the mouse hippocampus. Eur J Neurosci 31:2234-2246.
158. Szinyei C, Heinbockel T, Montagne J, Pape HC (2000) Putative cortical and thalamic inputs elicit convergent excitation in a population of GABAergic interneurons of the lateral amygdala. J Neurosci 20:8909-8915.
159. Takacs VT, Szonyi A, Freund TF, Nyiri G, Gulyas AI (2015) Quantitative ultrastructural analysis of basket and axo-axonic cell terminals in the mouse hippocampus. Brain structure & function 220:919-940.
160. Takahashi H, Magee JC (2009) Pathway interactions and synaptic plasticity in the dendritic tuft regions of CA1 pyramidal neurons. Neuron 62:102-111.
161. Takamori S, Rhee JS, Rosenmund C, Jahn R (2000) Identification of a vesicular glutamate transporter that defines a glutamatergic phenotype in neurons. Nature 407:189-194.
162. Takamori S, Rhee JS, Rosenmund C, Jahn R (2001) Identification of differentiation-associated brain-specific phosphate transporter as a second vesicular glutamate transporter (VGLUT2). J Neurosci 21:RC182.

163. Tamas G, Szabadics J (2004) Summation of unitary IPSPs elicited by identified axo-axonic interneurons. Cereb Cortex 14:823-826.
164. Tamas G, Szabadics J, Lorincz A, Somogyi P (2004) Input and frequency-specific entrainment of postsynaptic firing by IPSPs of perisomatic or dendritic origin. Eur J Neurosci 20:2681-2690.
165. Thome C, Kelly T, Yanez A, Schultz C, Engelhardt M, Cambridge SB, Both M, Draguhn A, Beck H, Egorov AV (2014) Axon-carrying dendrites convey privileged synaptic input in hippocampal neurons. Neuron 83:1418-1430.
166. Tye KM, Prakash R, Kim SY, Fenno LE, Grosenick L, Zarabi H, Thompson KR, Gradinaru V, Ramakrishnan C, Deisseroth K (2011) Amygdala circuitry mediating reversible and bidirectional control of anxiety. Nature 471:358-362.
167. Varoqueaux F, Jamain S, Brose N (2004) Neuroligin 2 is exclusively localized to inhibitory synapses. European journal of cell biology 83:449-456.
168. Vereczki V, Veres J, Muller K, Nagy G, Racz B, Barsy B, Hajos N (2016) Synaptic organization of perisomatic GABAergic inputs onto the principal cells of the mouse basolateral amygdala. Front Neuroanat 10:19.
169. Wang Y, Toledo-Rodriguez M, Gupta A, Wu C, Silberberg G, Luo J, Markram H (2004) Anatomical, physiological and molecular properties of Martinotti cells in the somatosensory cortex of the juvenile rat. J Physiol 561:65-90.
170. Washburn MS, Moises HC (1992) Electrophysiological and morphological properties of rat basolateral amygdaloid neurons in vitro. J Neurosci 12:4066-4079.
171. Watson RE, Jr., Wiegand SJ, Clough RW, Hoffman GE (1986) Use of cryoprotectant to maintain long-term peptide immunoreactivity and tissue morphology. Peptides 7:155-159.
172. Wefelmeyer W, Cattaert D, Burrone J (2015) Activity-dependent mismatch between axo-axonic synapses and the axon initial segment controls neuronal output. Proc Natl Acad Sci U S A 112:9757-9762.
173. Windels F, Crane JW, Sah P (2010) Inhibition dominates the early phase of up-states in the basolateral amygdala. Journal of neurophysiology 104:3433-3438.

174. Wolff SB, Grundemann J, Tovote P, Krabbe S, Jacobson GA, Muller C, Herry C, Ehrlich I, Friedrich RW, Letzkus JJ, Luthi A (2014) Amygdala interneuron subtypes control fear learning through disinhibition. Nature 509:453-458.

175. Woodruff AR, McGarry LM, Vogels TP, Inan M, Anderson SA, Yuste R (2011) State-dependent function of neocortical chandelier cells. J Neurosci 31:17872-17886.

176. Woodruff AR, Monyer H, Sah P (2006) GABAergic excitation in the basolateral amygdala. J Neurosci 26:11881-11887.

177. Woodruff AR, Sah P (2007a) Inhibition and synchronization of basal amygdala principal neuron spiking by parvalbumin-positive interneurons. Journal of neurophysiology 98:2956-2961.

178. Woodruff AR, Sah P (2007b) Networks of parvalbumin-positive interneurons in the basolateral amygdala. J Neurosci 27:553-563.

179. Zhu PJ, Lovinger DM (2005) Retrograde endocannabinoid signaling in a postsynaptic neuron/synaptic bouton preparation from basolateral amygdala. J Neurosci 25:6199-6207.

10. List of publications

Publications related to this thesis

Vereczki VK[1], **Veres JM**[1], Müller K, Nagy GA, Rácz B, Barsy B, Hájos N
Synaptic organization of perisomatic GABAergic inputs onto the principal cells of the mouse basolateral amygdala.
Frontiers in Neuroanatomy, 2016, Volume 10 Article 20
[1]equal contribution

Veres JM, Nagy GA, Vereczki VK, Andrási T, Hájos N
Strategically positioned inhibitory synapses of axo-axonic cells potently control principal neuron spiking in the basolateral amygdala.
Journal of Neuroscience, 2014 Dec 3;34(49):16194-206.

Other publications

Zemankovics R, **Veres JM**, Oren I, Hájos N
Feedforward inhibition underlies the propagation of cholinergically induced gamma oscillations from hippocampal CA3 to CA1.
Journal of Neuroscience, 2013 Jul 24;33(30):12337-51.

Holderith N, Németh B, Papp OI, **Veres JM**, Nagy GA, Hájos N
Cannabinoids attenuate hippocampal gamma oscillations by suppressing excitatory synaptic input onto CA3 pyramidal neurons and fast spiking basket cells.
Journal of Physiology, 2011 Oct 15;589(Pt 20):4921-34.

Cserép C, Szonyi A, **Veres JM**, Németh B, Szabadits E, de Vente J, Hájos N, Freund TF, Nyiri G
Nitric oxide signaling modulates synaptic transmission during early postnatal development.
Cerebral Cortex, 2011 Sep;21(9):2065-74.

11. Acknowledgements

First of all, I would like to thank all the energy and care of my mentor Norbert Hájos, who has been supervising my development with infinite enthusiasm, patience and devotion since my very first immunostaining, and who formed and inspired my scientific thinking profoundly. I would also like to say thanks for all the present and past members of the Laboratory of Network Neurophysiology. I'm glad that I have the opportunity to work in a great lab with inspiring atmosphere both scientifically and personally, having always someone ready for a brainstorming about the latest results or for a consolatory beer. Among them Rita Zemankovics, Gergő Szabó and Orsolya Papp contributed particularly much to my professional and personal development, thank you guys. It is also a great pleasure to work in the stimulating scientific environment the KOKI provides.

I would also like to say thanks to my friends and family, and specially to my parents, without their love and support I surely wouldn't become the person who I am. Köszönöm!